

Current-current operator contribution to the decay matrix in B -meson mixing at next-to-next-to-leading order of QCD

Marvin Gerlach^a, Ulrich Nierste^a, Pascal Reeck^a,
Vladyslav Shtabovenko^b, and Matthias Steinhauser^a

^a*Institut für Theoretische Teilchenphysik,
Wolfgang-Gaede Straße 1, Karlsruhe Institute of Technology (KIT)
76131 Karlsruhe, Germany*

^b*Theoretische Physik 1, Center for Particle Physics Siegen,
Universität Siegen, 57068 Siegen, Germany*

Abstract

We compute next-to-next-to-leading order perturbative corrections to the decay width difference of mass eigenstates and the charge-parity asymmetry a_{fs} in flavour-specific decays of neutral B mesons. In our calculation we take into account the full dependence on the charm and bottom quark masses for the current-current operator contributions up to three-loop order. Special emphasis is put on the proper construction of the so-called $|\Delta B| = 2$ theory such that Fierz symmetry is preserved. We provide updated phenomenological predictions, for $\Delta\Gamma$, $\Delta\Gamma/\Delta M$ and a_{fs} for the B_d and B_s system, including a detailed analysis of the uncertainties of our predictions. The calculated NNLO correction reduce the perturbative uncertainty of the leading term of the $1/m_b$ expansion of the width difference $\Delta\Gamma_s$ in the B_s system to the level of the current experimental error. The uncertainty of our prediction $\Delta\Gamma_s = (0.077 \pm 0.016) \text{ ps}^{-1}$ is dominated by the sub-leading term of this expansion. We further illustrate how better future measurements of $\Delta\Gamma_d$ and a_{fs}^d will help to gain a better understanding of B_d - \bar{B}_d mixing.

1 Introduction

Neutral B_q mesons mix with their antiparticles because the weak interaction permits transitions which change the beauty quantum number B by two units. $B_q - \bar{B}_q$ mixing requires the exchange of two virtual W bosons and is therefore a loop-induced process, mediated by the box diagram in Fig. 1. The valence quark q can be d or s ; since their masses are negligible, the corresponding box diagrams only differ by the elements of the Cabibbo-Kobayashi-Maskawa (CKM) matrix accompanying the W couplings. The time evolution of the two-state system ($|B_q\rangle, |\bar{B}_q\rangle$) is governed by the 2×2 matrix $M^q - i\Gamma^q/2$ built from the Hermitian mass and decay matrices M^q and Γ^q . To leading order (LO) in the strong coupling constant α_s , the off-diagonal elements of both matrices are calculated from the box diagram in Fig. 1. While M_{12}^q is dominated by the diagrams with one or two internal top quarks, only box diagrams with light quarks u, c contribute to Γ_{12}^q . The latter diagrams describe the interference between the decay amplitudes of $B_q \rightarrow f$ and $\bar{B}_q \rightarrow f$, which is related to the absorptive part of the $B_q \rightarrow \bar{B}_q$ box diagram.

The state $|B_q(t)\rangle$ of a meson tagged as B_q at time $t = 0$ evolves into a superposition of $|B_q\rangle$ and $|\bar{B}_q\rangle$ and experimental studies of time dependent decay rates $\Gamma(B_q(t) \rightarrow f)$ permit the determination of the three theoretical quantities $|M_{12}^q|$, $|\Gamma_{12}^q|$, and $\arg(-\Gamma_{12}^q/M_{12}^q)$ of the $B_q - \bar{B}_q$ complex. One defines

$$\begin{aligned}\Delta M_q &= M_H^q - M_L^q, \\ \Delta \Gamma_q &= \Gamma_L^q - \Gamma_H^q,\end{aligned}\tag{1}$$

where $M_{L,H}$ and $\Gamma_{L,H}$ denote the masses and widths of the lighter and heavier eigenstates

$$|B_{q,L}\rangle = p|B_q\rangle + q|\bar{B}_q\rangle, \quad |B_{q,H}\rangle = p|B_q\rangle - q|\bar{B}_q\rangle.\tag{2}$$

The coefficients p and q are found by diagonalising $M^q - i\Gamma^q/2$. Then theoretical and experimental quantities are related as

$$\begin{aligned}\Delta M_q &= 2|M_{12}^q|, & \Delta \Gamma_q &= 2|\Gamma_{12}^q| \cos \phi_q \\ \frac{\Delta \Gamma_q}{\Delta M_q} &= -\text{Re} \frac{\Gamma_{12}^q}{M_{12}^q}, & a_{\text{fs}}^q &= \text{Im} \frac{\Gamma_{12}^q}{M_{12}^q},\end{aligned}\tag{3}$$

where $\phi_q \equiv \arg(-\Gamma_{12}^q/M_{12}^q)$ is the small fundamental CP phase quantifying CP violation in mixing. a_{fs}^q denotes the charge-parity (CP) asymmetry in flavour-specific decays and quantifies CP violation in $B_q - \bar{B}_q$ mixing. Eqs. (3) receive negligible relative corrections of order $|\Gamma_{12}^q/M_{12}^q|^2 \sim 10^{-5}$. Furthermore, in a_{fs}^q we omit the quadratic terms in $\text{Im}[\Gamma_{12}^q/M_{12}^q] \lesssim 10^{-3}$.

The experimental situation is as follows:

$$\Delta M_s^{\text{exp}} = (17.7656 \pm 0.0057) \text{ ps}^{-1}, \tag{1} \tag{4}$$

$$\Delta \Gamma_s^{\text{exp}} = (0.082 \pm 0.005) \text{ ps}^{-1}, \tag{2} \tag{5}$$

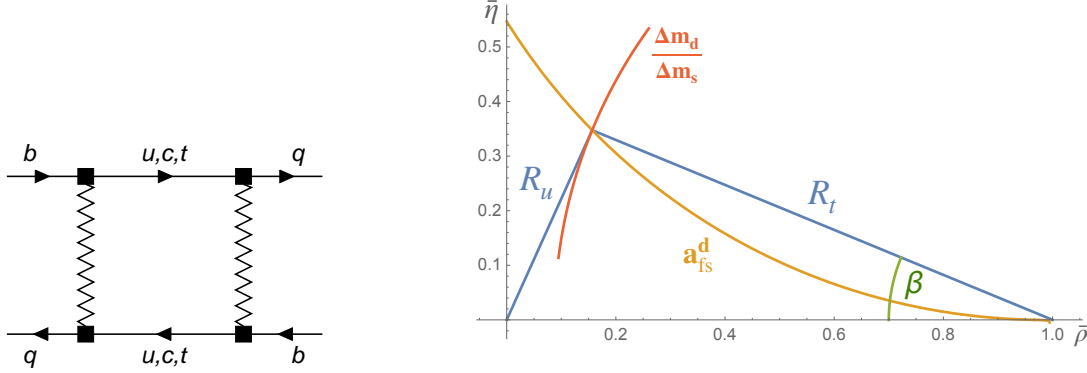


Figure 1: Left: box diagram describing $B_q - \bar{B}_q$ mixing with $q = d$ or s to leading order in QCD. Right: constraints from the three $B - \bar{B}$ mixing observables $\Delta M_d / \Delta M_s \propto R_t^2$, $a_{CP}(B_d(t) \rightarrow J/\psi K_S) \propto \sin(2\beta)$, and $a_{\text{fs}}^d \propto (\sin \beta) / R_t$ on the apex $(\bar{\rho}, \bar{\eta})$ of the CKM unitarity triangle.

$$a_{\text{fs}}^{s,\text{exp}} = -0.0006 \pm 0.0028, \quad [2] \quad (6)$$

$$\Delta M_d^{\text{exp}} = (0.5065 \pm 0.0019) \text{ ps}^{-1}, \quad [2] \quad (7)$$

$$\Delta \Gamma_d^{\text{exp}} = (0.7 \pm 6.6) \cdot 10^{-3} \text{ ps}^{-1}, \quad [2] \quad (8)$$

$$a_{\text{fs}}^{d,\text{exp}} = -0.0021 \pm 0.0017. \quad [2] \quad (9)$$

The last five numbers are averages from all available data, see Ref. [2] for the original references. $\Delta \Gamma_d^{\text{exp}}$ in Eq. (8) is calculated from $\Delta \Gamma_d / \Gamma_d = 0.001 \pm 0.010$ quoted in Ref. [2] and the B_d lifetime $1/\Gamma_d^{\text{exp}} = \tau(B_d) = (1.519 \pm 0.004) \text{ ps}^{-1}$.

In order to fully determine the three fundamental quantities $|M_{12}^q|$, $|\Gamma_{12}^q|$, and $\phi_q = \arg(-M_{12}^q/\Gamma_{12}^q)$ for both the B_d and B_s systems, one must measure all six quantities listed in Eqs. (4) to (9). Ideally, these measurements will be confronted with precise Standard Model (SM) predictions. While ΔM_q^{exp} accurately constrains $|M_{12}^q|$, the only precise information on a decay matrix element is on $\text{Re}(\Gamma_{12}^s/M_{12}^s)$ inferred from $\Delta \Gamma_s^{\text{exp}}/\Delta M_s^{\text{exp}}$.

The calculation of Γ_{12}^q involves two operator product expansions (OPE) which separate the strong interactions associated with the different energy scales $m_t, M_W \gg m_b \gg \Lambda_{\text{QCD}}$, where m_t , m_b , and M_W are the masses of top and bottom quark and W boson and $\Lambda_{\text{QCD}} \sim 400 \text{ MeV}$ is the hadronic scale. The first OPE amounts to the construction of the effective weak $|\Delta B| = 1$ Hamiltonian describing b decays mediated by virtual W bosons or top quarks in terms of dimension-six operators. The Wilson coefficients multiplying these operators can be calculated in perturbation theory and are known to next-to-leading order (NLO) [3–5] and next-to-next-to-leading order (NNLO) [6–8] of quantum chromodynamics (QCD). The numerically most important coefficients in the $|\Delta B| = 1$ Hamiltonian are those of the current-current operators describing the effect of W -mediated tree decays. Penguin operators related to W -top loops in the SM have a smaller, yet non-negligible effect on Γ_{12}^q . The second OPE is the Heavy Quark Expansion (HQE) which matches the

$B_q-\bar{B}_q$ mixing amplitude with two $\Delta B = 1$ operators onto local $\Delta B = 2$ operators, which amounts to an expansion in powers of Λ_{QCD}/m_b . The coefficients multiplying the $\Delta B = 2$ operators of the leading power are fully known at LO and NLO, including the contributions with one or two penguin operators [9–16]. NNLO corrections to the contribution from two current-current operators have been calculated first in the approximation of a large number of flavours [17–19], but a theoretical prediction matching the error of $\Delta\Gamma_s^{\text{exp}}$ in Eq. (5) calls for a full NNLO calculation of the current-current contribution. The numerical NNLO result for $\Delta\Gamma_s$ presented in Ref. [20] is based on an expansion of the three-loop integrals to second order in m_c/m_b , where m_c denotes the charm quark mass. This paper is devoted to a detailed description of the calculation including semi-analytic results. We go beyond Ref. [20] by evaluating the three-loop integrals up to order z^{50} where $z = m_c^2/m_b^2$.¹ Contributions from penguin operators are considered up to NLO and up to order z^1 .

Another focus of this paper is the application of our result to a phenomenological analysis of $\Delta\Gamma_d$ and a_{fs}^d , which can constrain models of new physics predicting sizeable contributions to Γ_{12}^d (see, e.g. Ref. [22]). Furthermore, a_{fs}^d can play an important role to constrain new physics in M_{12}^d : While we know the magnitude and phase of M_{12}^d well from ΔM_d and the mixing-induced CP asymmetry $a_{CP}(B_d(t) \rightarrow J/\psi K_S)$, the predictions of both quantities involve the parameters $\bar{\rho}, \bar{\eta}$ characterising the apex of the CKM unitarity triangle (UT). In fact, in the absence of new physics, the ratio $\Delta M_d/\Delta M_s$ pins down the side $R_t = \sqrt{\bar{\rho}^2 + \bar{\eta}^2}$ of the UT precisely, and $a_{CP}(B_d(t) \rightarrow J/\psi K_S) \propto \sin(2\beta)$ accurately determines the UT angle β . However, to *test* the SM description of $B_d-\bar{B}_d$ mixing one must determine $\bar{\rho}, \bar{\eta}$ from *other* observables. For example, β is well constrained by the opposing side $R_u \propto |V_{ub}/V_{cb}|$ of the UT, which is unfortunately affected by the “exclusive vs. inclusive” controversies on the measurements of $|V_{ub}|$ and $|V_{cb}|$ from semileptonic decays. Now [12]

$$a_{\text{fs}}^d \propto \frac{\sin \beta}{R_t} = \frac{\bar{\eta}}{\sqrt{(1 - \bar{\rho})^2 + \bar{\eta}^2}} \quad (10)$$

up to small and calculable corrections. Eq. (10) means that a precise measurement of a_{fs}^d defines a circle in the $(\bar{\rho}, \bar{\eta})$ plane. The requirement that the apex of the UT determined from $\Delta M_d/\Delta M_s$ and $a_{CP}(B_d(t) \rightarrow J/\psi K_S)$ lies on this circle probes the SM from $B_q-\bar{B}_q$ mixing observables *alone*, see Fig. 1. Moreover, $a_{\text{fs}}^d = \mathcal{O}(m_c^2/m_b^2)$, because Γ_{12}^d and M_{12}^d have the same phase for $m_c = 0$, so that $\text{Im}(\Gamma_{12}^d/M_{12}^d)$ vanishes in this limit. A small new-physics contribution $\phi_{12}^{d\Delta}$ to $\arg M_{12}^d$ will change β inferred from $a_{CP}(B_d(t) \rightarrow J/\psi K_S) \propto \sin(2\beta + \phi_{12}^{d\Delta})$ slightly, but significantly enhance a_{fs}^d because a_{fs}^d receives a contribution proportional to $\sin \phi_{12}^{d\Delta}$ unsuppressed by m_c^2/m_b^2 [12, 23].

The paper is organised as follows: In the next Section we discuss in detail the effective $\Delta B = 1$ and $\Delta B = 2$ theories. In the latter case we elaborate in detail on the construction of the evanescent operators such that Fierz symmetry is preserved in $D \neq 4$ dimensions

¹In Ref. [21] expansions around $\sqrt{z} = 1/20, 1/5$ and $3/10$ have been constructed, too. For the phenomenological application it is sufficient to use the expansion for $z \rightarrow 0$.

and discuss the mixing among the operators. Section 3 is dedicated to technical details concerning the computation of the amplitudes, and in Section 4 we show results for the matching coefficients for $m_c = 0$. Section 5 contains the phenomenological analysis of $\Delta\Gamma_q$, $\Delta\Gamma_q/\Delta M_q$ and a_{fs}^q . We conclude in Section 6. In Appendix A we discuss the renormalisation constants in the $\Delta B = 2$ theory and describe how to obtain them from the computer-readable file. In Appendix B we provide additional information on the Fierz transformation. In Appendix C we provide analytic results for the master integrals which are needed in the limit of massless charm quarks. Appendix D contains the coefficients which appear in the definition of the evanescent operators in the $\Delta B = 2$ theory keeping the dependence on the number of colours.

2 Effective theories

For the calculation of Γ_{12}^q we have to consider two effective theories which are successively constructed from the Standard Model. In a first step one integrates out the degrees of freedom with masses of the order of the electroweak scale to arrive at the $|\Delta B| = 1$ Hamiltonian $\mathcal{H}_{\text{eff}}^{|\Delta B|=1} = \mathcal{H}_{\text{eff}}^{\Delta B=1} + \text{h.c.}$ mentioned in the Introduction; the corresponding Wilson coefficients are known to NNLO. For our calculation we need the coefficients of the current-current operators [7], which emerge from tree-level W exchange. In a first step we write Γ_{12}^q from Eq. (3) as

$$\Gamma_{12}^q = \frac{1}{2M_{B_s}} \text{Abs}\langle B_q | i \int d^4x T \mathcal{H}_{\text{eff}}^{\Delta B=1}(x) \mathcal{H}_{\text{eff}}^{\Delta B=1}(0) | \bar{B}_q \rangle, \quad (11)$$

where “Abs” denotes the absorptive part of the matrix element. In a second step we perform a HQE which leads to an expansion of Γ_{12}^q in powers of $1/m_b$ in the so-called $\Delta B = 2$ theory. This step amounts to the expression of the bi-local matrix element in Eq. (11) as a sum of terms involving matrix elements of local $\Delta B = 2$ operators multiplied by new $\Delta B = 2$ matching coefficients, which depend on the $\Delta B = 1$ coefficients, the strong coupling constant α_s , and the quark masses m_c and m_b . Higher dimensions of the $\Delta B = 2$ operators correspond to higher powers of $1/m_b$ in the HQE. The $\Delta B = 2$ matching coefficients are calculated in perturbative QCD as an expansion in α_s . The main purpose of this work is the calculation of the leading-power coefficients to NNLO, i.e. three-loop accuracy. The essentials of the matching calculation between the $\Delta B = 1$ and $\Delta B = 2$ theories is described in Refs. [11–18]. We will therefore focus on the new features occurring first at NNLO, which are related to evanescent operators and the mixing with an operator related formally to power-suppressed terms.

2.1 $\Delta B = 1$ theory

For definiteness we consider Γ_{12}^s from now on, the generalisation to Γ_{12}^d is straightforward. On the $|\Delta B| = 1$ side of the matching we work with the operator basis [24]

$$\mathcal{H}_{\text{eff}}^{|\Delta B|=1} = \frac{4G_F}{\sqrt{2}} \left[-\lambda_t^s \left(\sum_{i=1}^6 C_i Q_i + C_8 Q_8 \right) - \lambda_u^s \sum_{i=1}^2 C_i (Q_i - Q_i^u) \right. \\ \left. + V_{us}^* V_{cb} \sum_{i=1}^2 C_i Q_i^{cu} + V_{cs}^* V_{ub} \sum_{i=1}^2 C_i Q_i^{uc} \right] + \text{h.c.}, \quad (12)$$

with

$$\lambda_a^s = V_{as}^* V_{ab}, \quad (13)$$

where $a = u, c, t$ and $\lambda_t = -\lambda_c - \lambda_u$. G_F stands for the Fermi constant. We need the current-current operators

$$\begin{aligned} Q_1 &= \bar{s}_L \gamma_\mu T^a c_L \bar{c}_L \gamma^\mu T^a b_L, & Q_2 &= \bar{s}_L \gamma_\mu c_L \bar{c}_L \gamma^\mu b_L, \\ Q_1^u &= \bar{s}_L \gamma_\mu T^a u_L \bar{u}_L \gamma^\mu T^a b_L, & Q_2^u &= \bar{s}_L \gamma_\mu u_L \bar{u}_L \gamma^\mu b_L, \\ Q_1^{cu} &= \bar{s}_L \gamma_\mu T^a u_L \bar{c}_L \gamma^\mu T^a b_L, & Q_2^{cu} &= \bar{s}_L \gamma_\mu u_L \bar{c}_L \gamma^\mu b_L, \\ Q_1^{uc} &= \bar{s}_L \gamma_\mu T^a c_L \bar{u}_L \gamma^\mu T^a b_L, & Q_2^{uc} &= \bar{s}_L \gamma_\mu c_L \bar{u}_L \gamma^\mu b_L. \end{aligned} \quad (14)$$

Here we introduced the left-chiral projector $P_L = (1 - \gamma_5)/2$ so that $q_L = P_L q$. The four-quark penguin operators Q_3, \dots, Q_6 and the chromomagnetic penguin operator Q_8 are not needed for the calculation presented in this paper; their definition can be found, e.g. in Refs. [15, 16, 24].

We employ dimensional regularisation in $D = 4 - 2\epsilon$ dimensions. The bare matrix elements of the operators in Eq. (14) feature ultraviolet (UV) divergent expressions with more than one Dirac matrix on each fermion line, which can be reduced to matrix elements of the operators in $\mathcal{H}_{\text{eff}}^{|\Delta B|=1}$ in four dimensions but not for $D \neq 4$. The renormalisation programme therefore involves evanescent operators; at NLO these are

$$\begin{aligned} E_1[Q_1] &= \bar{s}_L \gamma^{\mu_1} \gamma^{\mu_2} \gamma^{\mu_3} T^a c \bar{c} \gamma_{\mu_1} \gamma_{\mu_2} \gamma_{\mu_3} T^a b_L - 16Q_1, \\ E_1[Q_2] &= \bar{s}_L \gamma^{\mu_1} \gamma^{\mu_2} \gamma^{\mu_3} c \bar{c} \gamma_{\mu_1} \gamma_{\mu_2} \gamma_{\mu_3} b_L - 16Q_2. \end{aligned} \quad (15)$$

Similar evanescent operators are needed for Q_i^u , Q_i^{uc} and Q_i^{cu} with $i = 1, 2$; they are obtained by replacing one or both c fields with u fields in Eq. (15). We refer to $E_1[Q_{1,2}]$ as evanescent operators of the first generation and define the n -th generation operators as those with $2n$ more Dirac matrices in each fermion current than the corresponding physical operator. At NNLO one has to introduce the second-generation operators

$$\begin{aligned} E_2[Q_1] &= \bar{s}_L \gamma^{\mu_1} \gamma^{\mu_2} \gamma^{\mu_3} \gamma^{\mu_4} \gamma^{\mu_5} T^a c \bar{c} \gamma_{\mu_1} \gamma_{\mu_2} \gamma_{\mu_3} \gamma_{\mu_4} \gamma_{\mu_5} T^a b_L - 20E_1[Q_2] - 256Q_1, \\ E_2[Q_2] &= \bar{s}_L \gamma^{\mu_1} \gamma^{\mu_2} \gamma^{\mu_3} \gamma^{\mu_4} \gamma^{\mu_5} c \bar{c} \gamma_{\mu_1} \gamma_{\mu_2} \gamma_{\mu_3} \gamma_{\mu_4} \gamma_{\mu_5} b_L - 20E_1[Q_2] - 256Q_2, \end{aligned} \quad (16)$$

which occur in two-loop matrix elements of $Q_{1,2}$ and one-loop matrix elements of $E_1[Q_{1,2}]$. The renormalisation of the physical and evanescent $\Delta B = 1$ operators has extensively been discussed in the literature, see, e.g. Refs. [3–5, 7, 25, 26].

2.2 Physical operators in the $\Delta B = 2$ theory

In the following we present the basis of physical operators used in our calculation. At leading power in $1/m_b$, there are three physical operators which are chosen as

$$\begin{aligned} Q &= 4 (\bar{s}^c \gamma^\mu P_L b^c) (\bar{s}^d \gamma_\mu P_L b^d), \\ \tilde{Q}_S &= 4 (\bar{s}^c P_R b^d) (\bar{s}^d P_R b^c), \\ Q_S &= 4 (\bar{s}^c P_R b^c) (\bar{s}^d P_R b^d), \end{aligned} \tag{17}$$

where $P_R = (1 + \gamma_5)/2$ and c, d are the colour indices attached to quark fields. As in the $\Delta B = 1$ theory, we need evanescent operators with several Dirac matrices on each line, in analogy to Eqs. (15) and (16). These will be discussed in Section 2.3.

There is a special relation between the three physical operators,

$$R_0 = \frac{1}{2} Q + Q_S + \tilde{Q}_S, \tag{18}$$

which is an operator satisfying $\langle B_s | R_0 | \bar{B}_s \rangle = \mathcal{O}(1/m_b)$ [10]. Equation (18) can be used to trade Q_S for R_0 . In perturbation theory, $\langle B_s | R_0 | \bar{B}_s \rangle^{(n)} = \mathcal{O}(1/m_b)$ only holds beyond $n = 0$ (LO) if R_0 receives a special finite renormalisation, which is discussed in Section 2.5. The calculation of these finite renormalisation constants requires a subtle treatment of infrared (IR) singularities, to be discussed in Section 2.6.

In summary, we can trade the operators in Eq. (17) for linear combinations which are either evanescent or have power-suppressed matrix elements such that our basis of physical operators is $\{Q, \tilde{Q}_S, R_0\}$. The evanescent operators, which will be discussed in the following section, are unphysical, meaning that they vanish in $D \rightarrow 4$ dimensions and appear at intermediate steps, while their Wilson coefficients do not enter physical observables.

2.3 Evanescent operators in the $\Delta B = 2$ theory

In order to obtain results consistent with the low-energy matrix elements, we choose an operator basis that respects Fierz symmetry for the matrix elements of the physical operators. This is because our perturbative Wilson coefficients are combined with non-perturbative hadronic matrix elements, which are calculated in four dimensions, e.g. in lattice gauge theory. In such four-dimensional calculations an operator is trivially identical to its Fierz transform.

The relevance of Fierz symmetry is rooted in the fact that the $\Delta B = 2$ matrix elements can be calculated exactly in the limit $N_c \rightarrow \infty$, where $N_c = 3$ is the number of colours, in terms of meson masses and decay constants. In the case of \tilde{Q}_S this calculation involves a four-dimensional Fierz transform and only gives the correct result for physical observables if the Wilson coefficients of \tilde{Q}_S and its Fierz transform coincide for $N_c \rightarrow \infty$. It is further desirable to implement Fierz symmetry at all orders of $1/N_c$, so that in any calculation

of the hadronic matrix element one can easily choose the Fierz arrangement at wish. For further explanations see Appendix B.

To achieve Fierz symmetry in perturbation theory, one must define the evanescent operators appropriately [3, 25], and this step is part of the definition of the renormalisation scheme. Here “Fierz symmetry” means that the Wilson coefficient of a given operator O is identical to that of its Fierz transform O^F .

In the following, we will explicitly construct bases of evanescent operators obeying Fierz symmetry. Specifically, we impose the following conditions:

1. Renormalised matrix elements of physical operators are identical to those of their Fierz-transformed counterparts: $\lim_{d \rightarrow 4} \langle O \rangle^{\text{ren}} = \lim_{d \rightarrow 4} \langle O^F \rangle^{\text{ren}}$ at one-loop and two-loop level.
2. The operator definitions of the evanescent operators should not depend on the number of quark flavours N_f .
3. The large- N_c limit of the renormalised physical operator matrix elements fixes the leading term to be of order N_c^2 , see Appendix B. This constraint must be respected by the definition of the evanescent operators. Hence, the $\mathcal{O}(\epsilon)$ contributions of physical operators to the evanescent operators must be at most $\mathcal{O}(N_c^0)$ as $N_c \rightarrow \infty$.

One can check that enforcing these conditions leaves no ambiguity in the leading $\mathcal{O}(N_c^2)$ term of the renormalised physical operators in the large- N_c limit and ensures that they evaluate to the correct factorised results. Note that condition 1 must hold for any choice of IR regulator and is most easily implemented by choosing off-shell kinematics, for which no IR singularities occur.

To enforce the conditions 1 to 3 above, both the regular as well as the Fierz basis have to be defined. We first define the Fierz-transformed counterparts of the physical operators in Eq. (17), namely

$$\begin{aligned}\tilde{Q} &= Q^F = 4 (\bar{s}^c \gamma_\mu P_L b^d) (\bar{s}^d \gamma^\mu P_L b^c), \\ Q_S^F &= \frac{1}{12} Q_T - \frac{1}{6} \tilde{Q}_T, \\ \tilde{Q}_S^F &= \frac{1}{12} \tilde{Q}_T - \frac{1}{6} Q_T.\end{aligned}\tag{19}$$

Note that applying a Fierz transformation to Q leads directly to the operator \tilde{Q} which has the colour indices c, d contracted across the two spin lines. The operator Q and its evanescent operators renormalise separately from the operators Q_S and \tilde{Q}_S because even and odd numbers of gamma matrices do not mix. This is also true for the respective Fierz-transformed operators.

The operators Q_T and \tilde{Q}_T used in the definitions in Eq. (19) are

$$Q_T = 4 (\bar{s}^c \sigma^{\mu\nu} P_R b^c) (\bar{s}^d \sigma_{\mu\nu} P_R b^d),$$

Loop order	Inserted operators
Tree-level	$Q, E^{(1)}, E^{(2)}, E^{(3)}, E^{(4)}$
One-loop	$Q, E^{(1)}, E^{(2)}, E^{(3)}$
Two-loop	$Q, E^{(1)}, E^{(2)}$

Table 1: An example of which operators need to be inserted at which loop order to renormalise a second generation evanescent operator at NNLO, i.e. two-loop level. The physical operators are schematically denote by Q while $E^{(i)}$ stands for the i th generation evanescent operators.

$$\tilde{Q}_T = 4(\bar{s}^c \sigma^{\mu\nu} P_R b^d) (\bar{s}^d \sigma_{\mu\nu} P_R b^c), \quad (20)$$

where $\sigma^{\mu\nu} = \frac{i}{2}[\gamma^\mu, \gamma^\nu]$. This is a result of applying the Fierz identity

$$(P_R)_{\alpha\beta}(P_R)_{\gamma\delta} = \frac{1}{8}(\sigma^{\mu\nu} P_R)_{\alpha\delta}(\sigma_{\mu\nu} P_R)_{\gamma\beta} + \frac{1}{2}(P_R)_{\alpha\delta}(P_R)_{\gamma\beta}. \quad (21)$$

There is an infinite number of evanescent operators, but it is sufficient to include only a finite number to renormalise physical operators to a given order in perturbation theory. To renormalise n th generation evanescent operators to order $\mathcal{O}(\alpha_s^i)$, where physical operators are counted as 0th generation, we need to consider evanescent operators up to generation $k = n + i$ at tree-level. At loop order l , we need to include operators up to generation $k_l = k - l$. For illustration purposes, we list the necessary operators to renormalise a second generation evanescent operator to $\mathcal{O}(\alpha_s^2)$ in Tab. 1.

A small caveat here is that while the procedure above is sufficient to renormalise physical operators to a given order in α_s , it is necessary to renormalise evanescent operators to carry out the matching calculation described in Section 2.7 if those evanescent matrix elements appear at lower orders on the $\Delta B = 1$ side.

The evanescent operators of the first generation have the generic definitions

$$\begin{aligned} E_1^{(1)}[Q] &= Q - \tilde{Q}, \\ E_2^{(1)}[Q] &= 4(\bar{s}^c \gamma_{\mu_1} \gamma_{\mu_2} \gamma_{\mu_3} P_L b^d) (\bar{s}^d \gamma^{\mu_3} \gamma^{\mu_2} \gamma^{\mu_1} P_L b^c) - (4 + \tilde{f}\epsilon + \tilde{g}\epsilon^2) \tilde{Q}, \\ E_3^{(1)}[Q] &= 4(\bar{s}^c \gamma_{\mu_1} \gamma_{\mu_2} \gamma_{\mu_3} P_L b^c) (\bar{s}^d \gamma^{\mu_3} \gamma^{\mu_2} \gamma^{\mu_1} P_L b^d) - (4 + f\epsilon + g\epsilon^2) Q. \end{aligned} \quad (22)$$

For the operators $\{Q_S, \tilde{Q}_S\}$, which mix under renormalisation, the evanescent operators of the first generation are

$$\begin{aligned} E^{(1)}[Q_S] &= 4(\bar{s}^c \gamma_{\mu_1} \gamma_{\mu_2} P_R b^c) (\bar{s}^d \gamma^{\mu_2} \gamma^{\mu_1} P_R b^d) + (8 + \tilde{a}\epsilon + \tilde{b}\epsilon^2) \tilde{Q}_S \\ &\quad - (a\epsilon + b\epsilon^2) Q_S, \\ E^{(1)}[\tilde{Q}_S] &= 4(\bar{s}^c \gamma_{\mu_1} \gamma_{\mu_2} P_R b^d) (\bar{s}^d \gamma^{\mu_2} \gamma^{\mu_1} P_R b^c) + (8 + \tilde{a}_2\epsilon + \tilde{b}_2\epsilon^2) Q_S \end{aligned}$$

$$- (a_2\epsilon + b_2\epsilon^2) \tilde{Q}_S. \quad (23)$$

They appear in one-loop diagrams; for a NLO calculation one only needs the coefficients of the ϵ and not the ϵ^2 terms.

In the Fierz-transformed basis we can similarly define the first generation of evanescent operators as

$$\begin{aligned} E_1^{(1)}[Q^F] &= E_1^{(1)}[Q], \\ E_2^{(1)}[Q^F] &= E_2^{(1)}[Q], \\ E_3^{(1)}[Q^F] &= E_3^{(1)}[Q], \end{aligned} \quad (24)$$

i.e. we choose the ϵ and ϵ^2 coefficients to be identical for Q and Q^F . For the operators with an even number of γ matrices we allow for different coefficients in the evanescent operators

$$\begin{aligned} E^{(1)}[Q_S^F] &= -\frac{2}{3}(\bar{s}^c\gamma_{\mu_1}\gamma_{\mu_2}\sigma^{\mu\nu}\gamma^{\mu_2}\gamma^{\mu_1}P_Rb^d)(\bar{s}^d\sigma_{\mu\nu}P_Rb^c) \\ &\quad + \frac{1}{3}(\bar{s}^c\gamma_{\mu_1}\gamma_{\mu_2}\sigma^{\mu\nu}P_Rb^c)(\bar{s}^d\sigma_{\mu\nu}P_R\gamma^{\mu_2}\gamma^{\mu_1}b^d) \\ &\quad + \left(8 + \tilde{a}^F\epsilon + \tilde{b}^F\epsilon^2\right)\tilde{Q}_S^F - (a^F\epsilon + b^F\epsilon^2)Q_S^F, \\ E^{(1)}[\tilde{Q}_S^F] &= -\frac{2}{3}(\bar{s}^c\gamma_{\mu_1}\gamma_{\mu_2}\sigma^{\mu\nu}\gamma^{\mu_2}\gamma^{\mu_1}P_Rb^c)(\bar{s}^d\sigma_{\mu\nu}P_Rb^d) \\ &\quad + \frac{1}{3}(\bar{s}^c\gamma_{\mu_1}\gamma_{\mu_2}\sigma^{\mu\nu}P_Rb^d)(\bar{s}^d\sigma_{\mu\nu}P_R\gamma^{\mu_2}\gamma^{\mu_1}b^c) \\ &\quad + \left(8 + \tilde{a}_2^F\epsilon + \tilde{b}_2^F\epsilon^2\right)Q_S^F - (a_2^F\epsilon + b_2^F\epsilon^2)\tilde{Q}_S^F. \end{aligned} \quad (25)$$

Renormalising the $\langle Q \rangle^{(1),\text{ren}}$, $\langle Q_S \rangle^{(1),\text{ren}}$ and $\langle \tilde{Q}_S \rangle^{(1),\text{ren}}$ amplitudes in the standard basis and the $\langle \tilde{Q} \rangle^{(1),\text{ren}}$, $\langle Q_S^F \rangle^{(1),\text{ren}}$ and $\langle \tilde{Q}_S^F \rangle^{(1),\text{ren}}$ amplitudes in the Fierz-transformed basis, we can then impose condition 1. For the renormalised physical matrix elements in the standard basis we insert the operators in Eqs. (17), (22) and (23) in tree-level and one-loop diagrams with the corresponding renormalisation constants. Analogously, for the Fierz-transformed basis the calculation is carried out with tree-level and one-loop diagrams of the operators in Eqs. (19), (24) and (25), using the renormalisation constants of that basis. Note that the renormalisation programme must be done off-shell, and we choose vanishing external momenta with $m_b = m_s \neq 0$ on internal lines.

In order to compare the amplitudes, the results need to be mapped onto the same basis of operator matrix elements, which can be either those of the Fierz-transformed or the regular basis. However, since the renormalised amplitudes are finite, all evanescent pieces can be discarded and tree-level matrix elements of the Fierz-transformed operators identified with their regular counterparts. For example, we demand the coefficient of $\langle Q \rangle$ in the renormalised matrix element $\langle Q \rangle^{(1),\text{ren}}$ to be equal to the coefficient of $\langle \tilde{Q} \rangle$ in the

renormalised matrix element $\langle \tilde{Q} \rangle^{(1),\text{ren}}$. We arrive at the following result:

$$\begin{aligned} a &= a_2 = 0, & \tilde{a} &= \tilde{a}_2 = -8, \\ a^F &= a_2^F = 0, & \tilde{a}^F &= \tilde{a}_2^F = -8, \\ f &= \tilde{f} = -8. \end{aligned} \quad (26)$$

The evanescent operators obtained in this manner agree with the literature, see for example Refs. [11, 16, 25, 27].

At NNLO the ϵ^2 terms in Eqs. (22) to (25) matter. Furthermore, one encounters evanescent operators of the second generation:

$$\begin{aligned} E_1^{(2)}[Q] &= 4(\bar{s}^c \gamma_{\mu_1} \gamma_{\mu_2} \gamma_{\mu_3} \gamma_{\mu_4} \gamma_{\mu_5} P_L b^d) (\bar{s}^d \gamma^{\mu_5} \gamma^{\mu_4} \gamma^{\mu_3} \gamma^{\mu_2} \gamma^{\mu_1} P_L b^c) - (16 + \tilde{h}\epsilon + \tilde{k}\epsilon^2) \tilde{Q}, \\ E_2^{(2)}[Q] &= 4(\bar{s}^c \gamma_{\mu_1} \gamma_{\mu_2} \gamma_{\mu_3} \gamma_{\mu_4} \gamma_{\mu_5} P_L b^c) (\bar{s}^d \gamma^{\mu_5} \gamma^{\mu_4} \gamma^{\mu_3} \gamma^{\mu_2} \gamma^{\mu_1} P_L b^d) - (16 + h\epsilon + k\epsilon^2) Q. \end{aligned} \quad (27)$$

For Q_S and \tilde{Q}_S the corresponding evanescent operators are

$$\begin{aligned} E^{(2)}[Q_S] &= 4(\bar{s}^c \gamma_{\mu_1} \gamma_{\mu_2} \gamma_{\mu_3} \gamma_{\mu_4} P_R b^c) (\bar{s}^d \gamma^{\mu_4} \gamma^{\mu_3} \gamma^{\mu_2} \gamma^{\mu_1} P_R b^d) \\ &\quad + (128 + \tilde{c}\epsilon + \tilde{d}\epsilon^2) \tilde{Q}_S - (c\epsilon + d\epsilon^2) Q_S, \\ E^{(2)}[\tilde{Q}_S] &= 4(\bar{s}^c \gamma_{\mu_1} \gamma_{\mu_2} \gamma_{\mu_3} \gamma_{\mu_4} P_R b^d) (\bar{s}^d \gamma^{\mu_4} \gamma^{\mu_3} \gamma^{\mu_2} \gamma^{\mu_1} P_R b^c) \\ &\quad + (128 + \tilde{c}_2\epsilon + \tilde{d}_2\epsilon^2) Q_S - (c_2\epsilon + d_2\epsilon^2) \tilde{Q}_S. \end{aligned} \quad (28)$$

For the Fierz-transformed basis we again choose the same evanescent operators for Q and $Q^F = \tilde{Q}$,

$$\begin{aligned} E_1^{(2)}[Q^F] &= E_1^{(2)}[Q], \\ E_2^{(2)}[Q^F] &= E_2^{(2)}[Q], \end{aligned} \quad (29)$$

while for Q_S^F and \tilde{Q}_S^F we define the second generation evanescent operators as

$$\begin{aligned} E^{(2)}[Q_S^F] &\equiv -\frac{2}{3}(\bar{s}^c \gamma_{\mu_1} \gamma_{\mu_2} \gamma_{\mu_3} \gamma_{\mu_4} \sigma^{\mu\nu} \gamma^{\mu_4} \gamma^{\mu_3} \gamma^{\mu_2} \gamma^{\mu_1} P_R b^d) (\bar{s}^d \sigma_{\mu\nu} P_R b^c) \\ &\quad + \frac{1}{3}(\bar{s}^c \gamma_{\mu_1} \gamma_{\mu_2} \gamma_{\mu_3} \gamma_{\mu_4} \sigma^{\mu\nu} P_R b^c) (\bar{s}^d \sigma_{\mu\nu} P_R \gamma^{\mu_4} \gamma^{\mu_3} \gamma^{\mu_2} \gamma^{\mu_1} b^d) \\ &\quad + (128 + \tilde{c}^F\epsilon + \tilde{d}^F\epsilon^2) \tilde{Q}_S^F - (c^F\epsilon + d^F\epsilon^2) Q_S^F, \\ E^{(2)}[\tilde{Q}_S^F] &\equiv -\frac{2}{3}(\bar{s}^c \gamma_{\mu_1} \gamma_{\mu_2} \gamma_{\mu_3} \gamma_{\mu_4} \sigma^{\mu\nu} \gamma^{\mu_4} \gamma^{\mu_3} \gamma^{\mu_2} \gamma^{\mu_1} P_R b^c) (\bar{s}^d \sigma_{\mu\nu} P_R b^d) \\ &\quad + \frac{1}{3}(\bar{s}^c \gamma_{\mu_1} \gamma_{\mu_2} \gamma_{\mu_3} \gamma_{\mu_4} \sigma^{\mu\nu} P_R b^d) (\bar{s}^d \sigma_{\mu\nu} P_R \gamma^{\mu_4} \gamma^{\mu_3} \gamma^{\mu_2} \gamma^{\mu_1} b^c) \\ &\quad + (128 + \tilde{c}_2^F\epsilon + \tilde{d}_2^F\epsilon^2) Q_S^F - (c_2^F\epsilon + d_2^F\epsilon^2) \tilde{Q}_S^F. \end{aligned} \quad (30)$$

The comparison of the renormalised physical matrix elements is completely analogous to the NLO calculation. Renormalising the $\langle Q \rangle^{(2),\text{ren}}$, $\langle Q_S \rangle^{(2),\text{ren}}$ and $\langle \tilde{Q}_S \rangle^{(2),\text{ren}}$ amplitudes in the standard basis and the $\langle \tilde{Q} \rangle^{(2),\text{ren}}$, $\langle Q_S^F \rangle^{(2),\text{ren}}$ and $\langle \tilde{Q}_S^F \rangle^{(2),\text{ren}}$ amplitudes in the Fierz-transformed basis, we can then impose condition 1. Comparing just the N_f terms and enforcing condition 2, we obtain the remaining coefficients of order ϵ^2 in the first generation evanescent operators:

$$\begin{aligned} b &= b_2 = 4, & \tilde{b} &= \tilde{b}_2 = 0, \\ b^F &= b_2^F = 4, & \tilde{b}^F &= \tilde{b}_2^F = 0, \\ g &= \tilde{g} = 4. \end{aligned} \tag{31}$$

This is consistent with the literature, see for example Ref. [17].

From the remaining equations we get a solution space for the c , d , h and k coefficients of the second generation evanescent operators. We then solve the equations arising from condition 1 for $\{c, \tilde{c}, d, \tilde{d}, h, \tilde{h}\}$, leaving the rest of the constants undetermined, which marks a particular choice of a set of solutions. To further impose condition 3, we require the coefficients of N_c and N_c^2 in the solutions of the evanescent constants to vanish. This chosen solution set consistent with all physical conditions is given in Appendix D.

For concreteness, we can further pick a particular, convenient solution. For example, we can choose as many of the constants on the regular operator side to be equal to zero,

$$c = c_2 = \tilde{c} = d = d_2 = \tilde{d} = \tilde{d}_2 = 0, \tag{32}$$

and drop the ϵ^2 terms of the second generation evanescent operators of Q and \tilde{Q} ,

$$k = \tilde{k} = 0. \tag{33}$$

With these additional constraints, the remaining evanescent constants are fixed uniquely:

$$\begin{aligned} \tilde{c}_2 &= -1024, \\ c^F &= \frac{-256(534 - 344 N_c - 119 N_c^2 - 366 N_c^3 - 116 N_c^4 + 163 N_c^5)}{15(8 - 16 N_c^2 + 2 N_c^3 + 2 N_c^4 + N_c^5)}, \\ c_2^F &= \frac{256(92 + 46 N_c + 164 N_c^2 + 104 N_c^3 + 141 N_c^4 + 17 N_c^5)}{15(8 - 16 N_c^2 + 2 N_c^3 + 2 N_c^4 + N_c^5)}, \\ \tilde{c}^F &= \frac{-128(196 - 220 N_c + 26 N_c^2 - 445 N_c^3 + 256 N_c^4 + 226 N_c^5)}{15(8 - 16 N_c^2 + 2 N_c^3 + 2 N_c^4 + N_c^5)}, \\ \tilde{c}_2^F &= \frac{128(172 - 608 N_c - 138 N_c^2 - 730 N_c^3 + 120 N_c^4 + 25 N_c^5)}{15(8 - 16 N_c^2 + 2 N_c^3 + 2 N_c^4 + N_c^5)}, \\ d^F &= \frac{-32(1958 - 2608 N_c + 6957 N_c^2 - 3572 N_c^3 - 2697 N_c^4 + 1391 N_c^5)}{15(8 - 16 N_c^2 + 2 N_c^3 + 2 N_c^4 + N_c^5)}, \\ d_2^F &= \frac{64(92 + 46 N_c + 164 N_c^2 + 104 N_c^3 + 141 N_c^4 + 17 N_c^5)}{15(8 - 16 N_c^2 + 2 N_c^3 + 2 N_c^4 + N_c^5)}, \end{aligned}$$

$$\begin{aligned}
\tilde{d}^F &= \frac{-32(-964 - 1550 N_c + 2696 N_c^2 - 3610 N_c^3 + 411 N_c^4 + 1061 N_c^5)}{15(8 - 16 N_c^2 + 2 N_c^3 + 2 N_c^4 + N_c^5)}, \\
\tilde{d}_2^F &= \frac{32(1132 - 608 N_c - 2058 N_c^2 - 490 N_c^3 + 360 N_c^4 + 145 N_c^5)}{15(8 - 16 N_c^2 + 2 N_c^3 + 2 N_c^4 + N_c^5)}, \\
h &= \frac{-64(-98 - 158 N_c + 23 N_c^2 + 30 N_c^3)}{-14 - 14 N_c - 7 N_c^2 + 6 N_c^3}, \\
\tilde{h} &= -448.
\end{aligned} \tag{34}$$

This is a particularly nice solution because the second generation evanescent operators on the regular operator side for Q_S and \tilde{Q}_S have only one non-vanishing constant, \tilde{c}_2 . Moreover, this constant turns out to be N_c -independent. This is at the expense of the Fierz-transformed operators, which are significantly more complicated but for practical calculations not relevant since the Fierz-transformed basis is not used. The second generation evanescent operators for Q and \tilde{Q} have also been simplified by removing all ϵ^2 terms. A computer-readable file is provided for the specific choice given here, see Appendix D.

It is worth noting that the evanescent operators are now QCD-specific, i.e. they contain an explicit N_c dependence. This feature arises because we want the *renormalised* matrix elements to be invariant under a Fierz transformation, see condition 1.

For the matching calculation with the current-current operators of the $\Delta B = 1$ theory described in Section 2.7, evanescent operators of the second generation must be included in the matching to cancel IR poles and are renormalised at NNLO. For this purpose we do not need to specify the $\mathcal{O}(\epsilon)$ terms of evanescent operators of higher generations, but we need to define them with the correct vanishing ϵ -finite part. Therefore, we define the third generation as

$$\begin{aligned}
E_1^{(3)} &= 4(\bar{s}^c \gamma_{\mu_1} \gamma_{\mu_2} \gamma_{\mu_3} \gamma_{\mu_4} \gamma_{\mu_5} \gamma_{\mu_6} \gamma_{\mu_7} P_L b^d) (\bar{s}^d \gamma^{\mu_7} \gamma^{\mu_6} \gamma^{\mu_5} \gamma^{\mu_4} \gamma^{\mu_3} \gamma^{\mu_2} \gamma^{\mu_1} P_L b^c) \\
&\quad - (64 + \mathcal{O}(\epsilon)) \tilde{Q}, \\
E_2^{(3)} &= 4(\bar{s}^c \gamma_{\mu_1} \gamma_{\mu_2} \gamma_{\mu_3} \gamma_{\mu_4} \gamma_{\mu_5} \gamma_{\mu_6} \gamma_{\mu_7} P_L b^c) (\bar{s}^d \gamma^{\mu_7} \gamma^{\mu_6} \gamma^{\mu_5} \gamma^{\mu_4} \gamma^{\mu_3} \gamma^{\mu_2} \gamma^{\mu_1} P_L b^d) \\
&\quad - (64 + \mathcal{O}(\epsilon)) Q, \\
E^{(3)}[Q_S] &= 4(\bar{s}^c \gamma_{\mu_1} \gamma_{\mu_2} \gamma_{\mu_3} \gamma_{\mu_4} \gamma_{\mu_5} \gamma_{\mu_6} P_R b^c) (\bar{s}^d \gamma^{\mu_6} \gamma^{\mu_5} \gamma^{\mu_4} \gamma^{\mu_3} \gamma^{\mu_2} \gamma^{\mu_1} P_R b^d) \\
&\quad + (2048 + \mathcal{O}(\epsilon)) \tilde{Q}_S + \mathcal{O}(\epsilon) Q_S, \\
E^{(3)}[\tilde{Q}_S] &= 4(\bar{s}^c \gamma_{\mu_1} \gamma_{\mu_2} \gamma_{\mu_3} \gamma_{\mu_4} \gamma_{\mu_5} \gamma_{\mu_6} P_R b^d) (\bar{s}^d \gamma^{\mu_6} \gamma^{\mu_5} \gamma^{\mu_4} \gamma^{\mu_3} \gamma^{\mu_2} \gamma^{\mu_1} P_R b^c) \\
&\quad + (2048 + \mathcal{O}(\epsilon)) Q_S + \mathcal{O}(\epsilon) \tilde{Q}_S,
\end{aligned} \tag{35}$$

and the fourth generation as

$$\begin{aligned}
E_1^{(4)} &= 4(\bar{s}^c \gamma_{\mu_1} \gamma_{\mu_2} \gamma_{\mu_3} \gamma_{\mu_4} \gamma_{\mu_5} \gamma_{\mu_6} \gamma_{\mu_7} \gamma_{\mu_8} \gamma_{\mu_9} P_L b^d) (\bar{s}^d \gamma^{\mu_9} \gamma^{\mu_8} \gamma^{\mu_7} \gamma^{\mu_6} \gamma^{\mu_5} \gamma^{\mu_4} \gamma^{\mu_3} \gamma^{\mu_2} \gamma^{\mu_1} P_L b^c) \\
&\quad - (256 + \mathcal{O}(\epsilon)) \tilde{Q}, \\
E_2^{(4)} &= 4(\bar{s}^c \gamma_{\mu_1} \gamma_{\mu_2} \gamma_{\mu_3} \gamma_{\mu_4} \gamma_{\mu_5} \gamma_{\mu_6} \gamma_{\mu_7} \gamma_{\mu_8} \gamma_{\mu_9} P_L b^c) (\bar{s}^d \gamma^{\mu_9} \gamma^{\mu_8} \gamma^{\mu_7} \gamma^{\mu_6} \gamma^{\mu_5} \gamma^{\mu_4} \gamma^{\mu_3} \gamma^{\mu_2} \gamma^{\mu_1} P_L b^d)
\end{aligned}$$

$$\begin{aligned}
& - (256 + \mathcal{O}(\epsilon)) Q, \\
E^{(4)}[Q_S] &= 4(\bar{s}^c \gamma_{\mu_1} \gamma_{\mu_2} \gamma_{\mu_3} \gamma_{\mu_4} \gamma_{\mu_5} \gamma_{\mu_6} \gamma_{\mu_7} \gamma_{\mu_8} P_R b^c) (\bar{s}^d \gamma^{\mu_8} \gamma^{\mu_7} \gamma^{\mu_6} \gamma^{\mu_5} \gamma^{\mu_4} \gamma^{\mu_3} \gamma^{\mu_2} \gamma^{\mu_1} P_R b^d) \\
& + (32768 + \mathcal{O}(\epsilon)) \tilde{Q}_S + \mathcal{O}(\epsilon) Q_S, \\
E^{(4)}[\tilde{Q}_S] &= 4(\bar{s}^c \gamma_{\mu_1} \gamma_{\mu_2} \gamma_{\mu_3} \gamma_{\mu_4} \gamma_{\mu_5} \gamma_{\mu_6} \gamma_{\mu_7} \gamma_{\mu_8} P_R b^d) (\bar{s}^d \gamma^{\mu_8} \gamma^{\mu_7} \gamma^{\mu_6} \gamma^{\mu_5} \gamma^{\mu_4} \gamma^{\mu_3} \gamma^{\mu_2} \gamma^{\mu_1} P_R b^c) \\
& + (32768 + \mathcal{O}(\epsilon)) Q_S + \mathcal{O}(\epsilon) \tilde{Q}_S.
\end{aligned} \tag{36}$$

The $\mathcal{O}(\epsilon)$ terms can be kept as arbitrary constants, and it can be checked that they drop out of the physical matching coefficients at the end.

2.4 Renormalisation of the effective $\Delta B = 2$ theory

In the following we describe the generic renormalisation procedure for the effective $\Delta B = 2$ theory. We choose to renormalise the matching coefficients,

$$(\vec{C}^{\text{bare}}, \vec{C}_E^{\text{bare}}) = (\vec{C}^{\text{ren}}, \vec{C}_E^{\text{ren}}) Z \equiv (\vec{C}^{\text{ren}}, \vec{C}_E^{\text{ren}}) \begin{pmatrix} Z_{QQ} & Z_{QE} \\ Z_{EQ} & Z_{EE} \end{pmatrix}, \tag{37}$$

where the sub-matrices Z_{XY} with $XY \in \{QQ, EE\}$ of the matrix Z are understood to be an expansion in α_s , i.e.

$$(Z_{XY})_{ij} = \delta_{ij} + \frac{\alpha_s}{4\pi} \frac{1}{\epsilon} \left(Z_{XY}^{(1,1)} \right)_{ij} + \mathcal{O}(\alpha_s^2), \tag{38}$$

and for the QE part

$$(Z_{QE})_{ij} = \frac{\alpha_s}{4\pi} \frac{1}{\epsilon} \left(Z_{QE}^{(1,1)} \right)_{ij} + \mathcal{O}(\alpha_s^2). \tag{39}$$

The sub-matrix Z_{EQ} is special because it introduces *finite* counterterms [3, 25]:

$$(Z_{EQ})_{ij} = \frac{\alpha_s}{4\pi} \left(Z_{EQ}^{(1,0)} \right)_{ij} + \mathcal{O}(\alpha_s^2). \tag{40}$$

Note, however, that the α_s^2 terms may contain both ϵ^0 and $1/\epsilon$ terms.

To illustrate the meaning of the submatrices in Eq. (37) we consider Z_{QE} , which describes those counterterms to physical operators which are proportional to evanescent operators. When one assigns the counterterms to the Wilson coefficients instead of the operators, Z_{QE} involves a contribution to C_E^i which is proportional to $\frac{\alpha_s}{\epsilon} C^j$. The other submatrices correspond to the mixings among other subsets of operators. For our calculation we need Z_{XY} to two-loop order. One-loop results can be found in Ref. [16] and two-loop terms are presented in Appendix A. The renormalisation of the operator R_0 is also needed and is discussed in Section 2.5.

2.5 Renormalisation of the physical operators with a power-suppressed R_0

A proper treatment of the $\mathcal{O}(1/m_b)$ suppression of $\langle B_s | R_0 | \bar{B}_s \rangle$ requires a discussion of its renormalisation. The operator renormalisation involves three physical operators, which one can choose as $\{Q, \tilde{Q}_S, Q_S\}$ or $\{Q, \tilde{Q}_S, R_0\}$ because the renormalisation procedure is process-independent and the structure of the UV divergences is insensitive to the power suppression of $\langle B_s | R_0 | \bar{B}_s \rangle$. This power-suppression is a feature of the particular physical processes studied by us and calls for a finite counterterm.

The starting point of our discussion is the basis of physical operators $\{Q, \tilde{Q}_S, Q_S\}$, which is convenient because \tilde{Q}_S and Q_S do not mix with Q under renormalisation, meaning that their renormalisation constant is a 2×2 matrix. As described in Section 2.2 we will later trade Q_S for R_0 , which results in a 3×3 renormalisation matrix for Q, \tilde{Q}_S and R_0 . However, this does not simplify our calculation since we cannot discard R_0 at this point. This is because renormalisation belongs to the *off-shell* structure of our effective field theory while the power-suppression of $\langle B_s | R_0 | \bar{B}_s \rangle$ is an *on-shell* phenomenon.

The $\overline{\text{MS}}$ renormalised physical operators $\{Q, \tilde{Q}_S, Q_S\}$ are

$$Q = Z_Q Q^{\text{bare}} + \text{ev.}, \quad \begin{pmatrix} Q_S \\ \tilde{Q}_S \end{pmatrix} = Z_{Q_S \tilde{Q}_S} \begin{pmatrix} Q_S^{\text{bare}} \\ \tilde{Q}_S^{\text{bare}} \end{pmatrix} + \text{ev.}, \quad (41)$$

where we have suppressed the mixing with evanescent operators, which are discussed in Section 2.3. We implement the $\overline{\text{MS}}$ scheme by choosing $g^{\text{bare}} = \bar{\mu}^\epsilon Z_g g$ with $\bar{\mu}^2 = \mu^2 e^{-\gamma_E} / (4\pi)$, such that the renormalisation constants only involve poles. All fields in the operators are understood as bare, so the quark fields are renormalised separately.

We expand all renormalisation constants as

$$Z = 1 + \frac{\alpha_s}{4\pi} \left[\frac{Z^{(11)}}{\epsilon} + Z^{(10)} \right] + \left(\frac{\alpha_s}{4\pi} \right)^2 \left[\frac{Z^{(22)}}{\epsilon^2} + \frac{Z^{(21)}}{\epsilon} + Z^{(20)} \right].$$

For the $\overline{\text{MS}}$ constants in Eq. (41) one finds

$$\begin{aligned} Z_Q^{(11)} &= 2, & Z_Q^{(22)} &= -9 + \frac{2}{3}N_f, & Z_Q^{(21)} &= -\frac{45815}{516} + \frac{1}{9}N_f, \\ Z_{Q_S \tilde{Q}_S}^{(11)} &= \begin{pmatrix} -\frac{14}{3} & \frac{2}{3} \\ \frac{8}{3} & \frac{16}{3} \end{pmatrix}, & Z_{Q_S \tilde{Q}_S}^{(22)} &= \begin{pmatrix} \frac{337}{9} - \frac{14N_f}{9} & -\frac{31}{9} + \frac{2N_f}{9} \\ -\frac{124}{9} + \frac{8N_f}{9} & -\frac{128}{9} + \frac{16N_f}{9} \end{pmatrix}, \\ Z_{Q_S \tilde{Q}_S}^{(21)} &= \begin{pmatrix} \frac{547}{9} + \frac{22N_f}{27} & -\frac{227}{9} + \frac{2N_f}{27} \\ \frac{1235}{6} - \frac{19N_f}{27} & \frac{641}{18} - \frac{83N_f}{27} \end{pmatrix}, \end{aligned} \quad (42)$$

with the finite constants $Z^{(j0)}$ vanishing. Note that the $Z^{(21)}$ terms depend on the choice of the evanescent operators. Here we show the results in the basis as specified in Eqs. (31) to (34) and for $N_c = 3$.

It is possible to switch to the basis $\{Q, \tilde{Q}_S, R_0, E\}$, where E stands for the evanescent operators. This basis leads to the renormalisation matrix Z :

$$\begin{pmatrix} Q \\ \tilde{Q}_S \\ R_0 \\ E \end{pmatrix} = Z \begin{pmatrix} Q^{\text{bare}} \\ \tilde{Q}_S^{\text{bare}} \\ R_0^{\text{bare}} \\ E^{\text{bare}} \end{pmatrix}. \quad (43)$$

The results from the $\overline{\text{MS}}$ scheme for the $\{Q, \tilde{Q}_S, Q_S, E\}$ basis can be naively transformed to the $\{Q, \tilde{Q}_S, R_0, E\}$ basis by equating the renormalised matrix elements,

$$\begin{pmatrix} Q \\ \tilde{Q}_S \\ \frac{1}{2}Q + \tilde{Q}_S + Q_S \\ E \end{pmatrix}_{\{Q, Q_S, \tilde{Q}_S\}} = \begin{pmatrix} Q \\ \tilde{Q}_S \\ R_0 \\ E \end{pmatrix}_{\{Q, \tilde{Q}_S, R_0\}}^{\text{naive}}, \quad (44)$$

where Eqs. (41) and (43) are used to renormalise the left-hand side and right-hand side, respectively. The bare matrix elements of the two bases are related by Eq. (18). This transformation yields the “naive” renormalisation matrix of the $\{Q, \tilde{Q}_S, R_0, E\}$ basis,

$$Z^{\text{naive}} = (Z_1^{\text{naive}}, Z_2^{\text{naive}}, Z_3^{\text{naive}}, Z_4^{\text{naive}}), \quad (45)$$

where

$$\begin{aligned} Z_1^{\text{naive}} &= \begin{pmatrix} Z_Q \\ -\frac{1}{2} \left(Z_{Q_S \tilde{Q}_S} \right)_{21} \\ \frac{1}{2} \left(Z_Q - \left(Z_{Q_S \tilde{Q}_S} \right)_{11} - \left(Z_{Q_S \tilde{Q}_S} \right)_{21} \right) \\ Z_{EQ} - \frac{1}{2} Z_{EQ_S} \end{pmatrix}, \\ Z_2^{\text{naive}} &= \begin{pmatrix} 0 \\ - \left(Z_{Q_S \tilde{Q}_S} \right)_{21} + \left(Z_{Q_S \tilde{Q}_S} \right)_{22} \\ - \left(Z_{Q_S \tilde{Q}_S} \right)_{11} + \left(Z_{Q_S \tilde{Q}_S} \right)_{12} - \left(Z_{Q_S \tilde{Q}_S} \right)_{21} + \left(Z_{Q_S \tilde{Q}_S} \right)_{22} \\ Z_{E\tilde{Q}_S} - Z_{EQ_S} \end{pmatrix}, \\ Z_3^{\text{naive}} &= \begin{pmatrix} 0 \\ \left(Z_{Q_S \tilde{Q}_S} \right)_{21} \\ \left(Z_{Q_S \tilde{Q}_S} \right)_{11} + \left(Z_{Q_S \tilde{Q}_S} \right)_{21} \\ Z_{EQ_S} \end{pmatrix}, \end{aligned}$$

$$Z_4^{\text{naive}} = \begin{pmatrix} Z_{QE} \\ Z_{\tilde{Q}_S E} \\ \frac{1}{2}Z_{QE} + Z_{Q_S E} + Z_{\tilde{Q}_S E} \\ Z_{EE} \end{pmatrix}. \quad (46)$$

Beyond tree-level, however, the matrix element of R_0 is not suppressed by $1/m_b$ and one must add a finite renormalisation to R_0 , which is not captured by Eq. (46) [11]. This feature stems from the fact that the $\overline{\text{MS}}$ renormalised $\langle R_0 \rangle$ involves terms proportional to $\langle Q \rangle^{(0)}$ and $\langle \tilde{Q}_S \rangle^{(0)}$ in the operator basis $\{Q, \tilde{Q}_S, R_0\}$. Moreover, R_0 has an unsuppressed evanescent part which enters the calculation whenever IR singularities are regularised dimensionally, i.e. when matching calculations are performed for $D \neq 4$. This requires us to renormalise the evanescent part of R_0 in the same way as other evanescent operators [16].

To visualise how the finite renormalisation constants arise, it is instructive to consider the renormalised matrix element of R_0 as a linear combination of the renormalised Q , \tilde{Q}_S and Q_S matrix elements,

$$\langle R_0 \rangle = \frac{1}{2}\alpha_1 \langle Q \rangle + \alpha_2 \langle \tilde{Q}_S \rangle + \langle Q_S \rangle, \quad (47)$$

which we require to be $1/m_b$ -suppressed. Here and in the following we use the shorthand notation $\langle O \rangle$ to denote $\langle B_s | O | \bar{B}_s \rangle$. The constants α_1 and α_2 have an expansion in α_s ,

$$\alpha_i = 1 + \frac{\alpha_s}{4\pi}\alpha_i^{(1)} + \left(\frac{\alpha_s}{4\pi}\right)^2 \alpha_i^{(2)} + \mathcal{O}(\alpha_s^3). \quad (48)$$

The coefficient of one of the operators, which we choose to be Q_S , can be set to one. This corresponds to a perturbative redefinition of the evanescent part of R_0 . We discuss the calculation of $\alpha_{1,2}$ in detail in Section 2.6.

The $\alpha_i^{(j)}$ constants are UV-finite quantities and will appear as finite pieces in the renormalisation constants for R_0 . The true renormalisation matrix in the $\{Q, \tilde{Q}_S, R_0\}$ basis is obtained in the same way as the naive renormalisation matrix except that Eq. (44) is modified to read

$$\begin{pmatrix} Q \\ \tilde{Q}_S \\ \frac{1}{2}\alpha_1 Q + \alpha_2 \tilde{Q}_S + Q_S \\ E \end{pmatrix}_{\{Q, Q_S, \tilde{Q}_S\}} = \begin{pmatrix} Q \\ \tilde{Q}_S \\ R_0 \\ E \end{pmatrix}_{\{Q, \tilde{Q}_S, R_0\}}, \quad (49)$$

This leads to the correct renormalisation matrix

$$Z = (Z_1, Z_2, Z_3, Z_4), \quad (50)$$

where

$$\begin{aligned}
Z_1 &= \begin{pmatrix} Z_Q \\ -\frac{1}{2} \left(Z_{Q_S \tilde{Q}_S} \right)_{21} \\ \frac{1}{2} \left(\alpha_1 Z_Q - \left(Z_{Q_S \tilde{Q}_S} \right)_{11} - \alpha_2 \left(Z_{Q_S \tilde{Q}_S} \right)_{21} \right) \\ Z_{EQ} - \frac{1}{2} Z_{EQ_S} \end{pmatrix}, \\
Z_2 &= \begin{pmatrix} 0 \\ - \left(Z_{Q_S \tilde{Q}_S} \right)_{21} + \left(Z_{Q_S \tilde{Q}_S} \right)_{22} \\ - \left(Z_{Q_S \tilde{Q}_S} \right)_{11} + \left(Z_{Q_S \tilde{Q}_S} \right)_{12} - \alpha_2 \left(Z_{Q_S \tilde{Q}_S} \right)_{21} + \alpha_2 \left(Z_{Q_S \tilde{Q}_S} \right)_{22} \\ Z_{E\tilde{Q}_S} - Z_{EQ_S} \end{pmatrix}, \\
Z_3 &= \begin{pmatrix} 0 \\ \left(Z_{Q_S \tilde{Q}_S} \right)_{21} \\ \left(Z_{Q_S \tilde{Q}_S} \right)_{11} + \alpha_2 \left(Z_{Q_S \tilde{Q}_S} \right)_{21} \\ Z_{EQ_S} \end{pmatrix}, \\
Z_4 &= \begin{pmatrix} Z_{QE} \\ Z_{\tilde{Q}_SE} \\ \frac{1}{2} \alpha_1 Z_{QE} + Z_{Q_SE} + \alpha_2 Z_{\tilde{Q}_SE} \\ Z_{EE} \end{pmatrix}. \tag{51}
\end{aligned}$$

Here it becomes apparent that the coefficients α_1 and α_2 induce ϵ -finite renormalisation constants because they multiply the diagonal elements Z_Q and $(Z_{Q_S \tilde{Q}_S})_{22}$ whose leading term is one.

2.6 Determination of the finite renormalisation constants for R_0

The one-loop corrections $\alpha_1^{(1)}$ and $\alpha_2^{(1)}$ in Eq. (48) have been computed in Ref. [11] and the two-loop fermionic corrections in [17]. In the following we describe our calculation of the two-loop terms $\alpha_1^{(2)}$ and $\alpha_2^{(2)}$.

For the calculation of α_1 and α_2 it is important to distinguish UV and IR divergences since otherwise R_0 is accompanied by an unphysical evanescent operator that is not suppressed by $1/m_b$ [16]. In the matching calculation we want to use R_0 from Eq. (18) where α_1 and α_2 encode a finite UV renormalisation which guarantees the $1/m_b$ suppression of $\langle R_0 \rangle$. For this purpose we have to compute the operator matrix elements $\langle Q \rangle$, $\langle Q_S \rangle$ and $\langle \tilde{Q}_S \rangle$ up to two loops. Sample Feynman diagrams are shown in Fig. 2.

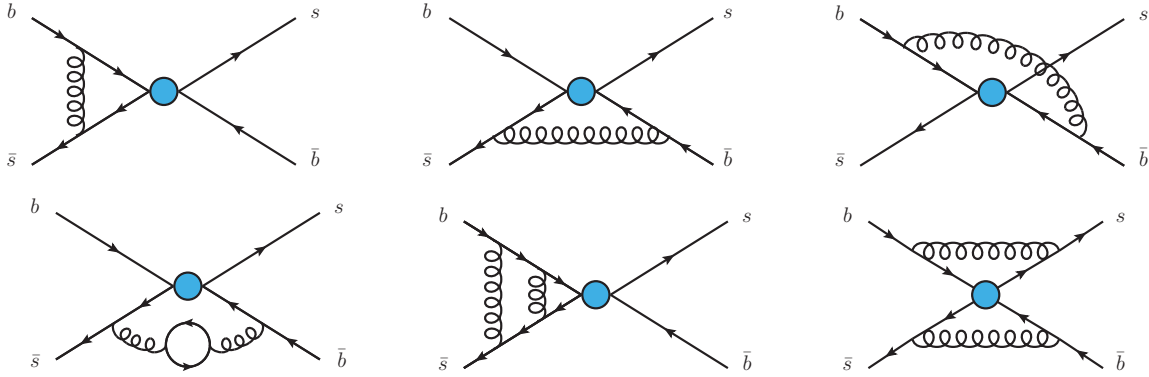


Figure 2: One- and two-loop Feynman diagrams needed for the calculation of α_1 and α_2 . The blob stands for the insertion of one of the operators Q , Q_S or \tilde{Q}_S .

For our calculation we use Feynman gauge and we isolate the UV divergences by introducing a gluon mass m_g in a minimal way into the gluon and ghost propagators via

$$\begin{aligned} \frac{i\delta^{ab}}{-p^2} \left(g^{\mu\nu} + \xi \frac{p^\mu p^\nu}{-p^2} \right) &\rightarrow \frac{i\delta^{ab}}{m_g^2 - p^2} \left(g^{\mu\nu} + \xi \frac{p^\mu p^\nu}{m_g^2 - p^2} \right), \\ \frac{i\delta^{ab}}{-p^2} &\rightarrow \frac{i\delta^{ab}}{m_g^2 - p^2}, \end{aligned} \quad (52)$$

where a and b are colour indices. Note that we have to consider the gluon propagator with a general gauge parameter ξ since we have to renormalise ξ . Our final results for α_1 and α_2 do not depend on the gauge parameter.

The calculation of the diagrams proceeds as described in Section 3. The charm quark appears in diagrams with a closed quark loop insertion into the gluon propagator, cf. Fig. 2. The charm-dependent contributions are taken from Ref. [17]. When preparing the amplitude, we expand in m_g in those contributions where no IR divergences are introduced. In the remaining parts we keep the gluon mass, also during reduction to the master integrals.

The matrix elements for Q , Q_S or \tilde{Q}_S are expressed in terms of the 23 master integrals shown in Fig. 3. Note that some of them have positive powers of m_g ; for example, the second diagram in the top row scales as m_g^4 . However, they may be multiplied with $1/m_g$ poles up to order six, which requires a careful expansion in m_g such that only in the final expression for the amplitude positive m_g terms are set to zero.

For the expansion of the master integrals we apply an asymptotic expansion (see, e.g. Ref. [28]) for $m_g \ll m_b$. In our case this means that all components of each loop momentum can either be soft (i.e., of order m_g) or hard (i.e., of order m_b), which splits each two-loop integral into several regions. Depending on the routing there is also the possibility that the sum or difference of the loop momenta is soft whereas the individual momenta are hard. For illustration we describe the procedure in detail for the second

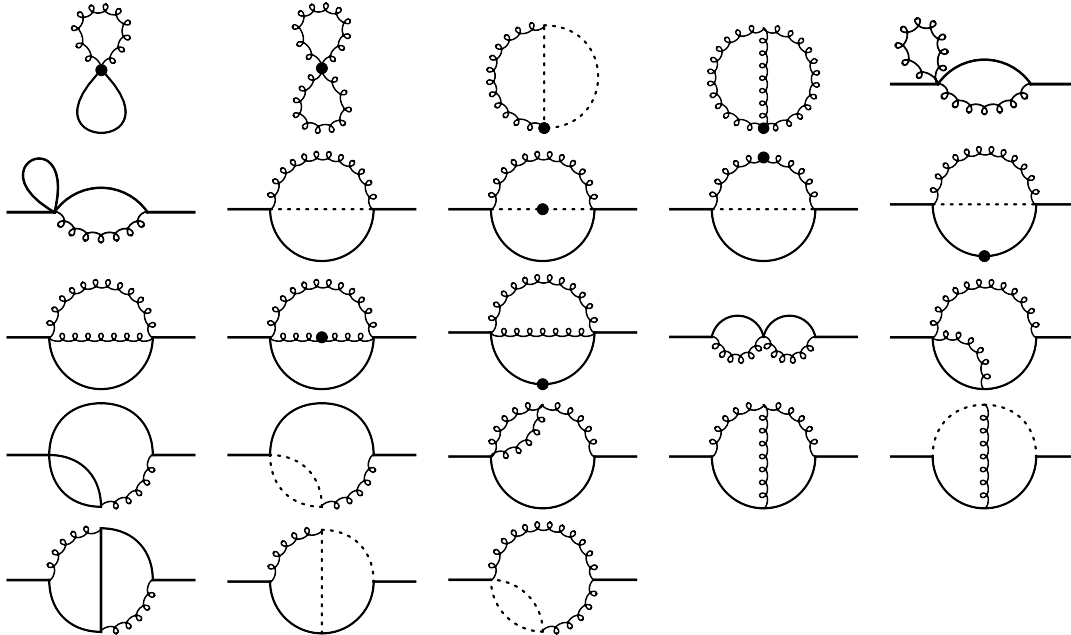


Figure 3: Two-loop master integrals where all lines represent scalar propagators. Solid and curly lines carry mass m_b and m_g , respectively. Dotted lines are massless. A dot on a line means that the corresponding propagator is squared.

master integral in the bottom row of Fig. 3, which has the following integrand

$$\frac{1}{(m_g^2 - p_1^2)(-p_1^2 - 2q \cdot p_1)(-p_2^2)(-p_2^2 - 2q \cdot p_2)(-(p_1 - p_2)^2)}, \quad (53)$$

with $q^2 = m_b^2$. Here we have to consider four regions. In case both loop momenta are hard we can perform a Taylor expansion of the first propagator in m_g and thus m_g disappears from the integrand. The resulting on-shell integral is well-known in the literature (see, e.g. Ref. [29]). Similarly, if both loop momenta are soft, the second and fourth propagators are expanded in p_1^2 and p_2^2 , respectively. With the proper choice of reference system a factor $1/m_b^2$ can be factored out and only a one-scale integral remains. In case one of the momenta is soft and the other is hard the two-loop integral factorises into two one-loop integrals which can be solved in a straightforward way.

For the operator matrix elements we have to perform the standard UV renormalisation for α_s and the external quark fields in the $\overline{\text{MS}}$ scheme and for the bottom quark mass in the on-shell scheme. Note that in principle a non-zero gluon mass can also be introduced in these constants. However, it only provides positive powers of m_g to α_1 and α_2 . Furthermore, the usual renormalisation constants for operator mixing have to be taken into account. As a consequence also evanescent operators enter the tree-level and one-loop matrix elements. As a non-standard counterterm we have to introduce a renormalisation constant for the gluon mass. It is determined from the requirement that the renormalised gluon propagator is transverse. Note that in intermediate steps the renormalisation constants for the gluon

wave function and the QCD gauge parameter are needed, too. Here it is possible to use the usual one-loop expressions in the $\overline{\text{MS}}$ scheme.

After renormalisation we obtain finite results for the operator matrix elements Q , Q_S and \tilde{Q}_S up to two loops. Note, however, that they still have a logarithmic dependence on m_g . After extracting α_1 and α_2 from the requirement that $\langle R_0 \rangle$ in Eq. (47) is $\mathcal{O}(1/m_b)$ the $\log(m_g)$ terms cancel since $\langle R_0 \rangle$ is IR finite. Of course, also α_1 and α_2 are IR finite. They are given by

$$\begin{aligned}
\alpha_1^{(1)} &= \frac{26}{3} + 8l_b, \\
\alpha_1^{(2)} &= \frac{904309}{3096} + \frac{17\pi^2}{3} + \frac{16\pi^2 \log(2)}{3} - 8\zeta(3) + \frac{649}{3}l_b + \frac{232}{3}l_b^2 \\
&\quad + N_L \left[-\frac{218}{27} - \frac{8\pi^2}{9} - \frac{104}{9}l_b - \frac{16}{3}l_b^2 \right] \\
&\quad + N_H \left[-\frac{434}{27} + \frac{16\pi^2}{9} - \frac{104}{9}l_b - \frac{16}{3}l_b^2 \right] \\
&\quad + N_V \left[-\frac{218}{27} - \frac{8\pi^2}{9} + \frac{8\pi^2\sqrt{z}}{3} - 16z + \frac{8\pi^2 z^{3/2}}{3} - \frac{302z^2}{27} - \frac{8\pi^2 z^2}{9} + \frac{304z^3}{225} \right. \\
&\quad + \frac{463z^4}{4900} + \frac{7976z^5}{297675} + \frac{1229z^6}{117612} - \frac{104}{9}l_b - \frac{16}{3}l_b^2 \\
&\quad \left. + \left(\frac{52z^2}{9} - \frac{32z^3}{45} - \frac{3z^4}{35} - \frac{32z^5}{945} - \frac{5z^6}{297} \right) \log(z) - \frac{4z^2}{3} \log^2(z) + \mathcal{O}(z^7) \right], \\
\alpha_2^{(1)} &= 8 + 16l_b, \\
\alpha_2^{(2)} &= \frac{3944}{9} + \frac{320\pi^2}{27} + 440l_b + \frac{752}{3}l_b^2 + \frac{32\pi^2 \log(2)}{3} - 16\zeta(3) \\
&\quad + N_L \left[-\frac{422}{27} - \frac{16\pi^2}{9} - \frac{208l_b}{9} - \frac{32}{3}l_b^2 \right] \\
&\quad + N_H \left[-\frac{854}{27} + \frac{32\pi^2}{9} - \frac{208}{9}l_b - \frac{32}{3}l_b^2 \right] \\
&\quad + N_V \left[-\frac{422}{27} - \frac{16\pi^2}{9} + \frac{16\pi^2\sqrt{z}}{3} - 32z + \frac{16\pi^2 z^{3/2}}{3} - \frac{604z^2}{27} - \frac{16\pi^2 z^2}{9} + \frac{608z^3}{225} \right. \\
&\quad + \frac{463z^4}{1225} + \frac{31904z^5}{297675} + \frac{1229z^6}{29403} - \frac{208}{9}l_b - \frac{32}{3}l_b^2 \\
&\quad \left. + \left(\frac{104z^2}{9} - \frac{64z^3}{45} - \frac{12z^4}{35} - \frac{128z^5}{945} - \frac{20z^6}{297} \right) \log(z) - \frac{8z^2}{3} \log^2(z) + \mathcal{O}(z^7) \right], \quad (54)
\end{aligned}$$

where $l_b = \log(\mu/m_b)$, N_L , N_H and N_V are the number of light (up, down, strange), bottom and charm quark flavours. N_c has been set to three. Note that the specific choice of $\mathcal{O}(\epsilon)$ coefficients given in Eq. (26) and Eqs. (31) to (34) has been used to simplify the expressions.

The terms of order α_s and the massless fermionic α_s^2 terms agree with Refs. [11] and [17],

respectively. All other terms are new. We also quote the higher order $z = m_c^2/m_b^2$ terms of the $\alpha_{1,2}^{(2)}$ constants, which stem from closed charm loops and have been calculated in Ref. [17].² For phenomenological applications the expansion to z^6 is sufficient as the relative contribution of the highest order term to $\alpha_{1,2}^{(2)}$ is smaller than 10^{-6} .

Let us remark that there are multiple possibilities to introduce the gluon mass. In our calculation we tested several approaches. For example, it is possible to omit m_g in the ξ -dependent term of the gluon propagator in Eq. (52) or to leave the ghost propagator massless. The various options require different expressions for Z_{m_g} and also lead to different results for the renormalised matrix elements for Q , Q_S and \tilde{Q}_S . However, in each case we obtain the same results for α_1 and α_2 .

2.7 Matching of $\Delta B = 1$ and $\Delta B = 2$ theory

We now switch back to the general case of $B_q - \bar{B}_q$ mixing with $q = d$ or s , because there are qualitative differences between the two systems, since the numerical suppression of the CKM sub-leading terms involving λ_u^q is much milder for $q = d$ than for $q = s$.

The off-diagonal element of the decay matrix can be written as [11]

$$\begin{aligned}\Gamma_{12}^q &= -(\lambda_c^q)^2 \Gamma_{12}^{cc} - 2\lambda_c^q \lambda_u^q \Gamma_{12}^{uc} - (\lambda_u^q)^2 \Gamma_{12}^{uu} \\ &= -(\lambda_t^q)^2 \left[\Gamma_{12}^{cc} + 2\frac{\lambda_u^q}{\lambda_t^q} (\Gamma_{12}^{cc} - \Gamma_{12}^{uc}) + \left(\frac{\lambda_u^q}{\lambda_t^q}\right)^2 (\Gamma_{12}^{uu} + \Gamma_{12}^{cc} - 2\Gamma_{12}^{uc}) \right],\end{aligned}\quad (55)$$

where for the sake of clarity, we omit the superscript q in the quantity Γ_{12}^{ab} . To obtain Γ_{12}^q , we calculate the absorptive part of a bi-local matrix element containing a time-ordered product of two $|\Delta B| = 1$ effective Hamiltonians. This yields

$$\Gamma_{12}^{ab} = \frac{G_F^2 m_b^2}{24\pi M_{B_q}} \left[H^{ab}(z) \langle B_q | Q | \bar{B}_q \rangle + \tilde{H}_S^{ab}(z) \langle B_q | \tilde{Q}_S | \bar{B}_q \rangle \right] + \mathcal{O}(\Lambda_{\text{QCD}}/m_b), \quad (56)$$

with $z = m_c^2/m_b^2$. It is worth highlighting again that R_0 does not appear because its matrix element is $1/m_b$ -suppressed in four dimensions thanks to the finite renormalisation outlined in Section 2.5.

In our phenomenological analysis we include in the matching coefficients $H^{ab}(z)$ and $\tilde{H}_S^{ab}(z)$ the LO and NLO corrections from current-current and penguin operators. Results for the former are exact in z and taken from Ref. [11]. The penguin contributions are expanded up to the linear term in z and can be found in Refs. [15, 16]. At NNLO our new contributions for the current-current operators Q_1 and Q_2 are included. For convenience of the reader we provide computer-readable results for the current-current contribution up to z^{10} on the website [30], where the specific choice of $\mathcal{O}(\epsilon)$ coefficients

²The original publication only contains terms up to z^3 . The higher order terms up to z^6 quoted here have been kindly provided to us by one of the authors, Artyom Hovhannisyan.

given in Eq. (26) and Eqs. (31) to (34) has been used to simplify the expressions. Our analysis also contains (in z expanded) NNLO and N³LO contributions involving the chromomagnetic operator (usually denoted by Q_8) [16]. Note that they are numerically tiny. For the $1/m_b$ suppressed terms see Refs. [10, 14].

Writing the amplitude \mathcal{M} of the $\bar{B}_q \rightarrow B_q$ transition calculated in the $\Delta B = 1$ theory as

$$\mathcal{M} = -(\lambda_c^q)^2 \mathcal{M}^{cc} - 2\lambda_c^q \lambda_u^q \mathcal{M}^{uc} - (\lambda_u^q)^2 \mathcal{M}^{uu}, \quad (57)$$

we obtain the matching condition [31]

$$\Gamma_{12}^{ab} = \frac{1}{M_{B_q}} \text{Im} \mathcal{M}^{ab}. \quad (58)$$

Since both the amplitude \mathcal{M} and the matrix elements of the local $\Delta B = 2$ transition operators have IR poles beyond LO, lower-order matching calculations need to be carried out beyond the finite ϵ^0 order. The two key issues here are the order in ϵ to which the amplitudes need to be evaluated as well as the generation of evanescent operators to be included in the local $\Delta B = 2$ matrix element. The order in ϵ is directly determined by the power of the IR poles, whereas the generations of evanescent operators on the $\Delta B = 2$ side follow the tree-level matrix elements of evanescent operators that appear on the $\Delta B = 1$ side. In the following we illustrate these two issues with a concrete matching calculation.

To obtain finite NNLO matching coefficients of the physical operators, the LO and NLO amplitudes need to be calculated to $\mathcal{O}(\epsilon^2)$ and $\mathcal{O}(\epsilon^1)$, respectively. This can be seen by expanding both sides of Eq. (58) in α_s and ϵ . We can consider the matching equation order by order by expanding the matching coefficients in α_s ,

$$H^{ab} = H^{(0),ab} + \frac{\alpha_s}{4\pi} H^{(1),ab} + \left(\frac{\alpha_s}{4\pi}\right)^2 H^{(2),ab} + \mathcal{O}(\alpha_s^3), \quad (59)$$

and defining analogous expansions for Γ_{12}^{ab} , \mathcal{M}^{ab} and the renormalised matrix elements $\langle O \rangle = \langle B | O | \bar{B} \rangle$. At LO we have

$$(\Gamma_{12}^{ab})^{(0)} = \frac{G_F^2 m_b^2}{24\pi M_{B_q}} \left[H_P^{(0),ab} \langle P \rangle^{(0)} + H_E^{(0),ab} \langle E \rangle^{(0)} \right]. \quad (60)$$

The operators P and E schematically stand for any physical and evanescent operator, respectively. To be explicit, the physical operators we choose are $\{Q, \tilde{Q}_S\}$ and the evanescent operators include R_0 in addition to the operators defined in Section 2.3. This is because after introducing finite renormalisation constants for R_0 , its matrix element vanishes in four dimensions, while in D dimensions $\langle R_0 \rangle$ possesses a power-unsuppressed evanescent piece [16].

On the $\Delta B = 1$ side, the LO amplitude is

$$\text{Im}(\mathcal{M}^{ab})^{(0)} = \frac{G_F^2 m_b^2}{24\pi} \left[(a^{(0,0)} + \epsilon a^{(0,1)} + \epsilon^2 a^{(0,2)} + \mathcal{O}(\epsilon^3)) \langle P \rangle^{(0)} \right]$$

$$+ (b^{(0,0)} + \epsilon b^{(0,1)} + \epsilon^2 b^{(0,2)} + \mathcal{O}(\epsilon^3)) \langle E \rangle^{(0)} \Big]. \quad (61)$$

Equating Eqs. (60) and (61), the LO matching coefficients can be read off,

$$\begin{aligned} H_P^{(0),ab} &= a^{(0,0)} + \epsilon a^{(0,1)} + \epsilon^2 a^{(0,2)} + \mathcal{O}(\epsilon^3), \\ H_E^{(0),ab} &= b^{(0,0)} + \epsilon b^{(0,1)} + \epsilon^2 b^{(0,2)} + \mathcal{O}(\epsilon^3). \end{aligned} \quad (62)$$

The procedure at NLO follows the same logic as the LO matching, but we encounter IR poles for the first time, which underlines the importance of keeping higher orders in ϵ . Starting on the $\Delta B = 2$ side, the first order correction is schematically

$$\begin{aligned} (\Gamma_{12}^{ab})^{(1)} &= \frac{G_F^2 m_b^2}{24\pi M_{B_q}} \left[H_P^{(0),ab} \langle P \rangle^{(1)} + H_P^{(1),ab} \langle P \rangle^{(0)} \right. \\ &\quad \left. + H_E^{(0),ab} \langle E \rangle^{(1)} + H_E^{(1),ab} \langle E \rangle^{(0)} \right]. \end{aligned} \quad (63)$$

The matrix elements can be written as a series in ϵ ,

$$\begin{aligned} \langle P \rangle^{(1)} &= \left(\frac{c^{(1,-1)}}{\epsilon} + c^{(1,0)} + \epsilon c^{(1,1)} \right) \langle P \rangle^{(0)} + \left(\frac{d^{(1,-1)}}{\epsilon} + d^{(1,0)} + \epsilon d^{(1,1)} \right) \langle E \rangle^{(0)}, \\ \langle E \rangle^{(1)} &= \left(e^{(1,0)} + \epsilon e^{(1,1)} \right) \langle P \rangle^{(0)} + \left(\frac{f^{(1,-1)}}{\epsilon} + f^{(1,0)} + \epsilon f^{(1,1)} \right) \langle E \rangle^{(0)}, \end{aligned} \quad (64)$$

where it is worth noting that the renormalised evanescent matrix elements are one order higher in ϵ than the renormalised physical operator matrix elements and hence do not have poles in front of $\langle P \rangle^{(0)}$. On the $\Delta B = 1$ side, the NLO amplitude is parametrised as

$$\begin{aligned} \text{Im}(\mathcal{M}^{ab})^{(1)} &= \frac{G_F^2 m_b^2}{24\pi} \left[\left(\frac{a^{(1,-1)}}{\epsilon} + a^{(1,0)} + \epsilon a^{(1,1)} + \mathcal{O}(\epsilon^2) \right) \langle P \rangle^{(0)} \right. \\ &\quad \left. + \left(\frac{b^{(1,-1)}}{\epsilon} + b^{(1,0)} + \epsilon b^{(1,1)} + \mathcal{O}(\epsilon^2) \right) \langle E \rangle^{(0)} \right]. \end{aligned} \quad (65)$$

Thus by inserting Eq. (64) into Eq. (63) and then equating with Eq. (65), the NLO matching coefficients can be extracted and read

$$\begin{aligned} H_P^{(1),ab} &= \frac{a^{(1,-1)}}{\epsilon} + a^{(1,0)} + \epsilon a^{(1,1)} - \left(\frac{c^{(1,-1)}}{\epsilon} + c^{(1,0)} + \epsilon c^{(1,1)} \right) H_P^{(0),ab} \\ &\quad - (e^{(1,0)} + \epsilon e^{(1,1)}) H_E^{(0),ab} + \mathcal{O}(\epsilon^2), \\ H_E^{(1),ab} &= \frac{b^{(1,-1)}}{\epsilon} + b^{(1,0)} + \epsilon b^{(1,1)} - \left(\frac{f^{(1,-1)}}{\epsilon} + f^{(1,0)} + \epsilon f^{(1,1)} \right) H_E^{(0),ab} \\ &\quad - \left(\frac{d^{(1,-1)}}{\epsilon} + d^{(1,0)} + \epsilon d^{(1,1)} \right) H_P^{(0),ab} + \mathcal{O}(\epsilon^2). \end{aligned} \quad (66)$$

We can now observe two important features: the cancellation of IR poles and the importance of ϵ parts of lower-order matching coefficients. The NLO matching coefficients reflect a physical quantity and need to be finite, meaning that

$$a^{(1,-1)} - c^{(1,-1)} H_P^{(0),ab} = \mathcal{O}(\epsilon), \quad (67)$$

which provides a strong cross-check for our calculation. Additionally, the ϵ parts of the LO matching coefficients enter the finite parts of the NLO matching coefficients. This can be seen from the pole $c^{(1,-1)}/\epsilon$ multiplying the LO matching coefficient $H_P^{(0),ab}$, resulting in a contribution of $a^{(0,1)}$ to the NLO matching coefficient $H_P^{(1),ab}$.

The matching procedure at NNLO is a natural extension of the NLO matching. The $\Delta B = 2$ side reads

$$\begin{aligned} (\Gamma_{12}^{ab})^{(2)} = \frac{G_F^2 m_b^2}{24\pi M_{B_q}} & \left[H_P^{(0),ab} \langle P \rangle^{(2)} + H_P^{(1),ab} \langle P \rangle^{(1)} + H_P^{(2),ab} \langle P \rangle^{(0)} \right. \\ & \left. + H_E^{(0),ab} \langle E \rangle^{(2)} + H_E^{(1),ab} \langle E \rangle^{(1)} + H_E^{(2),ab} \langle E \rangle^{(0)} \right], \end{aligned} \quad (68)$$

where the renormalised NNLO part of the matrix element can be written in analogy to Eq. (64) as

$$\begin{aligned} \langle P \rangle^{(2)} &= \left(\frac{c^{(2,-2)}}{\epsilon^2} + \frac{c^{(2,-1)}}{\epsilon} + c^{(2,0)} \right) \langle P \rangle^{(0)} + \left(\frac{d^{(2,-2)}}{\epsilon^2} + \frac{d^{(2,-1)}}{\epsilon} + d^{(2,0)} \right) \langle E \rangle^{(0)}, \\ \langle E \rangle^{(2)} &= \left(\frac{e^{(2,-1)}}{\epsilon} + e^{(2,0)} \right) \langle P \rangle^{(0)} + \left(\frac{f^{(2,-2)}}{\epsilon^2} + \frac{f^{(2,-1)}}{\epsilon} + f^{(2,0)} \right) \langle E \rangle^{(0)}. \end{aligned} \quad (69)$$

Similar to Eq. (65), the NNLO amplitude on the $\Delta B = 1$ side is parametrised as

$$\begin{aligned} \text{Im}(\mathcal{M}^{ab})^{(2)} = \frac{G_F^2 m_b^2}{24\pi} & \left[\left(\frac{a^{(2,-2)}}{\epsilon^2} + \frac{a^{(2,-1)}}{\epsilon} + a^{(2,0)} + \mathcal{O}(\epsilon) \right) \langle P \rangle^{(0)} \right. \\ & \left. + \left(\frac{b^{(2,-2)}}{\epsilon^2} + \frac{b^{(2,-1)}}{\epsilon} + b^{(2,0)} + \mathcal{O}(\epsilon) \right) \langle E \rangle^{(0)} \right]. \end{aligned} \quad (70)$$

Hence by inserting Eq. (69) into Eq. (68) and then equating with Eq. (70), the NNLO matching coefficients can be extracted and read

$$\begin{aligned} H_P^{(2),ab} &= \frac{a^{(2,-2)}}{\epsilon^2} + \frac{a^{(2,-1)}}{\epsilon} + a^{(2,0)} - e^{(1,0)} H_E^{(1),ab} - \left(\frac{c^{(1,-1)}}{\epsilon} + c^{(1,0)} \right) H_P^{(1),ab} \\ &\quad - \left(\frac{e^{(2,-1)}}{\epsilon} + e^{(2,0)} \right) H_E^{(0),ab} - \left(\frac{c^{(2,-2)}}{\epsilon^2} + \frac{c^{(2,-1)}}{\epsilon} + c^{(2,0)} \right) H_P^{(0),ab} + \mathcal{O}(\epsilon), \\ H_E^{(2),ab} &= \frac{b^{(2,-2)}}{\epsilon^2} + \frac{b^{(2,-1)}}{\epsilon} + b^{(2,0)} - \left(\frac{f^{(1,-1)}}{\epsilon} + f^{(1,0)} \right) H_E^{(1),ab} - \left(\frac{d^{(1,-1)}}{\epsilon} + d^{(1,0)} \right) H_P^{(1),ab} \end{aligned}$$

$$- \left(\frac{f^{(2,-2)}}{\epsilon^2} + \frac{f^{(2,-1)}}{\epsilon} + f^{(2,0)} \right) H_E^{(0),ab} - \left(\frac{d^{(2,-2)}}{\epsilon^2} + \frac{d^{(2,-1)}}{\epsilon} + d^{(2,0)} \right) H_P^{(0),ab} + \mathcal{O}(\epsilon). \quad (71)$$

As the matching coefficients need to be finite, all ϵ poles need to cancel. This provides another cross-check analogous to Eq. (67). Since the lower order matching coefficients are multiplied by poles in ϵ , it is now also apparent that the LO and NLO matching coefficients need to be extracted to $\mathcal{O}(\epsilon^2)$ and $\mathcal{O}(\epsilon)$, respectively.

For now we have discussed generic physical and evanescent operators, but it is also worth mentioning which evanescent operators need to be included in the matching. From Eq. (71) it is evident that both the LO and NLO evanescent matching coefficients, $H_E^{(0)}$ and $H_E^{(1)}$, will contribute to the physical matching coefficient at NNLO. Furthermore, from Eq. (68) we can see that $H_E^{(0)}$ and $H_E^{(1)}$ enter through the renormalised NNLO and NLO evanescent matrix elements, respectively. This means that all evanescent operators which appear as tree-level matrix elements at LO on the $\Delta B = 1$ side, i.e. in Eq. (61), need to be renormalised to NNLO on the $\Delta B = 2$ side. Similarly all evanescent operators that appear at NLO on the $\Delta B = 1$ side, i.e. in Eq. (65), need to be renormalised to NLO on the $\Delta B = 2$ side.

In our specific case where we consider two insertions of the current-current operators on the $\Delta B = 1$ side, the most complicated evanescent operators appearing at LO are the second generation evanescent operators defined in Eqs. (27) and (28). At NLO we also get the third generation evanescent operators from Eq. (35) and at NNLO we encounter the fourth generation evanescent operators from Eq. (36) for the first time. This means we renormalise the second, third and fourth generation evanescent operators to NNLO, NLO and LO (i.e. only tree-level), respectively. Incidentally this is exactly the hierarchy needed to renormalise a second generation evanescent operator at NNLO anyway.

3 Technicalities

For the calculation of the $\Delta B = 1$ and $\Delta B = 2$ amplitudes up to three and two loops, respectively, we have used two independent codes. Both of them use **qgraf** [32] for the generation of the amplitudes for the Feynman diagrams.

The implementation of the Feynman rules for the four-fermion operators requires special care. We find it convenient to split the four-particle vertices into two three-particle vertices each. The Feynman rules for the new vertices must be chosen such that one can reproduce the correct colour structure of the original vertex. This procedure ensures that relative signs between diagrams containing four-fermion operators are automatically correct. This is also common to both setups. All remaining steps are to a large extent different.

In the first setup we implemented the effective Hamiltonians in **FeynRules** [33]³ and

³In our calculation it is important to disable the automatic simplification of chains with more than

exporting the Feynman rules to **FeynArts** [34]. The relative signs of genuine four-fermion operators are then automatically fixed by **FeynCalc** [35–37] using the algorithm adapted from **FormCalc** [38]. In this way we were able to validate the approach based on the splitting of the four-particle vertices into two three-particle vertices each by comparing amplitudes of selected diagrams.

The first setup further uses **q2e** [39, 40] to rewrite the **qgraf** output to **FORM** [41]. Afterwards, each diagram is mapped to a predefined integral family with the help of **exp**. The manipulations of the amplitudes and the identification of scalar integrals of a given integral family is done with the help of in-house **FORM** code. For the decomposition into the different operator structures, tensor integrals up to rank ten have been implemented. More details are provided in Ref. [21]. Note that the first setup to compute the three-loop corrections is restricted to the first two terms in the expansion for $m_c/m_b \rightarrow 0$. Thus, in the integral families the charm quark is massless.

We use version 6 of **FIRE** [42] in combination with **LiteRed** [43] for the reduction to master integrals. The calculation of the latter is described in detail in Section C where also explicit results can be found.

The second setup uses **tapir** [44, 45] which automatically generates a number of auxiliary files which in the first setup have to be generated manually. This concerns in particular the definition of the integral families and the corresponding **FORM** code. In the second approach we aim for a full dependence on m_c . Thus, the integral families are significantly more involved as in the first approach. Altogether we have 320 different integral families.

A major difference to the first approach is also that here we use projectors instead of tensor integral reduction in order to obtain the coefficients of the various tensor structures. Details concerning the construction of the projectors can again be found in Ref. [21].

We perform the reduction within each integral family to master integrals with the program **Kira** [46, 47]. At this step, the program **ImproveMasters.m** [48] is very useful in order to choose a good basis of master integrals such that the coefficients only contain low-order polynomials in ϵ and x . We use **Kira** also for the minimisation of the master integrals across all families. Keeping only those master integrals which have an imaginary part and completing the system of differential equations as outlined in Ref. [21], we obtain 342 complex-valued master integrals.

For the computation of the master integrals we use the “expand and match” approach [49–52] and construct generalised series expansions around several values for $z = m_c^2/m_b^2$ (see Ref. [21] for more details) such that we cover the range relevant for all renormalisation schemes. For the phenomenological application it is sufficient to use the expansion around $z = 0$ up to z^{10} as the highest expansion term has a relative contribution of 10^{-6} to the coefficient of $(\alpha_s/(4\pi))^2$ at the largest value of z considered in the scale variation.

three Dirac matrices using the Chisholm identity. This is achieved by commenting the corresponding routine in the **Processing** section of the file **FeynArtsInterface.m**

4 Semi-analytic results

For illustration purposes, we present the first z^0 term of the semi-analytic expansion of the matching coefficient contributions from current-current operators. We provide computer-readable results up to z^{10} on the website [30].

The matching coefficients are as defined in Eqs. (56) and (59) and can be further decomposed by the respective contributions from the $\Delta B = 1$ Wilson coefficients,

$$H^{(n),ab} = \sum_{i,j \in \{1,\dots,6,8\}, j \geq i} C_i C_j p_{ij}^{(n),ab}, \quad (72)$$

and analogously for \tilde{H}_S . For the z^0 term the coefficients are identical for $ab \in \{uu, uc, cc\}$, so we omit these indices in the following. Our LO results read

$$\begin{aligned} p_{11}^{(0)} &= 0.31944, & p_{11}^{S,(0)} &= -0.55556, \\ p_{12}^{(0)} &= 0.16667, & p_{12}^{S,(0)} &= -1.33333, \\ p_{22}^{(0)} &= 1.0000, & p_{22}^{S,(0)} &= 1.0000. \end{aligned}$$

At NLO we obtain

$$\begin{aligned} p_{11}^{(1)} &= 3.2241 + 2.0802L_1 + 2.7593L_2, & p_{11}^{S,(1)} &= -0.72285 - 0.93827L_1 - 2.9630L_2, \\ p_{12}^{(1)} &= -11.134 - 11.963L_1 + 4.2222L_2, & p_{12}^{S,(1)} &= 12.230 + 3.2593L_1 - 7.1111L_2, \\ p_{22}^{(1)} &= -14.764 - 3.1111L_1 + 1.3333L_2, & p_{22}^{S,(1)} &= 0.64402 + 14.222L_1 + 5.3333L_2, \end{aligned}$$

and finally at NNLO we have

$$\begin{aligned} p_{11}^{(2)} &= 68.566 + 126.22L_1 + 39.642L_1^2 + 44.635L_2 + 53.132L_1L_2 - 5.7593L_2^2, \\ p_{11}^{S,(2)} &= -71.490 - 110.61L_1 - 14.848L_1^2 - 18.999L_2 - 50.436L_1L_2 + 38.519L_2^2, \\ p_{12}^{(2)} &= 6.5554 - 153.65L_1 - 129.70L_1^2 - 2.7358L_2 + 8.1975L_1L_2 - 0.22222L_2^2, \\ p_{12}^{S,(2)} &= 36.006 + 238.79L_1 + 2.1728L_1^2 + 28.880L_2 - 91.654L_1L_2 + 92.444L_2^2, \\ p_{22}^{(2)} &= -267.98 - 80.931L_1 + 53.111L_1^2 - 121.96L_2 - 29.926L_1L_2 - 25.333L_2^2, \\ p_{22}^{S,(2)} &= -396.55 - 146.85L_1 + 89.481L_1^2 + 30.694L_2 + 157.63L_1L_2 - 69.333L_2^2, \end{aligned}$$

where we have defined $L_1 = \ln(\mu_1/m_b)$ and $L_2 = \ln(\mu_2/m_b)$. An important cross-check of our results at three-loops is the calculation using analytical master integrals for $z = 0$. The details of the computation are in Appendix C. Here and in the following μ_1 is the scale at which the $\Delta B = 1$ Wilson coefficients are evaluated, while μ_2 is the scale at which the $\Delta B = 2$ operators are defined. The μ_1 dependence of the coefficients of the $\Delta B = 2$ operators decreases with increasing orders of α_s . The same holds true for the μ_2 dependence only in combination with the μ_2 dependence of the $\Delta B = 2$ matrix elements,

$\alpha_s(M_Z)$	$=$	0.1180 ± 0.0009	[53]	$m_c(3 \text{ GeV})$	$=$	$0.993 \pm 0.008 \text{ GeV}$	[54]
m_t^{pole}	$=$	$172.4 \pm 0.7 \text{ GeV}$	[53]	$m_b(m_b)$	$=$	$4.163 \pm 0.016 \text{ GeV}$	[55]
M_{B_s}	$=$	$5366.88 \pm 0.14 \text{ MeV}$	[53]	M_{B_d}	$=$	$5279.64 \pm 0.12 \text{ MeV}$	[53]
B_{B_s}	$=$	0.813 ± 0.034	[56]	B_{B_d}	$=$	0.806 ± 0.041	[56]
\tilde{B}'_{S,B_s}	$=$	1.31 ± 0.09	[56]	\tilde{B}'_{S,B_d}	$=$	1.20 ± 0.09	[56]
f_{B_s}	$=$	$0.2303 \pm 0.0013 \text{ GeV}$	[57–60]	f_{B_d}	$=$	$0.1905 \pm 0.0013 \text{ MeV}$	[57–60]

Table 2: Input parameters for the numerical analysis. The quoted m_t^{pole} corresponds to $m_t(m_t) = (162.6 \pm 0.7) \text{ GeV}$ in the $\overline{\text{MS}}$ scheme. We use the values for $B_{B_q} = B_{B_q}(\mu_2)$ and $\tilde{B}'_{S,B_q} = \tilde{B}'_{S,B_q}(\mu_2)$ with $\mu_2 = m_b^{\text{pole}}$.

which requires a calculation of the lattice-continuum matching to the appropriate order in α_s .

Let us briefly comment on the agreement of the matching coefficients obtained in this work with previous NNLO studies. The matching coefficients which form the basis of Ref. [20] have been reproduced as part of our calculation at intermediate steps. Note that the coefficients provided here and in the ancillary files are different because of the new operator basis used in this work, see Section 2.3.

We also reproduced the part of the NNLO matching coefficients which stems from closed charm quark loops as calculated in Ref. [17]. Note that the latter contributions are independent of the choice of the second generation evanescent operators. Ref. [20] also incorporated the previously published closed charm loop contributions, but missed a numerically small correction, which has been resolved now.

5 Phenomenology

In this Section we consider both the B_s and B_d system and discuss numerical results for the width difference $\Delta\Gamma_q$, the ratio $\Delta\Gamma_q/\Delta M_q$ and the CP asymmetry in flavours-specific decays a_{fs}^q . We find good numerical agreement with previous calculations in Ref. [20].

5.1 Input values and renormalisation schemes

In Tab. 2 we list the input values which we use for our numerical analysis. Using $m_b(m_b)$ and the two-loop relation to the pole mass we obtain $m_b^{\text{pole}} = 4.758 \text{ GeV}$. The pole mass is well-defined at any finite order of QCD, but suffers from a renormalon ambiguity of order Λ_{QCD} . While this feature is related to asymptotically large orders of perturbation theory, it is empirically known that perturbative series of physical quantities exhibit a poor convergence at low orders of α_s . Γ_{12}^q is proportional to two powers of m_b , and we

will present results for different renormalisation schemes for this overall factor m_b^2 . The results using the pole mass are for illustrative purposes only and are excluded from the final numerical values. For the bottom mass in the potential-subtracted (PS) scheme, we obtain $m_b^{\text{PS}} = 4.480$ GeV with the factorisation scale $\mu_f = 2$ GeV using the four-loop implementation in RunDec [61]. Furthermore, we need CKM parameters which are given by [62]

$$\begin{aligned}\frac{\lambda_u^d}{\lambda_t^d} &= (0.0105 \pm 0.0107) - (0.4259 \pm 0.0091)i, \\ \frac{\lambda_u^s}{\lambda_t^s} &= -(0.00877 \pm 0.00043) + (0.01858 \pm 0.00038)i.\end{aligned}\quad (73)$$

While only the ratio λ_u^q/λ_t^q enters Γ_{12}^q/M_{12}^q , in a direct calculation of $\Delta\Gamma_q$ using Eq. (3), the absolute values $|\lambda_t^d|$ and $|\lambda_t^s|$ are also needed, which depend on the value of $|V_{cb}|$. The current measurements from inclusive and exclusive decays are [63]

$$\begin{aligned}|V_{cb}^{\text{incl}}| &= (42.16 \pm 0.51) \times 10^{-3} \quad [64], \\ |V_{cb}^{\text{excl}}| &= (39.45 \pm 0.56) \times 10^{-3}, \quad [B \rightarrow (D, D^*)\ell\nu], \text{ FLAG average, } [2, 65\text{--}73],\end{aligned}\quad (74)$$

where for the inclusive $|V_{cb}|$ one can also use the result from Ref. [74], which leads to a similar result. The current SM fit which excludes measurements of $|V_{cb}|$ gives [62]

$$|V_{cb}^{\text{SM fit}}| = (41.60_{-0.58}^{+0.20}) \times 10^{-3}. \quad (75)$$

We obtain the following values for λ_t^q :

$$\begin{aligned}|\lambda_t^{d, \text{SM fit}}| &= (8.56_{-0.34}^{+0.08}) \times 10^{-3}, & |\lambda_t^{d, \text{excl}}| &= (8.12_{-0.20}^{+0.15}) \times 10^{-3}, \\ |\lambda_t^{s, \text{incl}}| &= (41.39 \pm 0.50) \times 10^{-3}, & |\lambda_t^{s, \text{excl}}| &= (38.73 \pm 0.55) \times 10^{-3}.\end{aligned}\quad (76)$$

Here $|\lambda_t^{d, \text{SM fit}}|$ is calculated from the 1σ best-fit result for $|V_{td}|$ and $|V_{tb}|$ found by the CKMfitter group from a global fit to the CKM parameters [62]. One cannot simply deduce which result one would find by fixing $|V_{cb}|$ to the value determined from exclusive semileptonic B decays, which would come with a poor p -value, from the results of Ref. [62]. Our $|\lambda_t^{d, \text{excl}}|$ is instead calculated by rescaling $|\lambda_t^{d, \text{SM fit}}|$ with the ratio of the two $|V_{cb}|^2$ values from Eqs. (74) and (75). The B_s system is easier because the involved CKM elements are fixed by CKM unitarity to $|V_{ts}| = (0.983 \pm 0.001)|V_{cb}|$ and $|V_{tb}| = 0.9991$ with essentially no sensitivity to other parameters. Thus we calculate $|\lambda_t^{s, \text{incl/excl}}|$ directly from $|V_{cb}^{\text{incl/excl}}|$ in this way.

The parameters B_{B_s} and \tilde{B}'_{S, B_s} in Tab. 2 are used to parametrise the matrix elements of the leading operators Q and \tilde{Q}_S as

$$\begin{aligned}\langle B_s | Q(\mu_2) | \bar{B}_s \rangle &= \frac{8}{3} M_{B_s}^2 f_{B_s}^2 B_{B_s}(\mu_2), \\ \langle B_s | \tilde{Q}_S(\mu_2) | \bar{B}_s \rangle &= \frac{1}{3} M_{B_s}^2 f_{B_s}^2 \tilde{B}'_{S, B_s}(\mu_2).\end{aligned}\quad (77)$$

Analogous formulae hold for the B_d system. Sum rule results for the matrix elements can be found in Refs. [75, 76]. They have, e.g. been used in Ref. [77, 78].

For the $1/m_b$ suppressed correction to Γ_{12}^q in Eq. (56) use for the overall factor m_b^2 the PS scheme. The matrix elements of the $1/m_b$ suppressed corrections calculated with lattice QCD are obtained from Refs. [56, 79] and are given by

$$\begin{aligned}
\langle B_s | R_0 | \bar{B}_s \rangle &= -(0.43 \pm 0.18) f_{B_s}^2 M_{B_s}^2, \\
\langle B_s | R_1 | \bar{B}_s \rangle &= (0.07 \pm 0.00) f_{B_s}^2 M_{B_s}^2, \\
\langle B_s | \tilde{R}_1 | \bar{B}_s \rangle &= (0.04 \pm 0.00) f_{B_s}^2 M_{B_s}^2, \\
\langle B_s | R_2 | \bar{B}_s \rangle &= -(0.18 \pm 0.07) f_{B_s}^2 M_{B_s}^2, \\
\langle B_s | \tilde{R}_2 | \bar{B}_s \rangle &= (0.18 \pm 0.07) f_{B_s}^2 M_{B_s}^2, \\
\langle B_s | R_3 | \bar{B}_s \rangle &= (0.38 \pm 0.13) f_{B_s}^2 M_{B_s}^2, \\
\langle B_s | \tilde{R}_3 | \bar{B}_s \rangle &= (0.29 \pm 0.10) f_{B_s}^2 M_{B_s}^2,
\end{aligned} \tag{78}$$

where explicit expressions for the operators can be found in Refs. [56, 80]. The results for the matrix elements of R_2 , \tilde{R}_2 , R_3 and \tilde{R}_3 can be found in Ref. [79] and we extract the remaining three matrix elements from [56]. For $\langle B_s | R_1 | \bar{B}_s \rangle$ and $\langle B_s | \tilde{R}_1 | \bar{B}_s \rangle$ the ratio of the bottom and strange quark masses is needed $m_b(\mu)/m_s(\mu) = 52.55 \pm 0.55$ [81].

The matrix elements of the $1/m_b$ suppressed corrections for the B_d system are given by

$$\begin{aligned}
\langle B_d | R_0 | \bar{B}_d \rangle &= -(0.35 \pm 0.19) f_{B_d}^2 M_{B_d}^2, \\
\langle B_d | R_1 | \bar{B}_d \rangle &= 0, \\
\langle B_d | \tilde{R}_1 | \bar{B}_d \rangle &= 0, \\
\langle B_d | R_X | \bar{B}_d \rangle &= \frac{f_{B_d}^2 M_{B_d}^2}{f_{B_s}^2 M_{B_s}^2} \langle B_s | R_X | \bar{B}_s \rangle,
\end{aligned} \tag{79}$$

where $R_X \in \{R_2, \tilde{R}_2, R_3, \tilde{R}_3\}$ [79]. The matrix elements of R_1 and \tilde{R}_1 are of order $10^{-3} f_{B_d}^2 M_{B_d}^2$ which is due to the additional suppression factor $m_d/m_s \approx 0.03$ as compared the corresponding quantities in the B_s system. The matrix element for R_0 is extracted from Ref. [56]. In the last expression in Eq. (79) flavour-SU(3) breaking effects beyond factorisation are neglected.

Following the matching procedure outlined in Section 2.7, we obtain an expression for Γ_{12}^{ab} where the α_s is renormalised in the $\overline{\text{MS}}$ scheme and the charm and bottom quark masses are in the on-shell scheme. In a first step we transform the parameter z in Eq. (56) to the $\overline{\text{MS}}$ scheme which introduces μ_c and μ_b , the renormalisation scales of \overline{m}_c and \overline{m}_b . For the overall factor m_b^2 we adapt three different renormalisation schemes: we either leave it in the pole scheme or transform it to the $\overline{\text{MS}}$ or PS mass [82]. The latter is an example for a so-called threshold mass. Alternatively we could have used the kinetic [83–85] or RS [86] schemes. Note that the scheme transformation of m_b^2 leads to a redefinition of $H^{ab}(z)$ and $\tilde{H}_S^{ab}(z)$ such that the scheme dependence of Γ_{12}^s is of higher order in α_s .

Let us next discuss our choices for the various renormalisation and matching scales which enter our analysis. For the matching scale between the full Standard Model to the $|\Delta B| = 1$ theory, μ_0 , we choose $\mu_0 = 165 \text{ GeV} \approx m_t(m_t)$. We do not vary μ_0 since it barely affects the physical quantities. The matching scale μ_1 and the renormalisation scales μ_b and μ_c are all of the order of the bottom quark mass. In our analysis we vary them simultaneously (i.e., $\mu_c = \mu_b = \mu_1$) between 2.1 GeV and 8.4 GeV with the central scale $\mu_1 = 4.2 \text{ GeV}$. For reference, at the central scale $\mu_1 = 4.2 \text{ GeV}$ we have $\bar{z} = (m_c(\mu_1)/m_b(\mu_1))^2 \approx 0.04955$.

The $|\Delta B| = 2$ operators are defined at the scale μ_2 which has to be kept fixed, because the μ_2 dependence only cancels in the product of $H^{ab}(z)$ and $\tilde{H}_S^{ab}(z)$ with their respective matrix elements. In our analysis we set $\mu_2 = m_b^{\text{pole}} = 4.758 \text{ GeV}$ which is computed from $m_b(m_b)$ to two-loop accuracy. The terms of order Λ_{QCD}/m_b in Γ_{12}^q are only known to LO, so that the μ_1 -dependence of these terms is non-negligible. In the numerical results, which we present below, the corresponding uncertainties will be displayed separately.

5.2 $\Delta\Gamma_q$ and $\Delta\Gamma_q/\Delta M_q$

5.2.1 B_s system

We start with the discussion of the B_s system and consider in a first step the ratio $\Delta\Gamma_s/\Delta M_s$.

For the numerical evaluation we use the values for the input parameters provided in Section 5.1. We vary each parameter within the given uncertainty which leads to the central value for $\Delta\Gamma_s/\Delta M_s$ and the corresponding uncertainties. The latter are added in quadrature and taking into account the 100% correlation of $\langle B_s | R_2 | \tilde{B}_s \rangle$ and $\langle B_s | \tilde{R}_2 | \tilde{B}_s \rangle$. In the following we provide separate uncertainties for the scale variation (“scale”), the leading-power bag parameters (“ $B\tilde{B}_S$ ”), matrix elements of the power-suppressed corrections (“ $1/m_b$ ”), and the variation of the remaining input parameters (“input”). In our three schemes we have

$$\begin{aligned} \frac{\Delta\Gamma_s}{\Delta M_s} &= \left(3.84_{-0.57}^{+0.53} \text{scale} \text{ }_{-0.19}^{+0.09} \text{scale, } 1/m_b \pm 0.11_{B\tilde{B}_S} \pm 0.78_{1/m_b} \pm 0.06_{\text{input}} \right) \times 10^{-3} \text{ (pole)}, \\ \frac{\Delta\Gamma_s}{\Delta M_s} &= \left(4.37_{-0.44}^{+0.23} \text{scale} \text{ }_{-0.19}^{+0.09} \text{scale, } 1/m_b \pm 0.12_{B\tilde{B}_S} \pm 0.78_{1/m_b} \pm 0.05_{\text{input}} \right) \times 10^{-3} \text{ (MS)}, \\ \frac{\Delta\Gamma_s}{\Delta M_s} &= \left(4.27_{-0.37}^{+0.36} \text{scale} \text{ }_{-0.19}^{+0.09} \text{scale, } 1/m_b \pm 0.12_{B\tilde{B}_S} \pm 0.78_{1/m_b} \pm 0.05_{\text{input}} \right) \times 10^{-3} \text{ (PS)}. \end{aligned} \quad (80)$$

The dominant uncertainty comes from the matrix elements of the power-suppressed corrections [56, 79]) followed by the renormalisation scale uncertainty from the variation of μ_1 in the leading-power term. The uncertainties from the leading-power bag parameters and from the scale variation in the $1/m_b$ piece are much smaller. The variation of the remaining input parameters is of minor relevance.

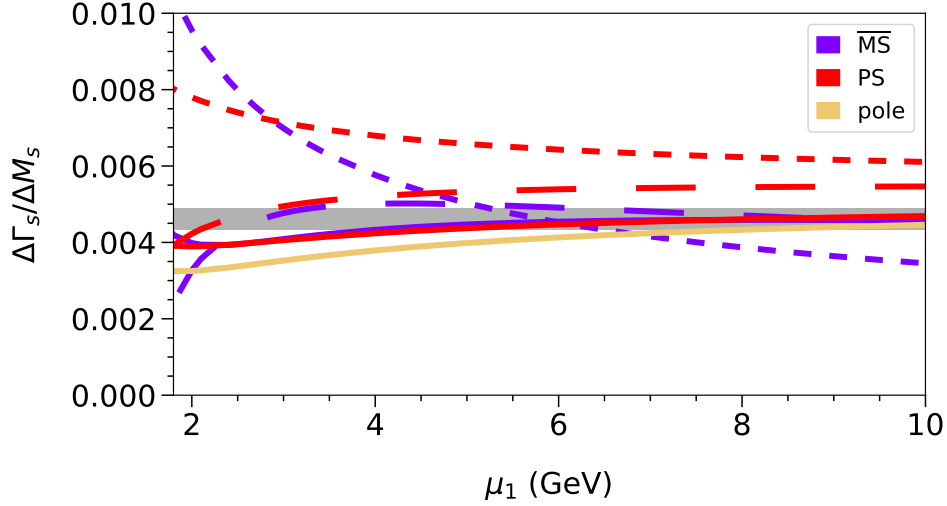


Figure 4: Renormalisation scale dependence at LO (short dashes), NLO (long dashes) and NNLO (solid) for $\Delta\Gamma_s/\Delta M_s$. The scale in the power-suppressed terms is kept fixed (so the displayed scale variation does not contain the uncertainties of the latter) while the scales $\mu_c = \mu_b = \mu_1$ are varied simultaneously. The grey band represents the experimental results.

In Fig. 4 we show the μ_1 dependence of $\Delta\Gamma_s/\Delta M_s$ with $\mu_1 = \mu_c = \mu_b$. The experimental result is shown as a grey band. To illustrate the effect of the NNLO calculation we vary the renormalisation scale only in the leading $1/m_b$ corrections; in the power-suppressed terms it is kept fixed. For the $\overline{\text{MS}}$ and PS schemes LO, NLO and NNLO results are shown. In both schemes we observe that the dependence on μ_1 decreases with increasing order in perturbation theory. For example, in the interval $[2.1, 8.4]$ GeV one observes a variation of $\Delta\Gamma_s/\Delta M_s$ in the $\overline{\text{MS}}$ scheme of about 123% at LO which reduces to 33% at NLO and 15% at NNLO, where we take the NNLO result as the reference point in each case and always include the $1/m_b$ corrections with the scale fixed at 4.2 GeV. For the PS scheme the corresponding numbers are {35%, 26%, 17%}. Let us stress that the NNLO results of both schemes are very close in the whole μ_1 interval.

It is interesting to consider the perturbative expansion at the central scale $\mu = 4.2$ GeV. In the PS scheme the NLO corrections are negative and reduce the LO predictions by about 22%. Also the NNLO corrections are negative and about a factor 1.6 smaller than at NLO. This is different for the $\overline{\text{MS}}$ scheme. Here the NNLO corrections amount to about 10% and are about a factor 1.1 larger than at NLO. This is because the central scale is close to $\mu_1 \approx 5$ GeV where the NLO corrections vanish. The situation is completely different at other values for μ_1 . For example, for $\mu_1 \approx 2.5$ GeV or $\mu_1 \approx 9$ GeV we observe NNLO corrections which are much smaller than the NLO ones, indicating a perfect behaviour of perturbation theory.

Both NNLO predictions lie inside the uncertainty band of experimental result for $\mu_1 \gtrsim 4$ GeV in the $\overline{\text{MS}}$ and for $\mu_1 \gtrsim 5$ GeV in the PS scheme. For smaller values the NLO $\overline{\text{MS}}$ curve lies within the uncertainty band for most of the μ_1 values. However, in the PS scheme the prediction is outside the band for $\mu_1 \gtrsim 3$ GeV.

For comparison we show in Fig. 4 also the NNLO result in the pole scheme. We observe a stronger dependence on μ_1 . Furthermore, the agreement with the experimental result is worse.

One of the benefits of the ratio $\Delta\Gamma_q/\Delta M_q$ is the reduced dependence on the hadronic matrix elements. ΔM_q only depends on the numerically dominant matrix element $\langle B_q | Q(\mu_2) | \overline{B}_q \rangle$ and thus the leading term of $\Delta\Gamma_q/\Delta M_q$ is independent of hadronic matrix elements. The numerically sub-leading terms are either proportional to $\langle B_q | \tilde{Q}_S(\mu_2) | \overline{B}_q \rangle / \langle B_q | Q(\mu_2) | \overline{B}_q \rangle$ (from the leading power in the $1/m_b$ expansion) or involve matrix elements from the $1/m_b$ contributions divided by $\langle B_q | Q(\mu_2) | \overline{B}_q \rangle$. To illustrate the relative size of the contributions, we show the decomposition of the central value from Eq. (80) in the $\overline{\text{MS}}$ scheme for the B_s system,

$$\frac{\Delta\Gamma_s}{\Delta M_s} = 4.37 \times 10^{-3} \approx \left(4.20 + 1.69 \tilde{Q}_S/Q - 1.53_{1/m_b} \right) \times 10^{-3} \text{ (}\overline{\text{MS}}\text{)}, \quad (81)$$

where the first number in the round brackets denotes the term independent of hadronic matrix elements, \tilde{Q}_S/Q the term proportional to the ratio of the leading order hadronic matrix elements and $1/m_b$ the contribution from the sub-leading terms in the HQE. Note that the sum of the latter two makes up less than 4% of the leading contribution and is of the order of the hadronic uncertainty of the leading $1/m_b$ contribution.

The most precise prediction for $\Delta\Gamma_s$ is obtained from the results in Eq. (80) combined with the experimental result [1]

$$\Delta M_s^{\text{exp}} = 17.7656 \pm 0.0057 \text{ ps}^{-1}. \quad (82)$$

Using Eq. (80) we obtain for the three renormalisation schemes

$$\begin{aligned} \Delta\Gamma_s &= \left(6.82_{-1.02_{\text{scale}}^{+0.94}}^{+0.16} \pm 0.19_{B\tilde{B}_S} \pm 1.39_{1/m_b} \pm 0.10_{\text{input}} \right) \times 10^{-2} \text{ps}^{-1} \text{ (pole)}, \\ \Delta\Gamma_s &= \left(7.76_{-0.79_{\text{scale}}^{+0.40}}^{+0.16} \pm 0.21_{B\tilde{B}_S} \pm 1.39_{1/m_b} \pm 0.09_{\text{input}} \right) \times 10^{-2} \text{ps}^{-1} \text{ (}\overline{\text{MS}}\text{)}, \\ \Delta\Gamma_s &= \left(7.58_{-0.66_{\text{scale}}^{+0.63}}^{+0.16} \pm 0.20_{B\tilde{B}_S} \pm 1.39_{1/m_b} \pm 0.09_{\text{input}} \right) \times 10^{-2} \text{ps}^{-1} \text{ (PS)}. \end{aligned} \quad (83)$$

For the final result for $\Delta\Gamma_s$ we only consider the $\overline{\text{MS}}$ and PS schemes. The total uncertainty in each scheme is obtained by adding the upper and lower bounds in quadrature, which are then symmetrised. Averaging the central values and the symmetrised uncertainties of the two schemes and obtain

$$\Delta\Gamma_s = (0.077 \pm 0.016) \text{ ps}^{-1}. \quad (84)$$

The comparison to Eq. (5) shows that the uncertainty is only bigger by about a factor of three than the experimental uncertainty and dominated by the $1/m_b$ corrections. Equation (83) shows that thanks to the NNLO calculation the perturbative uncertainty of the leading-power part as estimated from the scale dependence is only marginally larger than the current experimental error in Eq. (5). Clearly, a better calculation of the $1/m_b$ contribution is needed now.

In the analysis performed in Refs. [77, 78] the NLO result $\Delta\Gamma_s = (0.091 \pm 0.015) \text{ ps}^{-1}$ has been obtained, which we can compare to our NLO prediction of $\Delta\Gamma_s = (0.091 \pm 0.020) \text{ ps}^{-1}$, analogous to Eq. (84). As can be seen from Fig. 4 and as discussed above, the NNLO corrections shift the central value down. It is noteworthy that the central values for the two NLO predictions are quite close together, even though in Refs. [77, 78] only the leading term from the penguin operators is taken into account. For the operator matrix elements of the leading dimension-6 operators sum rule results from Refs. [75, 76] are used. Furthermore, the estimate of the uncertainties from renormalisation scale variation and the one from sub-leading matrix elements are smaller than in our analysis.

5.2.2 B_d system

Results for $\Delta\Gamma_d$ can be obtained by repeating the analysis performed for the B_s system after adjusting the relevant parameters. For the three renormalisation schemes we get

$$\begin{aligned}\frac{\Delta\Gamma_d}{\Delta M_d} &= \left(3.69^{+0.52}_{-0.57} \text{scale}^{+0.12}_{-0.20} \text{scale, } 1/m_b \pm 0.11_{B\tilde{B}_S} \pm 0.80_{1/m_b} \pm 0.06_{\text{input}} \right) \times 10^{-3} \text{ (pole)}, \\ \frac{\Delta\Gamma_d}{\Delta M_d} &= \left(4.21^{+0.23}_{-0.44} \text{scale}^{+0.12}_{-0.20} \text{scale, } 1/m_b \pm 0.12_{B\tilde{B}_S} \pm 0.80_{1/m_b} \pm 0.05_{\text{input}} \right) \times 10^{-3} \text{ (}\overline{\text{MS}}\text{)}, \\ \frac{\Delta\Gamma_d}{\Delta M_d} &= \left(4.11^{+0.35}_{-0.37} \text{scale}^{+0.12}_{-0.20} \text{scale, } 1/m_b \pm 0.12_{B\tilde{B}_S} \pm 0.80_{1/m_b} \pm 0.05_{\text{input}} \right) \times 10^{-3} \text{ (PS)}.\end{aligned}\tag{85}$$

From the results in Eq. (85) we obtain after multiplication with ΔM_d^{exp}

$$\begin{aligned}\Delta\Gamma_d &= \left(1.87^{+0.26}_{-0.29} \text{scale}^{+0.06}_{-0.10} \text{scale, } 1/m_b \pm 0.06_{B\tilde{B}_S} \pm 0.40_{1/m_b} \pm 0.03_{\text{input}} \right) \times 10^{-3} \text{ps}^{-1} \text{ (pole)}, \\ \Delta\Gamma_d &= \left(2.13^{+0.11}_{-0.23} \text{scale}^{+0.06}_{-0.10} \text{scale, } 1/m_b \pm 0.06_{B\tilde{B}_S} \pm 0.40_{1/m_b} \pm 0.03_{\text{input}} \right) \times 10^{-3} \text{ps}^{-1} \text{ (}\overline{\text{MS}}\text{)}, \\ \Delta\Gamma_d &= \left(2.08^{+0.18}_{-0.19} \text{scale}^{+0.06}_{-0.10} \text{scale, } 1/m_b \pm 0.06_{B\tilde{B}_S} \pm 0.40_{1/m_b} \pm 0.03_{\text{input}} \right) \times 10^{-3} \text{ps}^{-1} \text{ (PS)},\end{aligned}\tag{86}$$

where [2]

$$\Delta M_d^{\text{exp}} = (0.5065 \pm 0.0019) \text{ ps}^{-1}\tag{87}$$

has been used.

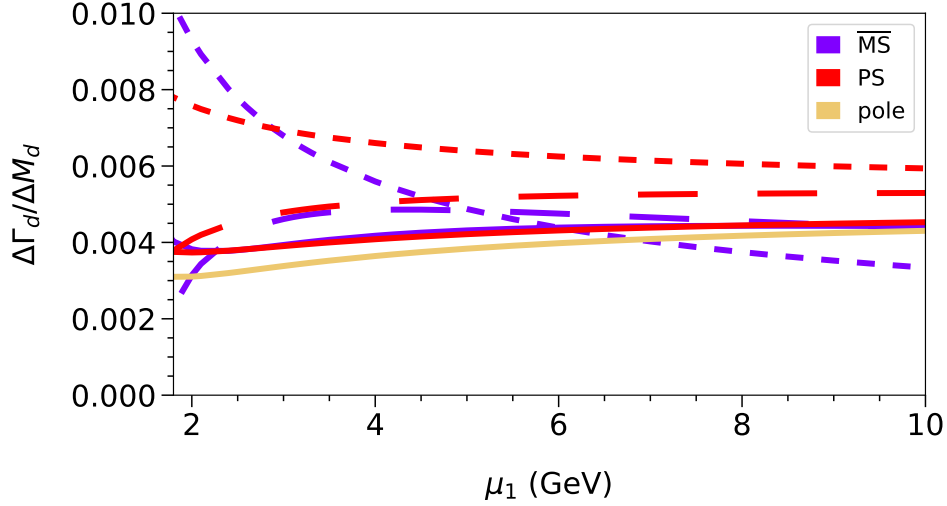


Figure 5: Renormalisation scale dependence at LO (short dashes), NLO (long dashes) and NNLO (solid) for $\Delta\Gamma_d/\Delta M_d$. The scale in the power-suppressed terms is kept fixed while the scales $\mu_c = \mu_b = \mu_1$ are varied simultaneously.

We add the various uncertainties in quadrature for the upper and lower bounds separately, symmetrise the total uncertainty in each scheme and average the results for the $\overline{\text{MS}}$ and PS schemes to obtain

$$\Delta\Gamma_d = (0.00211 \pm 0.00045) \text{ ps}^{-1}. \quad (88)$$

For the B_d system the pattern of the uncertainties is very similar to the B_s system: The dominant contribution comes from the matrix elements of the power-suppressed corrections, followed by the renormalisation scale uncertainty in the leading-power term, the uncertainty in the leading-power bag parameters and from the scale variation in the $1/m_b$ piece. Also for B_d the variation of the remaining input parameters is only a minor effect.

In Fig. 5 we show the μ_1 dependence of $\Delta\Gamma_d/\Delta M_d$. We refrain from showing the experimental results since the uncertainties are quite large and would cover the whole plot range. For the $\overline{\text{MS}}$ and PS scheme we again show LO, NLO and NNLO results and observe the same convergence pattern as for B_s . Also for B_d it is a welcome feature that the NNLO predictions for both renormalisation schemes are very close together. The NNLO prediction for the pole scheme is only shown for reference; it is not used for our final prediction.

In an alternative approach it is possible to obtain $\Delta\Gamma_d$ from $\Delta\Gamma_s/\Delta M_s$ after multiplying with the experimental value for ΔM_d . This is possible since the CKM-suppressed contribution to $\Delta\Gamma_d/\Delta M_d$ is only subleading. A priori it is expected to be numerically relevant due to $|\lambda_u^d/\lambda_t^d| \gg |\lambda_u^s/\lambda_t^s|$, but there are significant numerical cancellations in the sum of uc and uu contributions, which has been observed for the first time in Ref. [12]. Furthermore, the non-perturbative hadronic matrix elements for the B_s and B_d system

agree well within the uncertainties as can be seen in Tab. 2. Thus, the agreement of the central values for $\Delta\Gamma_d/\Delta M_d$ and $\Delta\Gamma_s/\Delta M_s$ is well below the uncertainties given in Eq. (80). Our results are given by

$$\begin{aligned}\Delta\Gamma_d &= \left(1.94^{+0.27}_{-0.29}{}^{+0.05}_{\text{scale}}{}^{-0.10}_{\text{scale}, 1/m_b} \pm 0.05_{B\tilde{B}_S} \pm 0.40_{1/m_b} \pm 0.03_{\text{input}}\right) \times 10^{-3}\text{ps}^{-1} \text{ (pole)}, \\ \Delta\Gamma_d &= \left(2.21^{+0.11}_{-0.22}{}^{+0.05}_{\text{scale}}{}^{-0.10}_{\text{scale}, 1/m_b} \pm 0.06_{B\tilde{B}_S} \pm 0.40_{1/m_b} \pm 0.03_{\text{input}}\right) \times 10^{-3}\text{ps}^{-1} \text{ (}\overline{\text{MS}}\text{)}, \\ \Delta\Gamma_d &= \left(2.16^{+0.18}_{-0.19}{}^{+0.05}_{\text{scale}}{}^{-0.10}_{\text{scale}, 1/m_b} \pm 0.06_{B\tilde{B}_S} \pm 0.40_{1/m_b} \pm 0.03_{\text{input}}\right) \times 10^{-3}\text{ps}^{-1} \text{ (PS)},\end{aligned}\tag{89}$$

Adding the various uncertainties in quadrature for the upper and lower bounds separately, symmetrising the total uncertainty in each scheme, and averaging the results for the $\overline{\text{MS}}$ and PS schemes, we obtain

$$\Delta\Gamma_d = (0.00219 \pm 0.00045) \text{ ps}^{-1}.\tag{90}$$

The comparison of Eqs. (86) and (89) shows good agreement in the central values well within the uncertainties. Also most of the individual uncertainties agree well for the two approaches to compute $\Delta\Gamma_d$.

The SM prediction of $\Delta\Gamma_s/\Delta M_s$ is almost completely independent of any CKM element, while the individual predictions for $\Delta\Gamma_s$ and ΔM_s depend on $|V_{cb}|$ (which determines $|V_{ts}| \simeq (0.982 \pm 0.001)|V_{cb}|$ from the unitarity of the CKM matrix), so that the ratio $\Delta\Gamma_s/\Delta M_s$ (or, equivalently, $\Delta\Gamma_s$ in Eq. (84) calculated from this ratio) probes, e.g. new physics in ΔM_s without the need for a resolution of the V_{cb} puzzle.

The situation is different for $\Delta\Gamma_d/\Delta M_d$, which depends on the apex $(\bar{\rho}, \bar{\eta})$ of the CKM unitarity triangle through λ_u^d/λ_t^d . Thus the SM predictions of $\Delta\Gamma_d/\Delta M_d$ in Eq. (85) and of $\Delta\Gamma_d$ in Eq. (90) assume that not only the predicted quantities are free from new-physics contributions, but also the observables entering the global fit determining $(\bar{\rho}, \bar{\eta})$. Coincidentally, if the fitted values for $(\bar{\rho}, \bar{\eta})$ and thus the value for λ_u^d/λ_t^d in Eq. (73) are correct, the linear and quadratic terms in the square bracket of Eq. (55) almost exactly cancel in $\Delta\Gamma_d$ (which is proportional to the real part of the square bracket) [12]. As a consequence, for the values in Eq. (73) we find $\Delta\Gamma_d/\Delta M_d \simeq \Delta\Gamma_s/\Delta M_s$.

5.2.3 $\Delta\Gamma_q/\Delta M_q$ versus $\Delta\Gamma_q$ and ΔM_q

We are now in the position to confront the ratio $\Delta\Gamma_q/\Delta M_q$ ($q = d, s$) with the individual predictions for $\Delta\Gamma_q$ and ΔM_q which is done in Fig. 6. The $|V_{cb}|$ controversy in Eq. (74) (red versus blue vertical and orange versus purple horizontal strips) prevents any conclusion on possible new physics from ΔM_d or ΔM_s alone. As stated above, the predictions for $\Delta\Gamma_s$ and ΔM_s depend on no other CKM parameters than $|V_{cb}|$ and we can label the corresponding predictions with “excl” and “incl”.

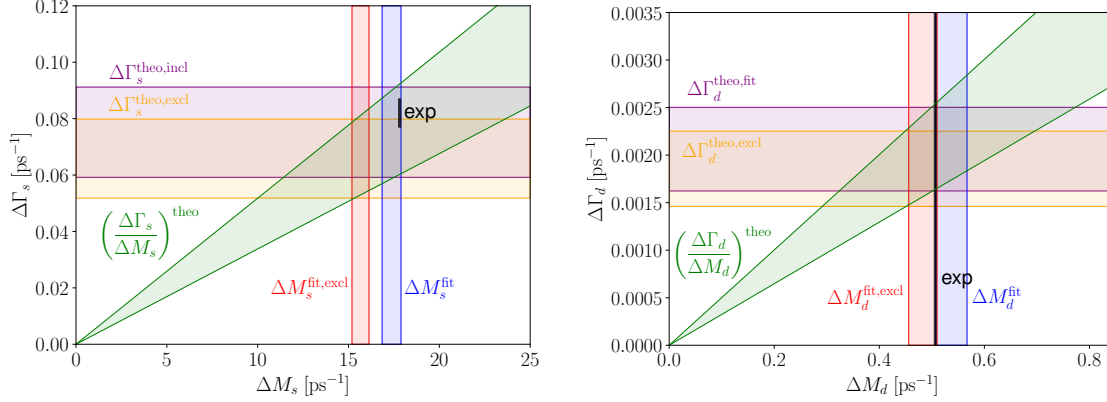


Figure 6: $\Delta\Gamma_q$ versus ΔM_q for the B_s (left) and B_d (right) schemes. The different horizontal and vertical coloured bands refer to different input values for $|V_{cb}|$. The bands for $\Delta\Gamma_s$ are obtained from a direct calculation according to Eq. (3) using the values for λ_t^s as given in Eq. (76). The band for ΔM_s^{fit} is obtained from the value and 1σ uncertainty given in Ref. [62] where ΔM_s was excluded from the fit. $\Delta M_s^{\text{fit,excl}}$ is the corresponding value rescaled by $|V_{cb}^{\text{excl}}|^2/|V_{cb}^{\text{SM fit}}|^2$. The bands for B_d are completely analogous with the exception of $\Delta\Gamma_d^{\text{theo,fit}}$, which was calculated using $|\lambda_t^{d,\text{SM fit}}|$. The experimental values shown are as given in Eqs. (4) to (8) with the uncertainty on ΔM_s scaled up by a factor of ten for visibility.

In the case of $\Delta\Gamma_d$ and ΔM_d we use the prediction using the CKM parameters from the global fit instead of the $|V_{cb}^{\text{incl}}|$ scenario. To this end we use the CKMFitter result from a fit in which ΔM_d has not been used to delimit the allowed region for ΔM_d . The fit result corresponds to $|\lambda_t^{d,\text{SM fit}}|$ in Eq. (76) which is then used for the band for $\Delta\Gamma_d$. For the case that the true value is $|V_{cb}^{\text{excl}}|$, one cannot easily determine the allowed regions in Fig. 6 because the small value of $|V_{cb}^{\text{excl}}|$ gives a very bad fit to $(\bar{\rho}, \bar{\eta})$. For simplicity, we choose the same $(\bar{\rho}, \bar{\eta})$ as for ΔM_d^{fit} , i.e. we simply rescale $\Delta\Gamma_d$ and ΔM_d by the corresponding values of $|V_{cb}|^2$ in Fig. 6, as explained after Eq. (76).

Clearly the experimental uncertainty of $\Delta\Gamma_d$ is much bigger than that of the theoretical prediction at present, calling for a better measurement.

In conclusion, a combined analysis of ΔM_q and $\Delta\Gamma_q$ adds important information because the SM prediction of $\Delta\Gamma_q/\Delta M_q$, shown as green wedge, is independent of $|V_{cb}|$ and one can disentangle the probe of new physics from the determination of CKM parameters.

5.3 a_{fs}^q

Before presenting our results for a_{fs}^q , let us briefly discuss possible measurements of the observable. A flavour-specific $B_q \rightarrow f$ decay is defined by the property that $B_q \rightarrow f$ is

allowed while $B_q \rightarrow \bar{f}$ and $\bar{B}_q \rightarrow f$ are forbidden. Here \bar{f} is the CP conjugate final state to f . Traditionally one uses semileptonic decays with $f = X\ell^+\nu_\ell$ and $\bar{f} = \bar{X}\ell^-\bar{\nu}_\ell$. But to gain statistics, it is desirable to include as many flavour-specific decays as possible into the measurement of a_{fs}^q . For instance, a_{fs}^d can be measured as well with $B_d \rightarrow J/\psi K^+\pi^-$, $B_d \rightarrow D_s^+ D^-$, $B_d \rightarrow D^- K^+$, and many more decays.

a_{fs}^q is related to the time-dependent decay rates as

$$\frac{\Gamma(\bar{B}_q(t) \rightarrow f) - \Gamma(B_q(t) \rightarrow \bar{f})}{\Gamma(\bar{B}_q(t) \rightarrow f) + \Gamma(B_q(t) \rightarrow \bar{f})} = a_{\text{fs}}^q + a_{\text{CP}}^{\text{dir}}, \quad (91)$$

where $B_q(t)$ denotes a meson tagged as B_q at time $t = 0$ with an analogous definition of $\bar{B}_q(t)$. For $t > 0$ a non-zero a_{fs}^q is generated, because an initially produced \bar{B}_q oscillates into B_q which then decays to f .

$$a_{\text{CP}}^{\text{dir}} = \frac{\Gamma(B_q \rightarrow f) - \Gamma(\bar{B}_q \rightarrow \bar{f})}{\Gamma(B_q \rightarrow f) + \Gamma(\bar{B}_q \rightarrow \bar{f})} \quad (92)$$

is the direct CP asymmetry in the studied decay. Usually $a_{\text{CP}}^{\text{dir}}$ is omitted when Eq. (91) is quoted, because $a_{\text{CP}}^{\text{dir}}$ is zero in the SM for semileptonic decays. Yet this is not true for e.g. $B_d \rightarrow J/\psi K^+\pi^-$ and $B_d \rightarrow D_s^+ D^-$.

It is well-known that a_{fs}^q can be measured without the need for flavour tagging. With the time-dependent untagged decay rate

$$\Gamma[f, t] = \Gamma(B_q(t) \rightarrow f) + \Gamma(\bar{B}_q(t) \rightarrow f). \quad (93)$$

one finds

$$a_{\text{fs,unt}}^q(t) \equiv \frac{\Gamma[f, t] - \Gamma[\bar{f}, t]}{\Gamma[f, t] + \Gamma[\bar{f}, t]} = a_{\text{CP}}^{\text{dir}} + \frac{a_{\text{fs}}^q}{2} \left(1 - (a_{\text{CP}}^{\text{dir}})^2\right) \left(1 - \frac{\cos(\Delta M_q t)}{\cosh(\Delta \Gamma_q t/2)}\right). \quad (94)$$

In all formulae terms of order $(a_{\text{fs}}^q)^2$ are neglected. While the time dependence drops out of Eq. (91), this is not the case for Eq. (94). Tracking the oscillatory time dependence helps to disentangle a_{fs}^q from $a_{\text{CP}}^{\text{dir}}$ and possible experimental detection asymmetries [87].

Our results for the CP asymmetry in flavour-specific decays for the B_s system read

$$\begin{aligned} a_{\text{fs}}^s &= \left(2.28_{-0.04}^{+0.01}_{\text{scale}} \pm 0.01_{\text{scale}, 1/m_b} \pm 0.01_{B\tilde{B}_S} \pm 0.06_{1/m_b} \pm 0.07_{\text{input}}\right) \times 10^{-5} \text{ (pole)}, \\ a_{\text{fs}}^s &= \left(2.25_{-0.19}^{+0.10}_{\text{scale}} \pm 0.01_{\text{scale}, 1/m_b} \pm 0.01_{B\tilde{B}_S} \pm 0.06_{1/m_b} \pm 0.07_{\text{input}}\right) \times 10^{-5} \text{ (}\overline{\text{MS}}\text{)}, \\ a_{\text{fs}}^s &= \left(2.31_{-0.07}^{+0.03}_{\text{scale}} \pm 0.01_{\text{scale}, 1/m_b} \pm 0.01_{B\tilde{B}_S} \pm 0.06_{1/m_b} \pm 0.07_{\text{input}}\right) \times 10^{-5} \text{ (PS)}, \end{aligned} \quad (95)$$

and for the B_d system we have

$$a_{\text{fs}}^d = - \left(5.21_{-0.09}^{+0.00}_{\text{scale}} \pm 0.03_{\text{scale}, 1/m_b} \pm 0.03_{B\tilde{B}_S} \pm 0.14_{1/m_b} \pm 0.16_{\text{input}}\right) \times 10^{-4} \text{ (pole)},$$

$$\begin{aligned}
a_{\text{fs}}^d &= - \left(5.15_{-0.43}^{+0.21}_{\text{scale}} \pm 0.03_{\text{scale}, 1/m_b} \pm 0.03_{B\tilde{B}_S} \pm 0.14_{1/m_b} \pm 0.16_{\text{input}} \right) \times 10^{-4} \text{ (}\overline{\text{MS}}\text{)}, \\
a_{\text{fs}}^d &= - \left(5.28_{-0.17}^{+0.08}_{\text{scale}} \pm 0.03_{\text{scale}, 1/m_b} \pm 0.03_{B\tilde{B}_S} \pm 0.14_{1/m_b} \pm 0.16_{\text{input}} \right) \times 10^{-4} \text{ (PS)}. \quad (96)
\end{aligned}$$

As before, we separately add the various uncertainties in quadrature for the upper and lower bounds, symmetrise the total uncertainty in each scheme, and average the results for the $\overline{\text{MS}}$ and PS schemes to obtain

$$\begin{aligned}
a_{\text{fs}}^s &= (2.28 \pm 0.14) \times 10^{-5}, \\
a_{\text{fs}}^d &= -(5.21 \pm 0.32) \times 10^{-4}. \quad (97)
\end{aligned}$$

To a large extent we observe the same pattern in the uncertainties as for $\Delta\Gamma_q/\Delta M_q$. However, there is an important difference since the uncertainty from the parameter variation is of the about the same size as the one from the power-suppressed operator matrix elements. This is due to the parameters λ_u^q/λ_t^q and m_c , which dominate the “input” uncertainties with contributions of comparable size.

Note that in the limit $m_c \rightarrow 0$ the CP asymmetries vanish. It is interesting to note that the contribution beyond the leading m_c contribution only amounts to 13% for both a_{fs}^s and a_{fs}^d in both the PS and $\overline{\text{MS}}$ scheme.

In the following, we discuss the dependence on the scale $\mu_1 = \mu_b = \mu_c$ in analogy to $\Delta\Gamma_q/\Delta M_q$ in the previous subsection. In particular, we focus again on the $\overline{\text{MS}}$ and PS schemes and show results for the pole scheme only for reference.

In Fig. 7 we show the μ_1 dependence of the leading $1/m_b$ contribution of a_{fs}^s and a_{fs}^d and keep the scale in the power-suppressed terms fixed. For the $\overline{\text{MS}}$ and PS scheme LO, NLO and NNLO predictions are shown. Similarly to Fig. 4 we observe in both schemes a decreased dependence on μ_1 for the higher order perturbative corrections. For both a_{fs}^s and a_{fs}^d the NNLO terms are about a factor of 3 smaller than the NLO corrections at the central scale $\mu_1 = 4.2$ GeV in the PS scheme. Both for a_{fs}^s and a_{fs}^d we observe a good convergence of the perturbative series and an overlap of the bands from the variation of μ_1 .

The NNLO prediction in the PS scheme is impressively flat and shows a variation of only about 5% for both a_{fs}^s and a_{fs}^d . For small values of μ_1 the $\overline{\text{MS}}$ and PS schemes agree. However, in contrast to Figs. 4 and 5, the μ_1 dependence in the $\overline{\text{MS}}$ is worse than the one in the PS scheme and a variation of about 13% is observed for both a_{fs}^s and a_{fs}^d .

The current experimental uncertainty for a_{fs}^d is too big to draw conclusions about possible deviations from the SM prediction. However, it is interesting to note that the NNLO predictions are well inside the experimental band.

For comparison we show in Fig. 7 also the NNLO prediction in the pole scheme. In contrast to $\Delta\Gamma_q/\Delta M_q$ it shows a flat behaviour and it is furthermore very close to the result in the PS scheme.

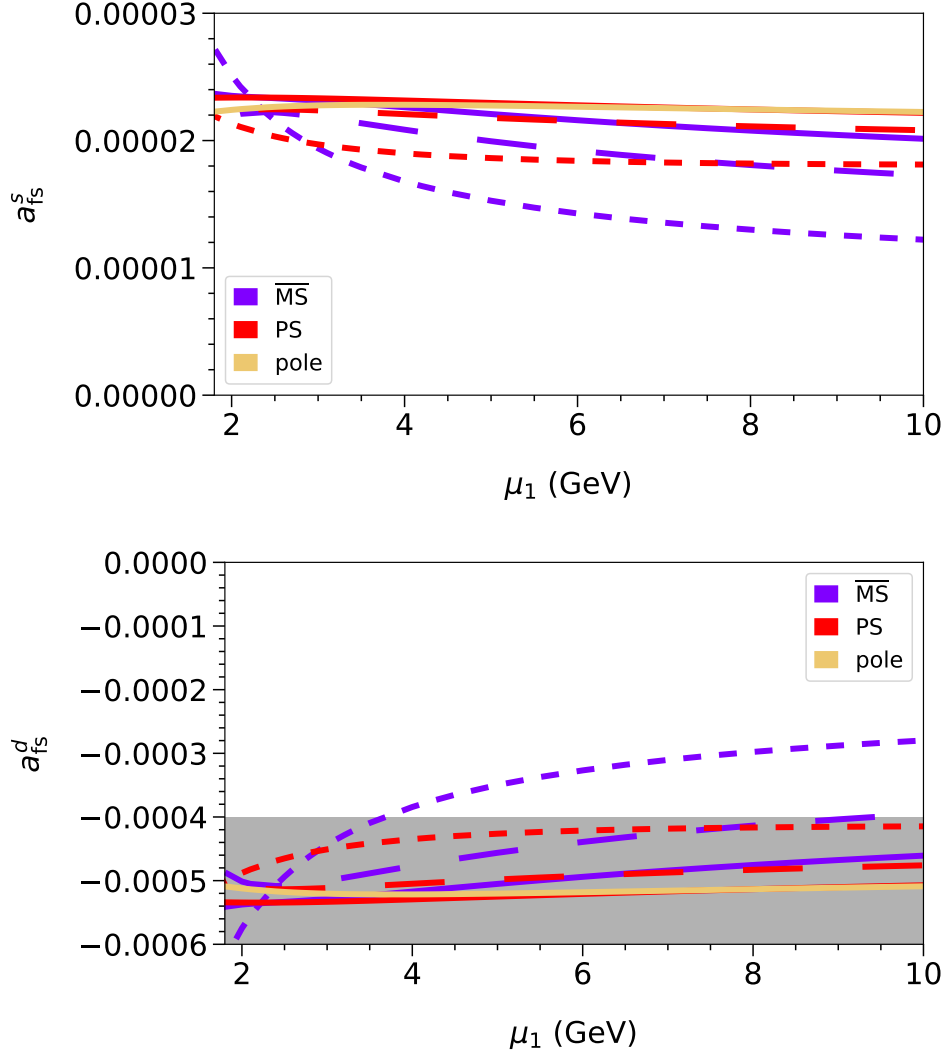


Figure 7: Renormalisation scale dependence at LO (short dashes), NLO (long dashes) and NNLO (solid) for a_{fs}^s (top) and a_{fs}^d (bottom). The scale in the power-suppressed terms is kept fixed. The grey band represents the 1σ experimental error of a_{fs}^d from Eq. (9).

Finally we come back to the plot on the right panel of Fig. 1 and discuss how a measurement of a_{fs}^d constrains the parameters $\bar{\rho}$ and $\bar{\eta}$ from the improved [88,89] Wolfenstein [90] parametrisation of the CKM matrix. We follow Ref. [12] and write a_{fs}^d as

$$a_{\text{fs}}^d = \left[a \text{Im} \frac{\lambda_u^d}{\lambda_t^d} + b \text{Im} \frac{(\lambda_u^d)^2}{(\lambda_t^d)^2} \right] \times 10^{-4}, \quad (98)$$

with

$$\frac{\lambda_u^d}{\lambda_t^d} = \frac{1 - \bar{\rho} - i\bar{\eta}}{(1 - \bar{\rho})^2 + \bar{\eta}^2} - 1. \quad (99)$$

$\overline{\text{MS}}$	LO	NLO	NNLO	PS	LO	NLO	NNLO
a_0	$8.20^{+4.20}_{-1.94}$	$10.47^{+0.76}_{-1.48}$	$11.46^{+0.51}_{-1.00}$	a_0	$9.53^{+1.17}_{-0.39}$	$11.18^{+0.26}_{-0.53}$	$11.77^{+0.18}_{-0.40}$
b_0	$0.069^{+0.037}_{-0.020}$	$0.112^{+0.043}_{-0.020}$	$0.134^{+0.042}_{-0.022}$	b_0	$0.081^{+0.011}_{-0.009}$	$0.122^{+0.027}_{-0.008}$	$0.140^{+0.034}_{-0.015}$

Table 3: Our results for the values a_0 and b_0 in the $\overline{\text{MS}}$ (left) and PS (right) schemes which form the basis of Fig. 8. Note that the uncertainty shown here refers to the perturbative scale uncertainty from varying $\mu_1 = \mu_b = \mu_c$ simultaneously between 2.1 GeV and 8.4 GeV.

From our calculation we can predict the quantities a and b in Eq. (98) to LO, NLO and NNLO. We separate a and b into the leading $1/m_b$ and sub-leading $1/m_b$ contributions,

$$\begin{aligned} a &= a_0 + a_1, \\ b &= b_0 + b_1, \end{aligned} \tag{100}$$

where the subscripts 0 and 1 indicate the leading and sub-leading terms, respectively. Our results for the leading term in the $\overline{\text{MS}}$ and PS schemes are given in Tab. 3. The sub-leading contributions read

$$\begin{aligned} a_1 &= 0.622^{+0.073}_{-0.020_{\text{scale}}, 1/m_b} \pm 0.43_{\text{para}}, \\ b_1 &= 0.091^{+0.011}_{-0.003_{\text{scale}}, 1/m_b} \pm 0.046_{\text{para}}, \end{aligned}$$

which are identical for all schemes and orders as they are only known to LO. The uncertainties given here are the perturbative scale uncertainty from varying $\mu_1 = \mu_b = \mu_c$ simultaneously between 2.1 GeV and 8.4 GeV and the combined uncertainties of all input parameters to our calculation. This means that all sources of uncertainties labelled with $B\tilde{B}_S$, $1/m_b$ and input in Eq. (96) have been added in quadrature. Therefore, our leading $1/m_b$ predictions a_0 and b_0 are free of input uncertainties.

If we use for the left-hand side of Eq. (98) the experimentally measured result and insert Eq. (99) into Eq. (98), we obtain a constraint in the $\bar{\rho}-\bar{\eta}$ plane. In Fig. 8 we show the constraints that would arise from an experimental measurement of $(a_{\text{fs}}^d)^{\text{exp}} = -5 \times 10^{-4}$. The plots on the top show LO, NLO and NNLO results for both the $\overline{\text{MS}}$ and PS schemes. The bands indicate the combined scale uncertainty of the leading and sub-leading terms in the HQE, which are obtained by varying $\mu_1 = \mu_b = \mu_c$ between 2.1 GeV and 8.4 GeV. The lower panel compares the NNLO results for both schemes. Furthermore, it contains results for $(a_{\text{fs}}^d)^{\text{exp}} = -1 \times 10^{-3}$ (green and red bands on the right). For reference we also show the currently favoured CKM triangle [62].

One observes that with increasing order of perturbation theory the widths of the bands decrease significantly. In the case of the $\overline{\text{MS}}$ scheme the NLO band is completely contained within the LO band. Furthermore, there is a significant overlap of the NNLO and NLO bands. In general, the uncertainties in the PS scheme are smaller. Here we observe only a small overlap of the NNLO and NLO bands. However, the NNLO band is completely contained in the NNLO band of the $\overline{\text{MS}}$.

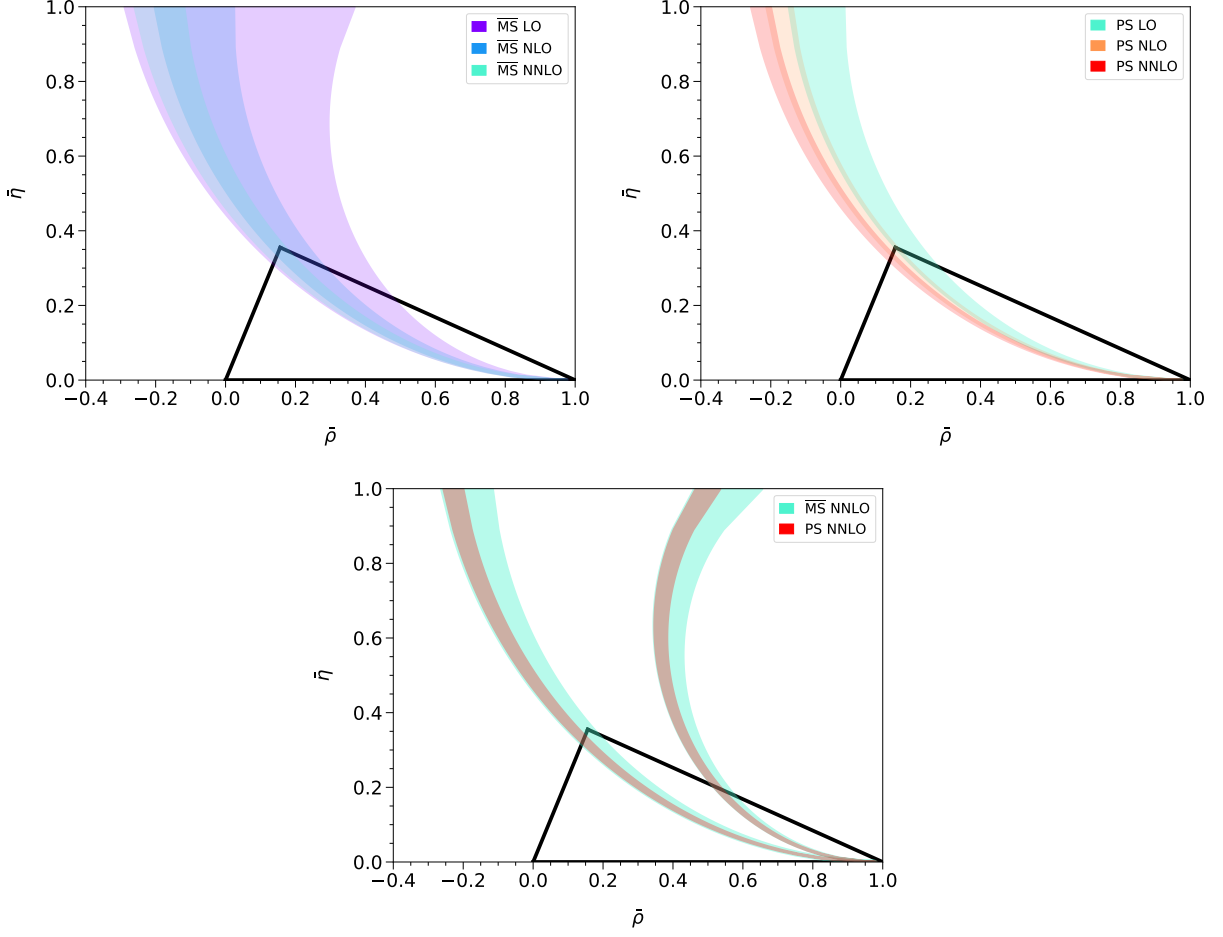


Figure 8: Constraints on the apex of the CKM triangle in the $(\bar{\rho}, \bar{\eta})$ plane, assuming a measurement of $(a_{\text{fs}}^d)^{\text{exp}} = -5 \times 10^{-4}$. In the top row LO, NLO and NNLO results are shown for the $\overline{\text{MS}}$ and PS scheme. In the lower panel we compare the NNLO results in both schemes and also show solutions for $(a_{\text{fs}}^d)^{\text{exp}} = -1 \times 10^{-3}$ (bands on the right). Note that the NNLO PS band is completely contained in the $\overline{\text{MS}}$ band. The current global average of the CKM triangle is shown in black [62].

Fig. 8 is an extension of Fig. 3 in Ref. [12] to NNLO, where it is worth noting that the authors of [12] chose to plot the constraints arising from the averages of the pole and $\overline{\text{MS}}$ schemes. The $\overline{\text{MS}}$ results that we provide, and which are the basis for our Fig. 8, are consistent with Ref. [12] up to NLO.

6 Conclusions

In this paper we have computed the NNLO corrections induced by current-current operators to the decay matrix element Γ_{12}^q appearing in $B_q - \bar{B}_q$ mixing. The result is expressed as a deep semi-analytic expansion in $z = m_c^2/m_b^2$, which for all relevant values of the charm and bottom quark masses is equivalent to an exact result.

The new results are used to perform a phenomenological analysis of the width difference $\Delta\Gamma_q$ and the CP asymmetry in flavour-specific B_q decays, a_{fs}^q , both for the B_s and the B_d system. The corrections of order α_s^2 significantly stabilise the dependence on the renormalisation scale and thus lead to a reduction of the uncertainties.

We provide computer-readable results for the matching coefficients [30] which can be combined with the non-perturbative matrix elements in a straightforward way.

For a further reduction of the uncertainty it would be important to obtain more precise results for the matrix elements of the dimension-7 operators. Furthermore, it is desirable to compute the corresponding NLO and NNLO contributions from the penguin operators to the leading term matching coefficient in the $1/m_b$ expansion. At the central scale their numerical effect is expected to be small. However, their inclusion could lead to an even more stable dependence on the renormalisation scale.

The calculated quantities permit to probe new physics in mass or decay matrix of the B_s and B_d systems from $B - \bar{B}$ mixing observables alone, without the information from a global fit to CKM parameters, which is sensitive to new physics as well. To this end more experimental effort on the determination of $\Delta\Gamma_d$ and $a_{\text{fs}}^{d,s}$ is highly desirable.

Acknowledgements

The work was supported by the Deutsche Forschungsgemeinschaft (DFG, German Research Foundation) under grant 396021762 — TRR 257 “Particle Physics Phenomenology after the Higgs Discovery”. We would like to thank Artyom Hovhannisyan for providing to us unpublished results from Ref. [17]. Pascal Reek would like to thank the Studienstiftung des deutschen Volkes for supporting him.

A Renormalisation constants of the $\Delta B = 2$ theory

Computer-readable files are provided for the renormalisation constants of the $\Delta B = 2$ theory up to α_s^2 and up to third⁴ generation evanescent operators in Ref. [30]. We supply the renormalisation constants in the $\{Q, Q_S, \tilde{Q}_S\}$ and $\{Q, \tilde{Q}_S, R_0\}$ bases. For the latter

⁴The third generation is not required for the current-current calculation, but we provide the renormalisation constants for completeness.

we quote the “naive” renormalisation constants as well as the ones that include the ϵ -finite renormalisation of R_0 , see Section 2.5. The specific choice of $\mathcal{O}(\epsilon)$ coefficients given in Eq. (26) and Eqs. (31) to (34) has been used here to simplify the expressions. The notation of the files and their contents is explained in the `README` file provided with them.

B Vacuum insertion approximation

The leading term of the $1/N_c$ expansion of the $\Delta B = 2$ matrix elements can be calculated analytically by factorising the matrix elements of the four-quark operators into two current matrix elements. At sub-leading order in $1/N_c$ the factorisation of the matrix element is an approximation, called vacuum insertion approximation (VIA). This is illustrated for \tilde{Q}_S in the following, highlighting the step in which Fierz symmetry is crucial.

With $\Gamma \equiv (1 + \gamma_5)$ we calculate this matrix element in VIA to find

$$\langle B_s | \tilde{Q}_S | \bar{B}_s \rangle \stackrel{\text{VIA}}{=} 2\Gamma_{jk}\Gamma_{lm} \left[\langle B_s | \bar{s}_j^\alpha b_k^\beta | 0 \rangle \langle 0 | \bar{s}_l^\beta b_m^\alpha | \bar{B}_s \rangle - \langle B_s | \bar{s}_j^\alpha b_m^\alpha | 0 \rangle \langle 0 | \bar{s}_l^\beta b_k^\beta | \bar{B}_s \rangle \right]. \quad (101)$$

Here j, k, l, m are Dirac indices and α, β are colour indices. While in the first term we immediately recognise the matrix element of the pseudoscalar current, we need a Fierz transformation to contract the indices of the Dirac matrices with those of the quark fields:

$$\langle B_s | \tilde{Q}_S | \bar{B}_s \rangle \stackrel{\text{VIA}}{=} 2 \langle B_s | \bar{s}^\alpha \Gamma b^\beta | 0 \rangle \langle 0 | \bar{s}^\beta \Gamma b^\alpha | \bar{B}_s \rangle - \langle B_s | \bar{s}^\alpha \Gamma^F b^\alpha | 0 \rangle \langle 0 | \bar{s}^\beta \Gamma^F b^\beta | \bar{B}_s \rangle \quad (102)$$

with

$$\Gamma_{jm}^F \Gamma_{lk}^F = \frac{1}{2} \Gamma_{jm} \Gamma_{lk} + \frac{1}{8} [\sigma_{\mu\nu} (1 + \gamma_5)]_{jm} [\sigma^{\mu\nu} (1 + \gamma_5)]_{lk}, \quad (103)$$

where only the first term gives a non-zero contribution to Eq. (102). Thus

$$\begin{aligned} \langle B_s | \tilde{Q}_S(\mu_2) | \bar{B}_s \rangle &\stackrel{\text{VIA}}{=} \left(\frac{2}{N_c} - 1 \right) \langle B_s | \bar{s} \gamma_5 b | 0 \rangle \langle 0 | \bar{s} \gamma_5 b | \bar{B}_s \rangle \\ &= \left(1 - \frac{2}{N_c} \right) \frac{f_{B_s}^2 M_{B_s}^4}{[m_b(\mu_2) + m_s(\mu_2)]^2}. \end{aligned} \quad (104)$$

Here M_{B_s} and f_{B_s} are mass and decay constant of the B_s meson, $N_c = 3$ is the number of colours, and we show the dependence of the matrix element on the renormalisation scale μ_2 at which our $\Delta B = 2$ operator \tilde{Q}_S is defined. In VIA the μ_2 dependence enters the result only through the quark masses $m_{b,s}(\mu_2)$.

Importantly, the VIA result in Eq. (104) is exact in the limit $N_c \rightarrow \infty$. The VIA result also includes a colour-suppressed term at $1/N_c$, which is referred to as the factorisable $1/N_c$ correction. Comparing VIA with the lattice-QCD prediction of $\langle B_s | \tilde{Q}_S | \bar{B}_s \rangle$ shows that VIA gives a good approximation, i.e. non-factorisable corrections are small. This is remarkable, because there is a large cancellation between 1 and $2/N_c$ in Eq. (104).

Since $\langle B_s | \tilde{Q}_S | \bar{B}_s \rangle$ is uniquely fixed in terms of quantities like f_{B_s} (which could be determined through other measurements), the Wilson coefficient of \tilde{Q}_S must be also unique in the large- N_c limit. This feature also means that the coefficient is Fierz-symmetric, because the large- N_c term in Eq. (104) stems from Γ^F . If one defined the evanescent operators in an arbitrary way, one would find arbitrary, scheme-dependent terms in the large- N_c part of the coefficient in order α_s and beyond, and there is no term in Eq. (104) to cancel this scheme-dependence.

In other words, \tilde{Q}_S and \tilde{Q}_S^F are identical in four dimensions and both evaluate to the same VIA result in Eq. (104). In the perturbative calculation one is entitled to either work with \tilde{Q}_S or \tilde{Q}_S^F and, of course, the final prediction for physical observables must be the same, which means that the coefficients \tilde{C}_S and \tilde{C}_S^F must be identical as well.

Since the VIA results are good approximations and furthermore are the reference values to which the lattice QCD results are normalised, it is desirable to impose Fierz symmetry also on the sub-leading terms in the colour counting, i.e. exactly. Furthermore, the leading N_c term is uniquely determined.

C Three-loop master integrals

Our phenomenological analysis is based on the approach where the master integrals are computed with the help of a semi-analytic method. However, an important cross check is provided by the analytic computation of the first expansion terms of order⁵ $(m_c^2/m_b^2)^0$ and $(m_c^2/m_b^2)^1$. In this section we briefly describe the computation of the corresponding three-loop master integrals. For the matching coefficient we only need the imaginary part of the master integrals. However, we find it more convenient to compute the complete diagrams and take the imaginary parts afterwards. All integrals have an on-shell external momentum $q^2 = m_b^2$ and internal lines which carry the mass m_b or are massless. Some integrals reduce to vacuum integrals.

For completeness we show in Fig. 9 the one- and two-loop master integrals needed for our calculation. Note that some of the three-loop master integrals factorise; for this reason there are also lower-loop integrals which do not have an imaginary part. The master integrals in Fig. 9 are also needed for the two-loop $\Delta B = 2$ calculation. Thus both real and imaginary parts have to be computed, which is straightforward using standard techniques (see, e.g. Ref. [28]). Analytic expressions for most of them can be found in Ref. [91].

The 27 three-loop master integrals which do not factorise into lower-loop integrals are shown in Fig. 10. Most of the integrals are not available in the literature. The four integrals with only massless propagators can be obtained from MINCER [92] (see,

⁵In this approach the contributions from a closed charm quark loop in the gluon propagator are not considered.

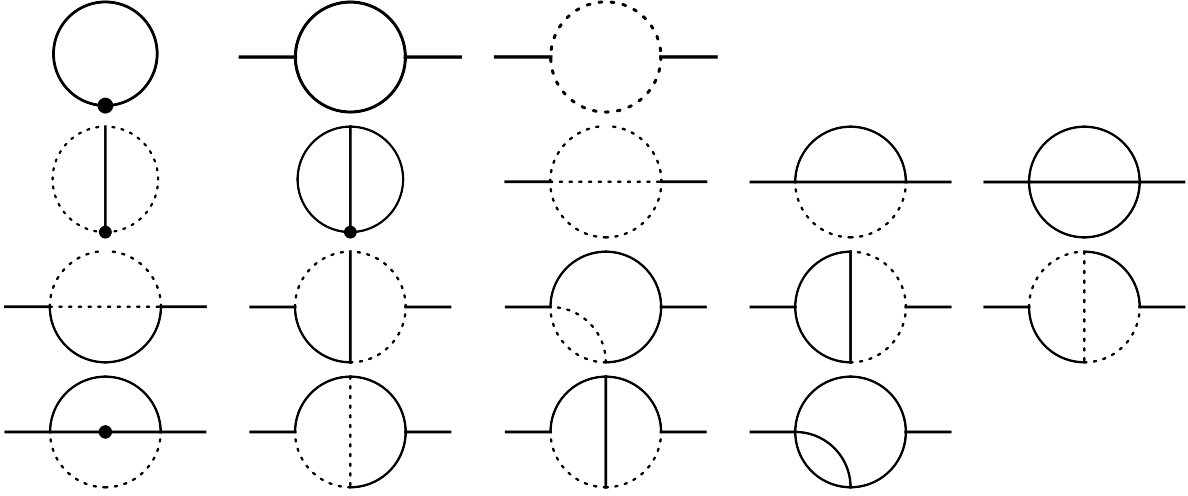


Figure 9: One- and two-loop master integrals. Solid and dotted lines denote massive (mass m_b) and massless propagators, respectively. A dot on a line denotes an additional power of the respective denominator.

e.g. also Refs. [93, 94]). Furthermore, some of them have been calculated in the context of the fermionic NNLO corrections and can be found in Ref. [17, 19]. Among multiple techniques available for the analytic evaluation of Feynman integrals (see, e.g. Ref. [95] for a recent overview), we have chosen the method of direct integration of the Feynman parametric representation using `HYPERINT` [96]. A detailed description of how to use `HYPERINT` for tackling this class of integrals can be found in [21]. Upon processing the results with `HYPERLOGPROCEDURES` [97] and `POLYLOGTOOLS` [98] we can rewrite the imaginary part of each master integral in terms of simple constants given by

$$\pi, \log(2), \zeta_2, \zeta_3, \zeta_4, \text{Cl}_2\left(\frac{\pi}{3}\right), \sqrt{3}, \text{Li}_4\left(\frac{1}{2}\right), \log\left(\frac{1+\sqrt{5}}{2}\right). \quad (105)$$

The real parts of the master integrals are admittedly much more complicated and still involve multiple constant GPLs, but since those are irrelevant for $\Delta\Gamma_s$, we do not discuss them here.

In the following we present the analytic results for the imaginary parts of those master integrals which have at least one massive line. We use the normalisation with $(e^{\gamma_E \epsilon}/(i\pi)^{D/2})^3$ and introduce

$$\text{Im}(I_i^3) = \pi M_i^{(3)}. \quad (106)$$

Our results for the non-trivial three-loop integrals read⁶

$$M_1^{(3)} = -\frac{1}{2\epsilon^2} - \frac{5}{2\epsilon} - \frac{17}{2} - \frac{3\zeta_2}{4} + \epsilon \left(-\frac{49}{2} - \frac{15\zeta_2}{4} + \frac{5\zeta_3}{2} \right)$$

⁶The results for purely massless integrals were taken from `MINCER` [92], cf. also Refs. [93, 94].

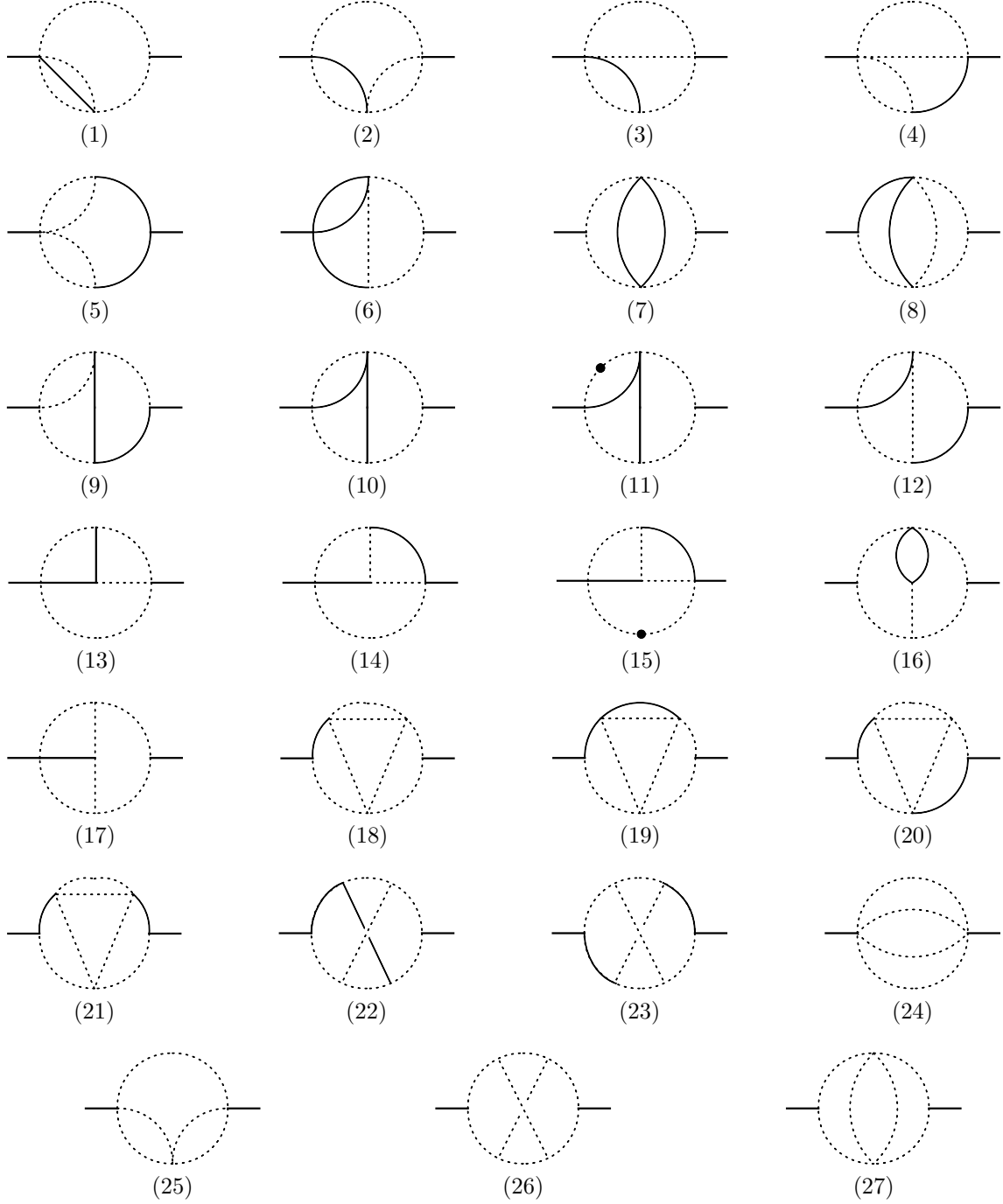


Figure 10: Three-loop master integrals arising from the $\Delta B = 1$ NNLO calculation. Solid and dotted lines denote massive (mass m_b) and massless propagators, respectively. A dot on a line denotes an additional power of the respective denominator.

$$+ \epsilon^2 \left(-\frac{129}{2} - \frac{51\zeta_2}{4} + \frac{25\zeta_3}{2} - \frac{57\zeta_4}{32} \right),$$

$$\begin{aligned}
M_2^{(3)} &= \frac{1}{2\epsilon} + \frac{11}{2} - \zeta_2 + \epsilon \left(\frac{77}{2} - \frac{33\zeta_2}{4} - 8\zeta_3 \right) + \epsilon^2 \left(\frac{439}{2} - \frac{195\zeta_2}{4} - \frac{107\zeta_3}{2} - \frac{123\zeta_4}{4} \right), \\
M_3^{(3)} &= \frac{1}{2\epsilon} + \frac{15}{4} + \epsilon \left(\frac{145}{8} - \frac{9\zeta_2}{4} \right) + \epsilon^2 \left(\frac{1155}{16} - \frac{135\zeta_2}{8} - \frac{11\zeta_3}{2} \right), \\
M_4^{(3)} &= \frac{7}{4} - \zeta_2 + \epsilon \left(\frac{175}{8} - \frac{9\zeta_2}{2} - 11\zeta_3 \right) + \epsilon^2 \left(\frac{2681}{16} - \frac{241\zeta_2}{8} - \frac{99\zeta_3}{2} - \frac{189\zeta_4}{4} \right), \\
M_5^{(3)} &= 2 - 2\sqrt{3}\text{Cl}_2 \left(\frac{\pi}{3} \right) + \zeta_2, \\
M_6^{(3)} &= \frac{1}{2\epsilon^2} + \frac{5}{2\epsilon} + \frac{15}{2} - \frac{\zeta_2}{4} - 2\zeta_3 + \epsilon \left(\frac{29}{2} + \frac{11\zeta_2}{4} - \frac{19\zeta_3}{2} + \frac{3\zeta_4}{2} \right), \\
M_7^{(3)} &= \frac{1}{\epsilon^2} + \frac{7}{\epsilon} + 33 - \frac{17\zeta_2}{2} - \frac{12\zeta_2}{\sqrt{5}} - \frac{48}{5}\zeta_2 \log \left(\frac{1+\sqrt{5}}{2} \right) + \frac{8\zeta_3}{5}, \\
M_8^{(3)} &= \frac{1}{2\epsilon^2} + \frac{7}{2\epsilon} + \frac{33}{2} - \frac{5\zeta_2}{4} - 2\zeta_3 + \epsilon \left(\frac{131}{2} - \frac{35\zeta_2}{4} - \frac{21\zeta_3}{2} - \frac{7\zeta_4}{2} \right), \\
M_9^{(3)} &= 1 + \epsilon(14 - 4\zeta_3) + \epsilon^2 \left(119 - \frac{9\zeta_2}{2} - 28\zeta_3 - 30\zeta_4 \right), \\
M_{10}^{(3)} &= \frac{1}{2\epsilon^2} + \frac{5}{2\epsilon} + \frac{15}{2} + \frac{3\zeta_2}{4} - 3\zeta_2 \log(2) + \frac{5\zeta_3}{4} + \epsilon \left(\frac{29}{2} + \frac{11\zeta_2}{4} \right. \\
&\quad \left. - 6\zeta_2 \log(2) + 4\zeta_3 + 8\text{Li}_4 \left(\frac{1}{2} \right) - \frac{33\zeta_4}{8} - 2\zeta_2 \log^2(2) + \frac{\log^4(2)}{3} \right), \\
M_{11}^{(3)} &= -\frac{\zeta_2}{\epsilon} - 2\zeta_2 - 3\zeta_2 \log(2) - \frac{7\zeta_3}{4} + \epsilon \left(-4\zeta_2 - 6\zeta_2 \log(2) - \frac{7\zeta_3}{2} \right. \\
&\quad \left. + 8\text{Li}_4 \left(\frac{1}{2} \right) - \frac{217\zeta_4}{8} - 2\zeta_2 \log^2(2) + \frac{\log^4(2)}{3} \right), \\
M_{12}^{(3)} &= \frac{1}{\epsilon} + 11 - \zeta_2 - \zeta_3 + \epsilon \left(77 - \frac{23\zeta_2}{2} - 13\zeta_3 - 7\zeta_4 \right), \\
M_{13}^{(3)} &= 1 - \zeta_2 + \zeta_3 + \epsilon(14 - 7\zeta_2 - 3\zeta_3 + 5\zeta_4), \\
M_{14}^{(3)} &= -2 + \zeta_2 - 3\zeta_2 \log(2) + \frac{13\zeta_3}{4} + \epsilon \left(-26 + 4\zeta_2 - 10\zeta_2 \log^2(2) \right. \\
&\quad \left. - 6\zeta_2 \log(2) + \frac{39\zeta_3}{2} + 40\text{Li}_4 \left(\frac{1}{2} \right) - \frac{65\zeta_4}{8} + \frac{5\log^4(2)}{3} \right), \\
M_{15}^{(3)} &= -\frac{\zeta_2}{\epsilon} - 2\zeta_2 - 3\zeta_2 \log(2) - \frac{39\zeta_3}{4} + \epsilon \left(-4\zeta_2 - 6\zeta_2 \log(2) \right. \\
&\quad \left. - 10\zeta_2 \log^2(2) - \frac{39\zeta_3}{2} + 40\text{Li}_4 \left(\frac{1}{2} \right) - \frac{629\zeta_4}{8} + \frac{5\log^4(2)}{3} \right), \\
M_{16}^{(3)} &= -16 + \frac{24\zeta_2}{\sqrt{5}} - \frac{24}{5}\zeta_2 \log \left(\frac{1+\sqrt{5}}{2} \right) - \frac{56\zeta_3}{5},
\end{aligned}$$

$$\begin{aligned}
M_{17}^{(3)} &= 4\zeta_4, \\
M_{18}^{(3)} &= 6\zeta_4, \\
M_{19}^{(3)} &= 5\zeta_4, \\
M_{20}^{(3)} &= \frac{27}{4}\zeta_4, \\
M_{21}^{(3)} &= 6\zeta_4, \\
M_{22}^{(3)} &= \frac{27}{4}\zeta_4, \\
M_{23}^{(3)} &= \frac{61}{4}\zeta_4, \\
M_{24}^{(3)} &= \frac{1}{12} + \frac{71\epsilon}{72} + \epsilon^2 \left(\frac{3115}{432} - \frac{7\zeta_2}{8} \right) + \epsilon^3 \left(\frac{109403}{2592} - \frac{497\zeta_2}{48} - \frac{29\zeta_3}{12} \right) \\
&\quad + \epsilon^4 \left(\frac{3386467}{15552} - \frac{21805\zeta_2}{288} - \frac{2059\zeta_3}{72} + \frac{291\zeta_4}{64} \right), \\
M_{25}^{(3)} &= \frac{1}{\epsilon} + 10 + \epsilon \left(64 - \frac{21\zeta_2}{2} \right) \\
&\quad + \epsilon^2(336 - 105\zeta_2 - 23\zeta_3) + \epsilon^3 \left(1584 - 672\zeta_2 - 230\zeta_3 + \frac{1017\zeta_4}{16} \right), \\
M_{26}^{(3)} &= 0, \\
M_{27}^{(3)} &= \frac{1}{\epsilon^2} + \frac{7}{\epsilon} + 31 - \frac{21\zeta_2}{2} + \epsilon \left(103 - \frac{147\zeta_2}{2} + 7\zeta_3 \right) \\
&\quad + \epsilon^2 \left(235 - \frac{651\zeta_2}{2} + 49\zeta_3 + \frac{1737\zeta_4}{16} \right), \tag{107}
\end{aligned}$$

with the Clausen function

$$\text{Cl}_2 \left(\frac{\pi}{3} \right) = \text{Im} \left(\text{Li}_2(e^{i\frac{\pi}{3}}) \right) \approx 1.014941. \tag{108}$$

Notice that while the massless 8-line integral $I_{26}^{(3)}$ does have a cut, its imaginary part vanishes at $\mathcal{O}(\epsilon^0)$ since the integral itself is finite and proportional to $1/m_b^6$. The imaginary part together with $\log(m_b)$ terms start contributing $\mathcal{O}(\epsilon)$.

In Eqs. 107 we set m_b to unity, since the corresponding prefactor can be trivially recovered using dimensional analysis

$$M_i^{(3)} \rightarrow m_b^{12-2n_p-6\epsilon} \mu^{6\epsilon} M_i^{(3)}, \tag{109}$$

where n_p denotes the number of propagators (including dots) present in the given integral.

All these results have been checked numerically with the help of `pySecDec` [99–101] at different values of m_b using the default precision of the QMC integrator.

D Full results for the $\Delta B = 2$ evanescent operator definitions

Imposing condition 3 on the equations arising from condition 1 for $\{c, \tilde{c}, d, \tilde{d}, h, \tilde{h}\}$, we obtain a particular solution for the constants appearing in the second generation evanescent operators consistent with all physical conditions from Section 2.3. It is given by:

$$\begin{aligned}
c &= \frac{1}{15 N_c^3 (2 + N_c^2)} \left(45568 - 54272 N_c - 151808 N_c^2 - 55808 N_c^3 - 6656 N_c^4 \right. \\
&\quad \left. + 22528 N_c^5 + c^F (-48 - 576 N_c^2 + 30 N_c^3 - 96 N_c^4 + 15 N_c^5) \right. \\
&\quad \left. + \tilde{c}_2^F (-240 N_c - 300 N_c^3 + 90 N_c^5) + d^F (192 + 384 N_c^2 + 144 N_c^4) \right) \\
\tilde{c} &= \frac{1}{15 N_c^3 (2 + N_c^2)} \left(-59392 - 20992 N_c - 177664 N_c^2 - 63616 N_c^3 - 48640 N_c^4 \right. \\
&\quad \left. + 2816 N_c^5 + \tilde{c}^F (-48 - 576 N_c^2 + 30 N_c^3 - 96 N_c^4 + 15 N_c^5) \right. \\
&\quad \left. + c_2^F (-240 N_c - 300 N_c^3 + 90 N_c^5) + \tilde{d}^F (192 + 384 N_c^2 + 144 N_c^4) \right) \\
d &= \frac{1}{30 N_c^3 (2 + N_c^2)} \left(79744 - 94976 N_c - 265664 N_c^2 - 112384 N_c^3 + 21952 N_c^4 \right. \\
&\quad \left. + 47424 N_c^5 + c^F (-84 - 1008 N_c^2 - 93 N_c^4) + \tilde{c}_2^F (-420 N_c - 600 N_c^3 + 195 N_c^5) \right. \\
&\quad \left. + d^F (336 + 672 N_c^2 + 60 N_c^3 + 252 N_c^4 + 30 N_c^5) \right) \\
\tilde{d} &= \frac{1}{30 N_c^3 (2 + N_c^2)} \left(-103936 - 36736 N_c - 310912 N_c^2 - 123008 N_c^3 - 74560 N_c^4 \right. \\
&\quad \left. + 11328 N_c^5 + \tilde{c}^F (-84 - 1008 N_c^2 - 93 N_c^4) + c_2^F (-420 N_c - 600 N_c^3 + 195 N_c^5) \right. \\
&\quad \left. + \tilde{d}^F (336 + 672 N_c^2 + 60 N_c^3 + 252 N_c^4 + 30 N_c^5) \right) \\
h &= \frac{4}{-14 - 14 N_c - 7 N_c^2 + 6 N_c^3} \left(1568 + 2528 N_c - 368 N_c^2 - 480 N_c^3 \right. \\
&\quad \left. + k (-4 - 4 N_c - 2 N_c^2 + N_c^3) + \tilde{k} (-10 - 20 N_c + 5 N_c^2 + 5 N_c^3) \right) \\
c_2 &= \frac{3584}{5} + c_2^F + \frac{12}{5} \tilde{c}^F - \frac{8}{5} \tilde{d}^F \\
\tilde{c}_2 &= \frac{3456}{5} + \frac{12}{5} c^F + \tilde{c}_2^F - \frac{8}{5} d^F \\
d_2 &= \frac{896}{5} + \frac{1}{4} c_2^F + \frac{3}{5} \tilde{c}^F - \frac{2}{5} \tilde{d}^F \\
\tilde{d}_2 &= \frac{2144}{5} + \frac{3}{5} c^F + \frac{1}{4} \tilde{c}_2^F - \frac{2}{5} d^F \\
d_2^F &= \frac{1}{4} c_2^F \\
\tilde{d}_2^F &= 256 + \frac{1}{4} \tilde{c}_2^F
\end{aligned}$$

$$\tilde{h} = -448 + 4\tilde{k} \quad (110)$$

It can be checked that the leading $\mathcal{O}(N_c^2)$ term of the renormalised physical matrix elements does not depend on the remaining undetermined constant in the evanescent operator definitions.

We provide the generic solution quoted above as well as the specific choice given in Eq. (26) and Eqs. (31) to (34) in computer-readable format which can be downloaded from Ref. [30]. The notation of the files and their contents are described in a separate **README** file.

References

- [1] LHCb collaboration, *Precise determination of the B_s^0 - \bar{B}_s^0 oscillation frequency*, *Nature Phys.* **18** (2022) 1 [2104.04421].
- [2] HFLAV collaboration, *Averages of b -hadron, c -hadron, and τ -lepton properties as of 2021*, *Phys. Rev. D* **107** (2023) 052008 [2206.07501].
- [3] A.J. Buras and P.H. Weisz, *QCD Nonleading Corrections to Weak Decays in Dimensional Regularization and 't Hooft-Veltman Schemes*, *Nucl. Phys. B* **333** (1990) 66.
- [4] A.J. Buras, M. Jamin, M.E. Lautenbacher and P.H. Weisz, *Effective Hamiltonians for $\Delta S = 1$ and $\Delta B = 1$ nonleptonic decays beyond the leading logarithmic approximation*, *Nucl. Phys. B* **370** (1992) 69.
- [5] A.J. Buras, M. Jamin, M.E. Lautenbacher and P.H. Weisz, *Two loop anomalous dimension matrix for $\Delta S = 1$ weak nonleptonic decays I: $\mathcal{O}(\alpha_s^2)$* , *Nucl. Phys. B* **400** (1993) 37 [hep-ph/9211304].
- [6] P. Gambino, M. Gorbahn and U. Haisch, *Anomalous Dimension Matrix for Radiative and Rare Semileptonic B Decays Up to Three Loops*, *Nucl. Phys. B* **673** (2003) 238 [hep-ph/0306079].
- [7] M. Gorbahn and U. Haisch, *Effective Hamiltonian for non-leptonic $|\Delta F| = 1$ decays at NNLO in QCD*, *Nucl. Phys. B* **713** (2005) 291 [hep-ph/0411071].
- [8] M. Gorbahn, U. Haisch and M. Misiak, *Three-loop mixing of dipole operators*, *Phys. Rev. Lett.* **95** (2005) 102004 [hep-ph/0504194].
- [9] A.J. Buras, W. Slominski and H. Steger, *$B^0 - \bar{B}^0$ Mixing, CP Violation and the B Meson Decay*, *Nucl. Phys. B* **245** (1984) 369.
- [10] M. Beneke, G. Buchalla and I. Dunietz, *Width Difference in the $B_s - \bar{B}_s$ System*, *Phys. Rev. D* **54** (1996) 4419 [hep-ph/9605259].

- [11] M. Beneke, G. Buchalla, C. Greub, A. Lenz and U. Nierste, *Next-to-leading order QCD corrections to the lifetime difference of B_s mesons*, *Phys. Lett. B* **459** (1999) 631 [[hep-ph/9808385](#)].
- [12] M. Beneke, G. Buchalla, A. Lenz and U. Nierste, *CP Asymmetry in Flavor Specific B Decays beyond Leading Logarithms*, *Phys. Lett. B* **576** (2003) 173 [[hep-ph/0307344](#)].
- [13] M. Ciuchini, E. Franco, V. Lubicz and F. Mescia, *Next-to-leading order QCD corrections to spectator effects in lifetimes of beauty hadrons*, *Nucl. Phys. B* **625** (2002) 211 [[hep-ph/0110375](#)].
- [14] A. Lenz and U. Nierste, *Theoretical update of $B_s - \bar{B}_s$ mixing*, *JHEP* **06** (2007) 072 [[hep-ph/0612167](#)].
- [15] M. Gerlach, U. Nierste, V. Shtabovenko and M. Steinhauser, *Two-loop QCD penguin contribution to the width difference in $B_s - \bar{B}_s$ mixing*, *JHEP* **07** (2021) 043 [[2106.05979](#)].
- [16] M. Gerlach, U. Nierste, V. Shtabovenko and M. Steinhauser, *The width difference in $B - \bar{B}$ mixing at order α_s and beyond*, *JHEP* **04** (2022) 006 [[2202.12305](#)].
- [17] H.M. Asatrian, A. Hovhannisyan, U. Nierste and A. Yeghiazaryan, *Towards next-to-next-to-leading-log accuracy for the width difference in the $B_s - \bar{B}_s$ system: fermionic contributions to order $(m_c/m_b)^0$ and $(m_c/m_b)^1$* , *JHEP* **10** (2017) 191 [[1709.02160](#)].
- [18] H.M. Asatrian, H.H. Asatryan, A. Hovhannisyan, U. Nierste, S. Tumasyan and A. Yeghiazaryan, *Penguin contribution to the width difference and CP asymmetry in $B_q - \bar{B}_q$ mixing at order $\alpha_s^2 N_f$* , *Phys. Rev. D* **102** (2020) 033007 [[2006.13227](#)].
- [19] A. Hovhannisyan and U. Nierste, *Addendum to: Towards next-to-next-to-leading-log accuracy for the width difference in the $B_s - \bar{B}_s$ system: fermionic contributions to order $(m_c/m_b)^0$ and $(m_c/m_b)^1$* , *JHEP* **06** (2022) 090 [[2204.11907](#)].
- [20] M. Gerlach, U. Nierste, V. Shtabovenko and M. Steinhauser, *Width Difference in the $B - \bar{B}$ System at Next-to-Next-to-Leading Order of QCD*, *Phys. Rev. Lett.* **129** (2022) 102001 [[2205.07907](#)].
- [21] P. Reek, V. Shtabovenko and M. Steinhauser, *B meson mixing at NNLO: technical aspects*, *JHEP* **08** (2024) 002 [[2405.14698](#)].
- [22] G. Alonso-Álvarez, G. Elor and M. Escudero, *Collider signals of baryogenesis and dark matter from B mesons: A roadmap to discovery*, *Phys. Rev. D* **104** (2021) 035028 [[2101.02706](#)].

- [23] S. Laplace, Z. Ligeti, Y. Nir and G. Perez, *Implications of the CP asymmetry in semileptonic B decay*, *Phys. Rev. D* **65** (2002) 094040 [[hep-ph/0202010](#)].
- [24] K.G. Chetyrkin, M. Misiak and M. Munz, $|\Delta F| = 1$ *nonleptonic effective Hamiltonian in a simpler scheme*, *Nucl. Phys. B* **520** (1998) 279 [[hep-ph/9711280](#)].
- [25] S. Herrlich and U. Nierste, *Evanescent operators, scheme dependences and double insertions*, *Nucl. Phys. B* **455** (1995) 39 [[hep-ph/9412375](#)].
- [26] S. Herrlich and U. Nierste, *The Complete $|\Delta S| = 2$ - Hamiltonian in the next-to-leading order*, *Nucl. Phys. B* **476** (1996) 27 [[hep-ph/9604330](#)].
- [27] M. Gorbahn, S. Jager, U. Nierste and S. Trine, *The supersymmetric Higgs sector and $B - \bar{B}$ mixing for large $\tan \beta$* , *Phys. Rev. D* **84** (2011) 034030 [[0901.2065](#)].
- [28] V.A. Smirnov, *Analytic tools for Feynman integrals*, vol. 250 (2012), 10.1007/978-3-642-34886-0.
- [29] J. Fleischer and O.V. Tarasov, *SHELL2: Package for the calculation of two loop on-shell Feynman diagrams in FORM*, *Comput. Phys. Commun.* **71** (1992) 193.
- [30] Ancillary files at: <https://www.ttp.kit.edu/preprints/2025/ttp25-016/>.
- [31] U. Nierste, *Three Lectures on Meson Mixing and CKM phenomenology*, in *Helmholtz International Summer School on Heavy Quark Physics*, pp. 1–38, 3, 2009 [[0904.1869](#)].
- [32] P. Nogueira, *Abusing QGRAF*, *Nucl. Instrum. Meth. A* **559** (2006) 220.
- [33] A. Alloul, N.D. Christensen, C. Degrande, C. Duhr and B. Fuks, *FeynRules 2.0 - A complete toolbox for tree-level phenomenology*, *Comput. Phys. Commun.* **185** (2014) 2250 [[1310.1921](#)].
- [34] T. Hahn, *Generating Feynman diagrams and amplitudes with FeynArts 3*, *Comput. Phys. Commun.* **140** (2001) 418 [[hep-ph/0012260](#)].
- [35] R. Mertig, M. Bohm and A. Denner, *FEYN CALC: Computer algebraic calculation of Feynman amplitudes*, *Comput. Phys. Commun.* **64** (1991) 345.
- [36] V. Shtabovenko, R. Mertig and F. Orellana, *New Developments in FeynCalc 9.0*, *Comput. Phys. Commun.* **207** (2016) 432 [[1601.01167](#)].
- [37] V. Shtabovenko, R. Mertig and F. Orellana, *FeynCalc 9.3: New features and improvements*, *Comput. Phys. Commun.* **256** (2020) 107478 [[2001.04407](#)].
- [38] T. Hahn and M. Perez-Victoria, *Automatized one loop calculations in four-dimensions and D-dimensions*, *Comput. Phys. Commun.* **118** (1999) 153 [[hep-ph/9807565](#)].

- [39] R. Harlander, T. Seidensticker and M. Steinhauser, *Complete corrections of $\mathcal{O}(\alpha\alpha_s)$ to the decay of the Z boson into bottom quarks*, *Phys. Lett. B* **426** (1998) 125 [[hep-ph/9712228](#)].
- [40] T. Seidensticker, *Automatic application of successive asymptotic expansions of Feynman diagrams*, in *6th International Workshop on New Computing Techniques in Physics Research: Software Engineering, Artificial Intelligence Neural Nets, Genetic Algorithms, Symbolic Algebra, Automatic Calculation*, 5, 1999 [[hep-ph/9905298](#)].
- [41] J. Kuipers, T. Ueda, J.A.M. Vermaseren and J. Vollinga, *FORM version 4.0*, *Comput. Phys. Commun.* **184** (2013) 1453 [[1203.6543](#)].
- [42] A.V. Smirnov and F.S. Chukharev, *FIRE6: Feynman Integral REduction with modular arithmetic*, *Comput. Phys. Commun.* **247** (2020) 106877 [[1901.07808](#)].
- [43] R.N. Lee, *LiteRed 1.4: a powerful tool for reduction of multiloop integrals*, *J. Phys. Conf. Ser.* **523** (2014) 012059 [[1310.1145](#)].
- [44] M. Gerlach, F. Herren and M. Lang, *tapir: A tool for topologies, amplitudes, partial fraction decomposition and input for reductions*, *Comput. Phys. Commun.* **282** (2023) 108544 [[2201.05618](#)].
- [45] M. Gerlach, *Three-loop topology analysis of neutral B-meson mixing with tapir*, *J. Phys. Conf. Ser.* **2438** (2023) 012156 [[2205.07483](#)].
- [46] P. Maierhöfer, J. Usovitsch and P. Uwer, *Kira—A Feynman integral reduction program*, *Comput. Phys. Commun.* **230** (2018) 99 [[1705.05610](#)].
- [47] J. Klappert, F. Lange, P. Maierhöfer and J. Usovitsch, *Integral reduction with Kira 2.0 and finite field methods*, *Comput. Phys. Commun.* **266** (2021) 108024 [[2008.06494](#)].
- [48] A.V. Smirnov and V.A. Smirnov, *How to choose master integrals*, *Nucl. Phys. B* **960** (2020) 115213 [[2002.08042](#)].
- [49] M. Fael, F. Lange, K. Schönwald and M. Steinhauser, *A semi-analytic method to compute Feynman integrals applied to four-loop corrections to the $\overline{\text{MS}}$ -pole quark mass relation*, *JHEP* **09** (2021) 152 [[2106.05296](#)].
- [50] M. Fael, F. Lange, K. Schönwald and M. Steinhauser, *Massive Vector Form Factors to Three Loops*, *Phys. Rev. Lett.* **128** (2022) 172003 [[2202.05276](#)].
- [51] M. Fael, F. Lange, K. Schönwald and M. Steinhauser, *Singlet and nonsinglet three-loop massive form factors*, *Phys. Rev. D* **106** (2022) 034029 [[2207.00027](#)].
- [52] M. Fael, F. Lange, K. Schönwald and M. Steinhauser, *Massive three-loop form factors: Anomaly contribution*, *Phys. Rev. D* **107** (2023) 094017 [[2302.00693](#)].

- [53] PARTICLE DATA GROUP collaboration, *Review of particle physics*, *Phys. Rev. D* **110** (2024) 030001.
- [54] K.G. Chetyrkin, J.H. Kuhn, A. Maier, P. Maierhofer, P. Marquard, M. Steinhauser et al., *Addendum to “Charm and bottom quark masses: An update”*, 1710.04249.
- [55] K. Chetyrkin, J.H. Kuhn, A. Maier, P. Maierhofer, P. Marquard, M. Steinhauser et al., *Precise Charm- and Bottom-Quark Masses: Theoretical and Experimental Uncertainties*, *Theor. Math. Phys.* **170** (2012) 217 [1010.6157].
- [56] R.J. Dowdall, C.T.H. Davies, R.R. Horgan, G.P. Lepage, C.J. Monahan, J. Shigemitsu et al., *Neutral B-meson mixing from full lattice QCD at the physical point*, *Phys. Rev. D* **100** (2019) 094508 [1907.01025].
- [57] A. Bazavov et al., *B- and D-meson leptonic decay constants from four-flavor lattice QCD*, *Phys. Rev. D* **98** (2018) 074512 [1712.09262].
- [58] C. Hughes, C.T.H. Davies and C.J. Monahan, *New methods for B meson decay constants and form factors from lattice NRQCD*, *Phys. Rev. D* **97** (2018) 054509 [1711.09981].
- [59] ETM collaboration, *Mass of the b quark and B -meson decay constants from $N_f=2+1+1$ twisted-mass lattice QCD*, *Phys. Rev. D* **93** (2016) 114505 [1603.04306].
- [60] HPQCD collaboration, *B-Meson Decay Constants from Improved Lattice Nonrelativistic QCD with Physical u, d, s, and c Quarks*, *Phys. Rev. Lett.* **110** (2013) 222003 [1302.2644].
- [61] F. Herren and M. Steinhauser, *Version 3 of RunDec and CRunDec*, *Comput. Phys. Commun.* **224** (2018) 333 [1703.03751].
- [62] CKMfitter Group (J. Charles et al.), updated results and plots available at: <http://ckmfitter.in2p3.fr>, *Eur. Phys. J* **C41** (2005) 1 [hep-ph/0406184].
- [63] FLAVOUR LATTICE AVERAGING GROUP (FLAG) collaboration, *FLAG Review 2024*, 2411.04268.
- [64] M. Bordone, B. Capdevila and P. Gambino, *Three loop calculations and inclusive V_{cb}* , *Phys. Lett. B* **822** (2021) 136679 [2107.00604].
- [65] MILC collaboration, *$B \rightarrow D\ell\nu$ form factors at nonzero recoil and $|V_{cb}|$ from 2+1-flavor lattice QCD*, *Phys. Rev. D* **92** (2015) 034506 [1503.07237].
- [66] HPQCD collaboration, *$B \rightarrow D\ell\nu$ form factors at nonzero recoil and extraction of $|V_{cb}|$* , *Phys. Rev. D* **92** (2015) 054510 [1505.03925].

- [67] FERMILAB LATTICE, MILC collaboration, *Semileptonic form factors for $B \rightarrow D^* \ell \nu$ at nonzero recoil from 2 + 1-flavor lattice QCD: Fermilab Lattice and MILC Collaborations*, *Eur. Phys. J. C* **82** (2022) 1141 [2105.14019].
- [68] JLQCD collaboration, *$B \rightarrow D^* \ell \nu_\ell$ semileptonic form factors from lattice QCD with Möbius domain-wall quarks*, *Phys. Rev. D* **109** (2024) 074503 [2306.05657].
- [69] BABAR collaboration, *Measurement of $|V_{cb}|$ and the Form-Factor Slope in $\bar{B} \rightarrow D \ell^- \bar{\nu}_\ell$ Decays in Events Tagged by a Fully Reconstructed B Meson*, *Phys. Rev. Lett.* **104** (2010) 011802 [0904.4063].
- [70] BELLE collaboration, *Measurement of the decay $B \rightarrow D \ell \nu_\ell$ in fully reconstructed events and determination of the Cabibbo-Kobayashi-Maskawa matrix element $|V_{cb}|$* , *Phys. Rev. D* **93** (2016) 032006 [1510.03657].
- [71] BELLE collaboration, *Measurement of the CKM matrix element $|V_{cb}|$ from $B^0 \rightarrow D^{*-} \ell^+ \nu_\ell$ at Belle*, *Phys. Rev. D* **100** (2019) 052007 [1809.03290].
- [72] BELLE collaboration, *Measurement of differential distributions of $B \rightarrow D^* \ell \bar{\nu}_\ell$ and implications on $|V_{cb}|$* , *Phys. Rev. D* **108** (2023) 012002 [2301.07529].
- [73] BELLE-II collaboration, *Determination of $|V_{cb}|$ using $\bar{B}^0 \rightarrow D^{*+} \ell^- \bar{\nu}_\ell$ decays with Belle II*, *Phys. Rev. D* **108** (2023) 092013 [2310.01170].
- [74] F. Bernlochner, M. Fael, K. Olschewsky, E. Persson, R. van Tonder, K.K. Vos et al., *First extraction of inclusive V_{cb} from q^2 moments*, *JHEP* **10** (2022) 068 [2205.10274].
- [75] M. Kirk, A. Lenz and T. Rauh, *Dimension-six matrix elements for meson mixing and lifetimes from sum rules*, *JHEP* **12** (2017) 068 [1711.02100].
- [76] L. Di Luzio, M. Kirk, A. Lenz and T. Rauh, *ΔM_s theory precision confronts flavour anomalies*, *JHEP* **12** (2019) 009 [1909.11087].
- [77] A. Lenz and G. Tetlalmatzi-Xolocotzi, *Model-independent bounds on new physics effects in non-leptonic tree-level decays of B-mesons*, *JHEP* **07** (2020) 177 [1912.07621].
- [78] J. Albrecht, F. Bernlochner, A. Lenz and A. Rusov, *Lifetimes of b-hadrons and mixing of neutral B-mesons: theoretical and experimental status*, *Eur. Phys. J. ST* **233** (2024) 359 [2402.04224].
- [79] HPQCD collaboration, *Lattice QCD matrix elements for the $B_s^0 - \bar{B}_s^0$ width difference beyond leading order*, *Phys. Rev. Lett.* **124** (2020) 082001 [1910.00970].
- [80] FERMILAB LATTICE, MILC collaboration, *$B_{(s)}^0$ -mixing matrix elements from lattice QCD for the Standard Model and beyond*, *Phys. Rev. D* **93** (2016) 113016 [1602.03560].

- [81] B. Chakraborty, C.T.H. Davies, B. Galloway, P. Knecht, J. Koponen, G.C. Donald et al., *High-precision quark masses and QCD coupling from $n_f = 4$ lattice QCD*, *Phys. Rev. D* **91** (2015) 054508 [1408.4169].
- [82] M. Beneke, *A Quark mass definition adequate for threshold problems*, *Phys. Lett. B* **434** (1998) 115 [hep-ph/9804241].
- [83] I.I.Y. Bigi, M.A. Shifman, N. Uraltsev and A.I. Vainshtein, *High power n of m_b in beauty widths and $n = 5 \rightarrow \infty$ limit*, *Phys. Rev. D* **56** (1997) 4017 [hep-ph/9704245].
- [84] A. Czarnecki, K. Melnikov and N. Uraltsev, *NonAbelian dipole radiation and the heavy quark expansion*, *Phys. Rev. Lett.* **80** (1998) 3189 [hep-ph/9708372].
- [85] M. Fael, K. Schönwald and M. Steinhauser, *Relation between the $\overline{\text{MS}}$ and the kinetic mass of heavy quarks*, *Phys. Rev. D* **103** (2021) 014005 [2011.11655].
- [86] A. Pineda, *Determination of the bottom quark mass from the $\Upsilon(1S)$ system*, *JHEP* **06** (2001) 022 [hep-ph/0105008].
- [87] U. Nierste, *CP asymmetry in flavor-specific B decays*, in *Proceedings of 39th Rencontres de Moriond on Electroweak Interactions and Unified Theories*, pp. 445–450, 6, 2004 [hep-ph/0406300].
- [88] A.J. Buras, M.E. Lautenbacher and G. Ostermaier, *Waiting for the top quark mass, $K^+ \rightarrow \pi^+ \nu \bar{\nu}$, $B_s^0 - \bar{B}_s^0$ mixing and CP asymmetries in B decays*, *Phys. Rev. D* **50** (1994) 3433 [hep-ph/9403384].
- [89] S. Herrlich and U. Nierste, *Indirect CP violation in the neutral kaon system beyond leading logarithms*, *Phys. Rev. D* **52** (1995) 6505 [hep-ph/9507262].
- [90] L. Wolfenstein, *Parametrization of the Kobayashi-Maskawa Matrix*, *Phys. Rev. Lett.* **51** (1983) 1945.
- [91] J. Fleischer, M.Y. Kalmykov and A.V. Kotikov, *Two loop selfenergy master integrals on-shell*, *Phys. Lett. B* **462** (1999) 169 [hep-ph/9905249].
- [92] S.A. Larin, F.V. Tkachov and J.A.M. Vermaseren, *The FORM version of MINCER*, .
- [93] S. Bekavac, *Calculation of massless Feynman integrals using harmonic sums*, *Comput. Phys. Commun.* **175** (2006) 180 [hep-ph/0505174].
- [94] P.A. Baikov and K.G. Chetyrkin, *Four Loop Massless Propagators: An Algebraic Evaluation of All Master Integrals*, *Nucl. Phys. B* **837** (2010) 186 [1004.1153].

- [95] S. Weinzierl, *Feynman Integrals. A Comprehensive Treatment for Students and Researchers*, UNITEXT for Physics, Springer (2022), 10.1007/978-3-030-99558-4, [2201.03593].
- [96] E. Panzer, *Algorithms for the symbolic integration of hyperlogarithms with applications to Feynman integrals*, *Comput. Phys. Commun.* **188** (2015) 148 [1403.3385].
- [97] O. Schnetz, *Generalized single-valued hyperlogarithms*, 2111.11246.
- [98] C. Duhr and F. Dulat, *PolyLogTools — polylogs for the masses*, *JHEP* **08** (2019) 135 [1904.07279].
- [99] S. Borowka, G. Heinrich, S. Jahn, S.P. Jones, M. Kerner, J. Schlenk et al., *pySecDec: a toolbox for the numerical evaluation of multi-scale integrals*, *Comput. Phys. Commun.* **222** (2018) 313 [1703.09692].
- [100] S. Borowka, G. Heinrich, S. Jahn, S.P. Jones, M. Kerner and J. Schlenk, *A GPU compatible quasi-Monte Carlo integrator interfaced to pySecDec*, *Comput. Phys. Commun.* **240** (2019) 120 [1811.11720].
- [101] G. Heinrich, S. Jahn, S.P. Jones, M. Kerner, F. Langer, V. Magerya et al., *Expansion by regions with pySecDec*, *Comput. Phys. Commun.* **273** (2022) 108267 [2108.10807].